5-5-2020

One-step Coassembly of Nanocoatings and Effects of the Deposition Methods

Sonia Chavez
University of Connecticut - Storrs, sonia.chavez@uconn.edu

One-step Coassembly of Nanocoatings and Effects of the Deposition Methods

Sonia Elena Chavez, Ph.D.

University of Connecticut, 2020

Organic/inorganic hybrid nanocoatings with a nacre like structure have attracted high interest because of their outstanding properties. A one-step coassembly method has previously been developed to prepare polyvinyl alcohol (PVA)/montmorillonite (MMT) nanocoatings with a high concentration of well-aligned MMT nanosheets. To obtained these coatings, dip coating is commonly used for flow-induced orientation.

In this dissertation, different coating methods are investigated to explore alternatives to overcome the deficiencies of dip coating. Spray coating is a versatile method that has virtually no limitation on substrate size or shape. Spray coating was varied through time and number of cycles. In addition, a rotational coating method was developed to apply continuous centripetal acceleration (4.0 to 48.8 m/s^2) to the nanosheets while drying to decrease production time. Both methods were proven to fabricate nanocoatings with sufficient performance for various applications.

While PVA is an ideal polymer binder, it is often desirable to introduce other binders with specific functionalities for new application development. As such, chitosan was selected to introduce antimicrobial properties to the nanocoatings. By introducing chitosan into the system, the resultant nanocoatings maintain a high O_2 barrier, possess antimicrobial properties, and are more sustainable.

Sonia Elena Chavez

University of Connecticut, 2020

Paper is a versatile material but not ideal for packaging applications due to its porous structure. As such, a method was developed to impregnate the PVA/MMT nanocoating into the pores of paper, as well as to coat the surface, to significantly improve the water vapor barrier.

In addition, an impregnation method was developed to form free-standing films, which usually are hard to be delaminated from the substrate if prepared via traditional coating methods. An all-MMT inorganic film was first prepared by casting a dispersion containing well-exfoliated MMT nanosheets and then impregnated with polyvinylidene fluoride (PVDF). The impregnation of PVDF helped further align the MMT nanosheets and improve the mechanical properties of the final product.

Overall, two new coating methods were developed for one-step coassembly of nanocoatings, an additional polymer binder and a new substrate were explored, and an impregnation method was developed. More importantly, this work may inspire the invention of new processing methods to prepare nacre-like structures.

One-step Co-Assembly of MMT Nanocoatings and Effects of the Deposition Methods

Sonia Elena Chavez

B.S. DePaul University, **2012**

M.S. DePaul University, **2014**

A Dissertation

Submitted in Partial Fulfillment of the

Requirements for the Degree of

Doctor of Philosophy

at the

University of Connecticut

2020

APPROVAL PAGE

Doctor of Philosophy Dissertation

One-step Co-Assembly of MMT Nanocoatings and Effects of the Deposition Methods

Presented by

Sonia Elena Chavez, B.S., M.S.

Major Advisor

_____

Dr. Luyi Sun

Co-Advisor

_____

Dr. Montgomery T. Shaw

Associate Advisor

_____

Dr. Richard Parnas

University of Connecticut

2020

Acknowledgement

I would like to sincerely thank Dr. Luyi Sun for his guidance and support throughout my Ph.D. study. Without his guidance, I would not have accomplished everything I have done so far. I am very grateful to have him as my mentor. In addition, I would like to thank Dr. Montgomery T. Shaw for the guidance he gave throughout my work. Without his expertise, I would not have been able to complete this work. Also, I would like to thank Dr. Mu-Ping Nieh for all his help with my SAXS results. I would like to thank my committee members Dr. Richard Parnas, Dr. Jie He, and Dr. Puxian Gao.

I would like to thank Hao Ding, Andrew Smith, Brandon Williams, Zaili Hou, and all my lab mates for their help in my research. In addition, to my undergraduate students that helped in material preparation and characterization, especially Gina Ducati, Joyce Caliendo, Karen Martinez, Allyson Barrett, and Sana Tanveer Khan.

Finally, I would like to thank my family for their love and support, Andres Chavez, Maria Chavez, Luz Chavez, and Albert Arevalo.

Table of Contents

CHAPTER 1. INTRODUCTION 1

CHAPTER 2. SPRAY COATING METHOD FOR PREPARING PVA/MMT NANOCOATINGS 15

2.1 INTRODUCTION 15

2.2 EXPERIMENTAL 16

2.2.1 Materials 16
2.2.2 Preparation of MMT/PVA dispersion 16
2.2.3 Preparation of nanocoatings via spray coating 17
2.2.4 Characterization 18

2.3 RESULTS AND DISCUSSION 20

2.4 CONCLUSION 32

CHAPTER 3. DEVELOPMENT OF ROTATIONAL COATING AS A FACILE METHOD FOR ONE-STEP COASSEMBLY OF NANOCOATINGS 36

3.1 INTRODUCTION 36

3.2 EXPERIMENTAL 37

3.2.1 Materials 37
3.2.2 Preparation of PVA/MMT dispersion 37
3.2.3 PVA/MMT nanocoating preparation 37

3.3 CHARACTERIZATION 38

3.4 RESULTS AND DISCUSSION 39

3.5 CONCLUSION 45

CHAPTER 4. SUSTAINABLE MULTIFUNCTIONAL NANOCOATINGS FROM ONE-STEP COASSEMBLY 49

4.1 INTRODUCTION 49

4.2 EXPERIMENTAL 50

4.2.1 Materials 50
4.2.2 Preparation of CH/PVA/MMT dispersions 50
4.2.3 Preparation of nanocoatings on PLA Films 51
4.2.4 Characterization 52

4.3 RESULTS AND DISCUSSION 53

4.4 CONCLUSION 66

CHAPTER 5. IMPROVING BARRIER PROPERTIES OF PAPER FOR POTENTIAL PACKAGING APPLICATIONS 71

5.1 INTRODUCTION 71

5.1.1 Materials 72
5.1.2 Preparation of PVA/MMT dispersion 72
5.1.3 Preparation of nanocoatings on paper substrates 73

5.2 RESULTS AND DISCUSSION 76

5.3 CONCLUSION 83

CHAPTER 6. POLYMER/CLAY NANOCOMPOSITE FILMS FROM AN IMPREGNATION METHOD 87

6.1 INTRODUCTION 87

6.2 EXPERIMENTAL 89

6.2.1 Materials 89
6.2.2 Preparation of PVDF/MMT nanocomposite films 89
6.2.3 Characterization 90

6.3 RESULTS AND DISCUSSION 90

6.4 CONCLUSION 99

CHAPTER 7. SUMMARY 103

Figure of Contents

Figure 1. Schematic of different types of morphology generated by a layered compound and a polymer. 1

Figure 2. Schematic of one-step coassembly (not drawn to scale). 4

Figure 3. Structure of montmorillonite. 5

Figure 4. Structure of (A) polyvinyl alcohol and (B) glutaraldehyde. 5

Figure 5. Co-crosslinking reaction between PVA and MMT using GA. 6

Figure 6. Spray Coating experimental set up. 18

Figure 7. Schematic and experimental set up for spray coating a polymer film. 21

Figure 8. Optical microscopy images of PET-PVA/MMT-50-1.5-C samples spray coated for 45 s for 1 (A), 2 (B), or (C) 3 cycles, and (D) optical microscopy image of a pristine PET film. 22

Figure 9. (A) Transmittance of the spray coated PET films and (B) turbidity of the spray coated nanocoatings. 24

Figure 10. Turbidity of the spray coated nanocoatings at 400 nm. 25

Figure 11. XRD patterns of the formed nanocoatings. 26

Figure 12. TEM image of the cross section of the nanocoating spray coated for 45 s and 3 cycles. 28

Figure 13. SAXS characterization of the spray coated PET-PVA/MMT-50-1.5-C-45s:3×. (A) 2D SAXS patterns of the coated film, (B) Bragg's patterns of the coated film, and (C) scattered intensity as a function of incident beam to the sample angle; the solid line represents the best fitting line of the Gaussian fit with the R^2 equal to 0.999. 29

Figure 14. O_2 Permeability of PVA/MMT-50-1.5-C nanocoatings. 31

Figure 15. Schematic of the experimental procedures to fabricate nanocoatings via rotational coating. 38

Figure 16. (A) Transmittance of the coated PET films and (b) turbidity of the PVA/MMT nanocoatings prepared at various centripetal accelerations. 40

Figure 17. Turbidity at 400 nm of the PVA/MMT nanocoatings prepared at various centripetal accelerations. 41

Figure 18. XRD patterns of the coated PET films at various centripetal accelerations. 43

Figure 19. Permeability of the formed nanocoatings at various centripetal accelerations. 44

Figure 20. Schematic of the fabrication of CH/PVA/MMT nanocoatings via one-step coassembly. 54

Figure 21. UV-Vis spectra of the coated PLA films. 55

Figure 22. XRD patterns of the coated PLA films and MMT control. 56

Figure 23. TEM images of the cross section of the nanocoatings. (A) CH(7)/PVA(C)/MMT-30-0.5-C, (B) CH(7)/PVA(C)/MMT-50-0.5-C, and (C) CH(7)/PVA(C)/MMT-70-0.5-C. 58

Figure 24. 2D SAXS patterns of (A) CH(7)/PVA(3)/MMT-30-0.5-C, (B) CH(7)/PVA(3)/MMT-50-0.5-C, (C) CH(7)/PVA(3)/MMT-70-0.5-C samples at various φ. 60

Figure 25. SAXS patterns of the formed nanocoatings. (A) CH(7)/PVA(3)/MMT-50-0.5-C, (B) CH(7)/PVA(3)/MMT-70-0.5-C, (C) CH(7)/PVA(3)/MMT-30-0.5-C, and (D) scattering intensity as a function of incident beam to the sample angle with the solid line representing the Gaussian fit. The R^2 values from the fitting for CH(7)/PVA(3)/MMT-50-0.5-C, CH(7)/PVA(3)/MMT-30-0.5-C, and CH(7)/PVA(3)/MMT-70-0.5-C are 0.9998, 0.9980, and 0.9999, respectively. 61

Figure 26. Permeability of various nanocoatings. (A) nanocoatings with various MMT %, (B) nanocoatings with various wt. %, and (C) nanocoatings with various CH/PVA ratios. 64

Figure 27. Bacterial viability of the coated PLA films with various formulations. 65

Figure 28. Schematic of the procedures to prepare PVA/MMT nanocoatings on paper substrates (not drawn to scale). 74

Figure 29. Schematic of the benchtop method to test the WVTR of the coated regular paper and cotton paper. 76

Figure 30. XRD patterns of the coated regular paper and cotton paper. 77

Figure 31. SEM images of the cotton paper (A) and (B), the coated cotton paper (C) and (D), the regular paper (E) and (F), and the coated regular paper (G) and (H). 80

Figure 32. Images of the combustion process of the samples: (A) regular paper, (B) coated regular paper, (C) cotton paper, and (D) coated cotton paper. 82

Figure 33. Residues of (A) the coated paper and (B) the coated cotton paper. 83

Figure 34. Schematic of the procedures to fabricate a PVDF/MMT nanocomposite film. 90

Figure 35. XRD patterns of the formed all-MMT and PVDF/MMT nanocomposite films. 92

Figure 36. (A) TGA and (B) DTGA thermograms of the PVDF, all-MMT, and PVDF/MMT nanocomposite freestanding film. 93

Figure 37. All-MMT (A) and PVDF/MMT (B) nanocomposite freestanding films wrapping around a 1.0 mm rod. 95

Figure 38. Representative stress-strain curves of the formed free-standing films. 96

Figure 39. Images of (A) combustibility testing (1300 ℃) of PVDF/MMT thin film under a butane torch for 12 s and (B) surface morphology after combustibility testing. 98

Table of Contents

Table 1. Barrier properties of various coated PET films..... 30

Table 2. Barrier properties of the coated PET films at various centripetal accelerations. 44

Table 3. Compositions of the dispersions to prepare nanocoatings on PLA films. 51

Table 4. Oxygen barrier properties of the coated PLA films. 63

Table 5. WVTRs of the coated regular paper and cotton paper. 81

Table 6. Mechanical properties of the formed PVDF/MMT free-standing films. 96

Table 7. Barrier properties of the formed PVDF/MMT nanocomposite film. 99

Table 8. Turbidity of the nanocoatings produced by rotational coating and spray coating. 104

Table 9. O_2 permeability of the nanocoatings by dip coating, rotational coating, and spray coating. 105

Chapter 1. **Introduction**

Polymer nanocomposites continue to attract high interest due to their excellent mechanical,[1, 2] gas barrier,[3, 4] flame retardant[5, 6] performance and various functionalities such as ionic conductivity,[7, 8] corrosion resistance,[9, 10] antimicrobial properties,[11-13] etc. Therefore, they have found widespread application in optics, electronics, energy fields, and food packaging.[1, 14-16] The ability to achieve the required properties for these applications is attributed to the two-phase system.

When introducing inorganic fillers into a polymer matrix, the formed morphology usually dictates the properties of the resultant nanocomposites. The morphologies (Figure 1) of the polymer/layered compound nanocomposites can be typically categorized as one of the following: phase-separated,[17, 18] intercalated,[7, 19] and exfoliated.[17, 18]

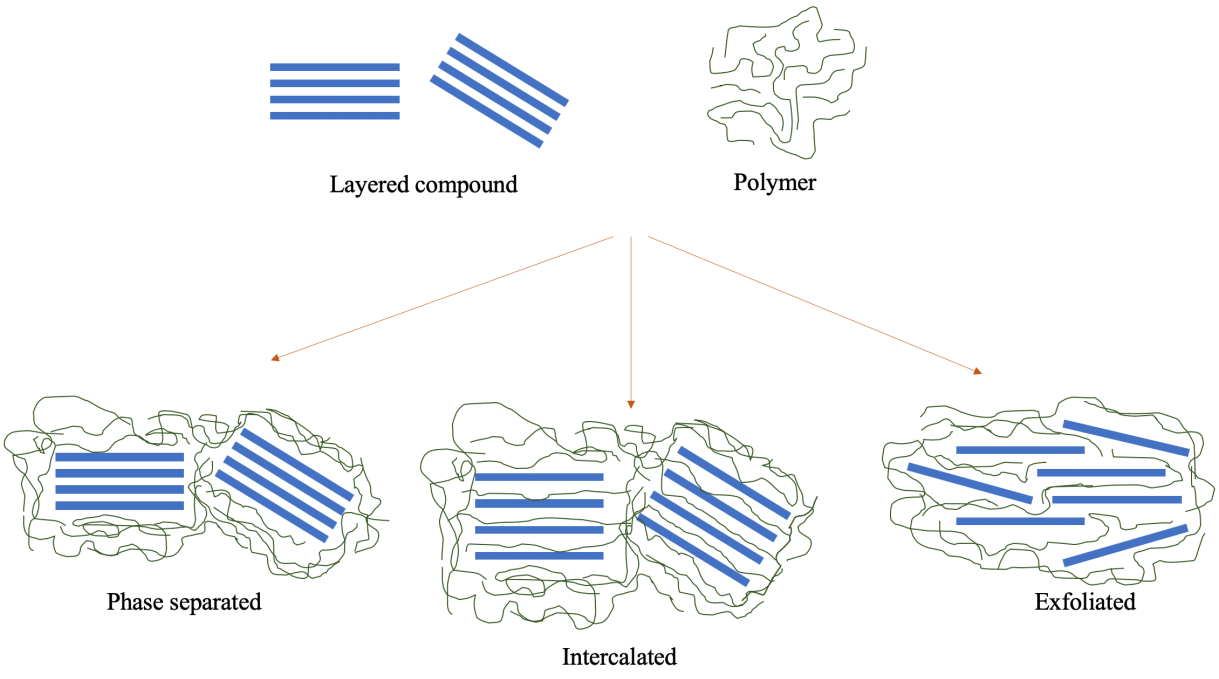

Figure 1. Schematic of different types of morphology generated by a layered compound and a polymer.

As shown in Figure 1, phase-separated nanocomposites form when the polymer cannot penetrate into the layered structure.[17] As a result, the d-spacing and the layered structures remain virtually identical to the starting state.[18] Alternatively, nanocomposites form an intercalated morphology when the polymer chains penetrate into the layered system but do not break the layered structure.[18, 19] On the other hand, nanocomposites possess an exfoliated morphology when the inorganic layers separate from each other, and the nanosheets are well dispersed in the polymer matrix, no longer maintaining a layered structure. Such well exfoliated and dispersed nanosheets will drastically improve the properties of the resultant nanocomposites.[18, 19]

Conventional processing methods have been widely used to prepare polymer nanocomposites. A common method is solvent mixing, during which layered nanosheets and polymer are mixed together in a proper solvent, usually with the assistance of ultrasonication, to achieve intercalation or exfoliation.[7] [19] This method decreases the chance of aggregation but typically has a long processing time and is difficult to scale up. To overcome some of these issues, direct mixing, i.e., compounding, can be adopted. Polymer pellets and nanoparticles are pre-mixed and then extruded using either a single- or twin-screw extruder.[7, 20, 21] Unfortunately, compounding usually requires a low nanofiller loading, as a high load will lead to an extremely high viscosity, and thus may not be able to achieve desired properties..[22] [21] *In situ* polymerization is another processing method and involves two steps.[19, 21, 23, 24] Even though, this method has some benefits it still has compatibility issues with high loadings of inorganic fillers, and a high level of dispersion needs to be completed before polymerization.[17, 21]

To advance the processing development of nanocomposites, some novel methods have been invented, including three-dimensional (3-D) printing,[24-26] electrophoretic deposition,[27-29]

layer-by-layer (LbL) self-assembly.[4, 30] But some of these methods are limited by the raw materials that can be used.[26, 31]

LbL self-assembly is a relatively versatile processing technique and is particularly ideal for the preparation of nanocomposite coatings (nanocoatings). Most charged materials, including inorganic nanosheets[14, 32] and organic electrolyts[33] can be used for LbL. With LbL self-assembly, alternating charged materials are assembled step by step to coat a substrate.[34] This method allows a buildup of different properties in each layer and allows for a better control of thickness. Even though this method has many advantages, it is difficult to scale up and is labor intensive.[35]

Many processing methods have paved the way for recent developments in nanocoatings, but several disadvantages arise with these methods. This includes limitations on sample size,[27, 31] raw materials,[28] and processing conditions[31] with possibly a low yield. To overcome these issues, a one-step coassembly method was developed.[35]

One-step coassembly involves the formation of nanocoatings using a low-viscosity dispersion containing both inorganic nanosheets and a polymer binder.[35] The goal is to achieve a high level of orientation of the nanosheets with the assistance of flow in the resultant nanocoating, thus resulting in outstanding mechanical and barrier properties.[35] To generate the nanocoating, the inorganic nanosheets are dispersed with a polymer binder through sonication. The dispersion is then applied to a substrate using dip coating to induce orientation with the flow, which is illustrated in Figure 2. This method allows for a decrease in material needed, tunable thickness, and the capability of scaling up. Also, dozens of layers are formed within one-step, promising for a broader range of applications.[35]

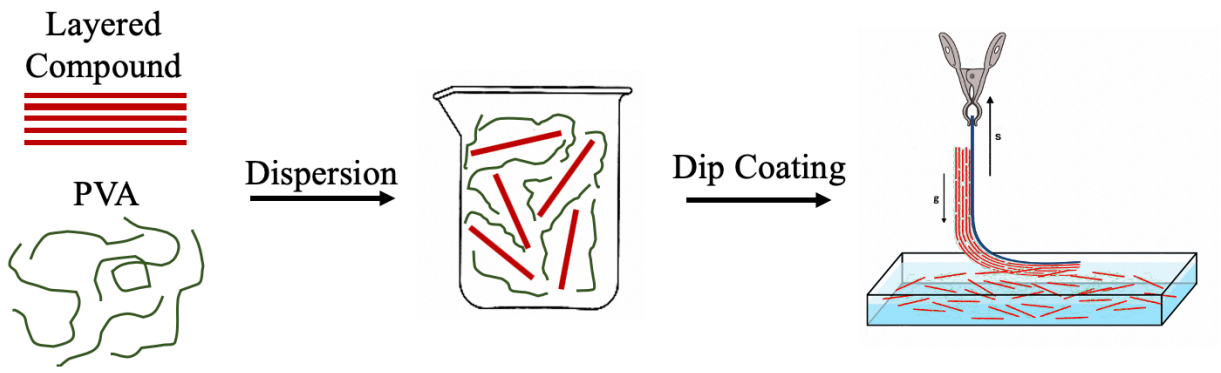

Figure 2. Schematic of one-step coassembly (not drawn to scale).

Montmorillonite (MMT) is an ideal nanofiller due to its ability to exfoliate in water, high mechanical properties, and low cost.[36, 37] MMT belongs to the 2:1 phyllosilicates family and smectite group. The structure of MMT (Figure ***3***) consists of an aluminum octahedral sheet sandwiched between two tetrahedral silica sheets.[17, 37] Due to the weak van der Waals forces holding the layers together, once in water, MMT will swell, and exfoliation can occur by shearing. Furthermore, MMT has a net negative charge, which helps to build polymer nanocomposites. Because of the above merits, MMT was used as the main inorganic nanosheets in this dissertation. The MMT nanosheets typically have a size of 260 ± 60 nm.[35]

Along with MMT, polyvinyl alcohol (PVA, Figure 4) was used as a main polymer binder in this dissertation due to its high water solubility and its strong interactions with MMT nanosheets, facilitating the coassembly process. In addition, glutaraldehyde (GA, Figure 4) can be used as a crosslinking agent to crosslink PVA, as well as co-crosslink PVA and MMT, as MMT nanosheets contain surface/edge hydroxyl groups as well.[35] The co-crosslinking schematic is illustrated in Figure 5. Crosslinking could be a very effective means to further improve the mechanical and physical properties of the resultant nanocoatings, as well as significantly improve the water stability of the nanocoatings, which is very necessary for some applications.

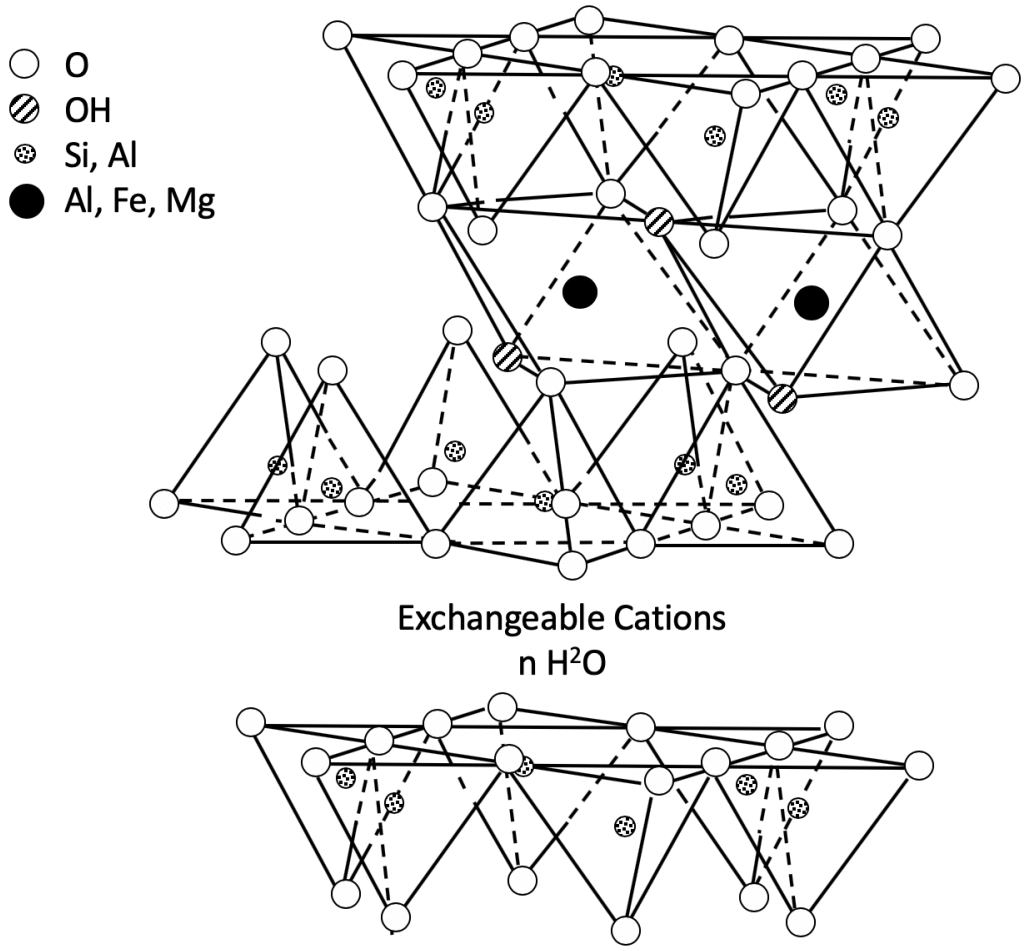

Figure 3. Structure of montmorillonite.

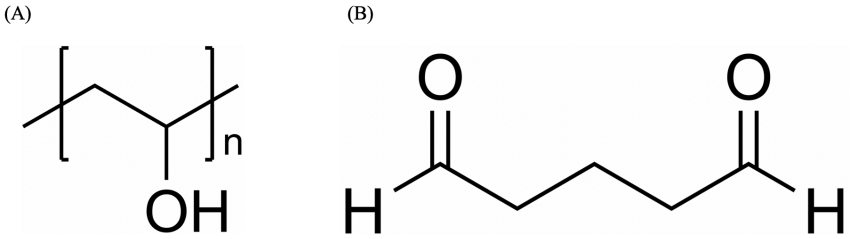

Figure 4. Structure of (A) polyvinyl alcohol and (B) glutaraldehyde.

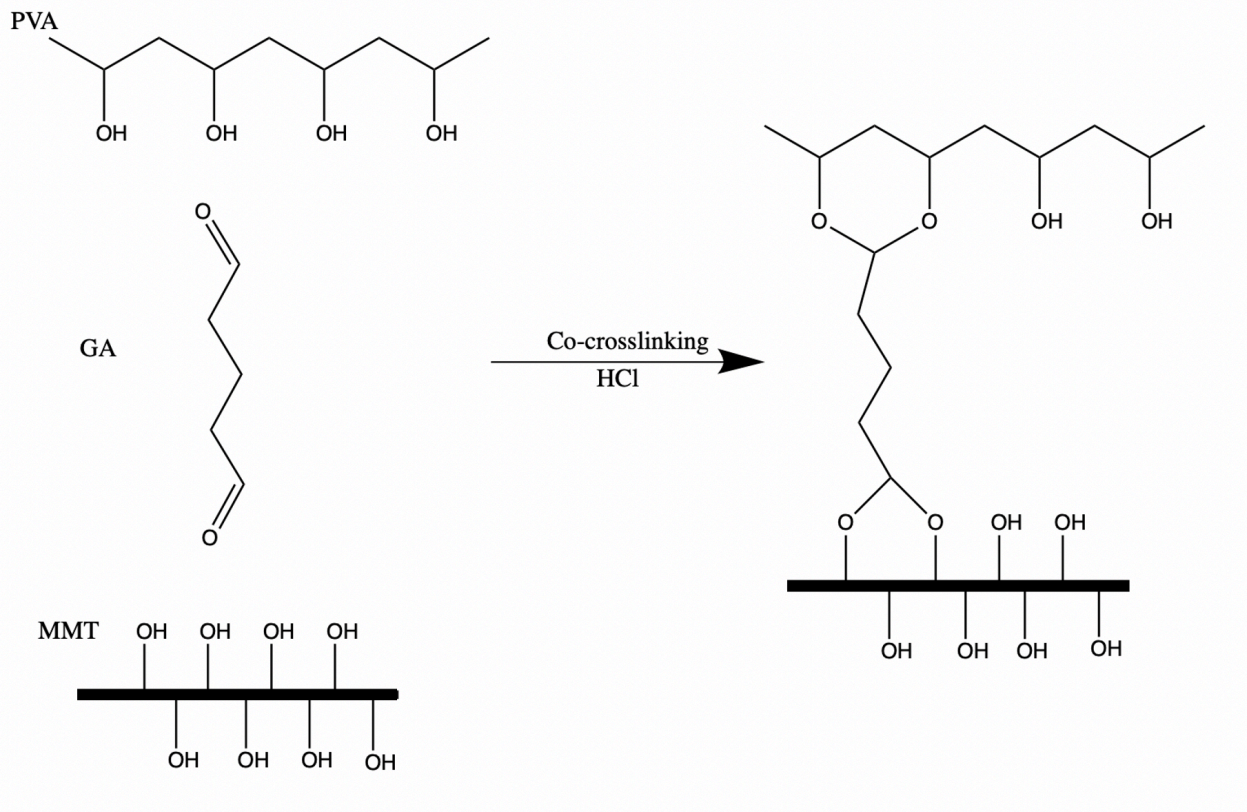

Figure 5. Co-crosslinking reaction between PVA and MMT using GA.

As stated before, dip coating is a facile method to induce flow of nanosheets and align them on the surface of various substrates to form nanocoatings. Previous work has shown that the formed nanocoatings can significantly improve the properties of the substrates, particularly barrier performance.[35] The process is completed through the evaporation of the solvent that is homogeneously spread on the surface, to form a solid film with a tunable thickness[38, 39]. Dip coating consists of several steps: immersion, dwelling, deposition, drainage, and evaporation.[39, 40] All of these stages are essential to the dip coating process, but drainage and evaporation stages are the primary factors determining the properties of the coating.[39]

During the drainage process, the dispersion drains from the substrate, and the entraining forces work to keep the fluid on the substrate.[39, 41] The deposition and drainage forces are what controls the thickness of the wet fluid on the substrate.[34, 36, 42] Afterwards, during solvent

evaporation, a film forms on the surface, with capillary and draining forces still acting on the wet dispersion.[39, 41] These regimes allow for dilute dispersion to develop thin films on the substrate. Dip coating is an excellent method but has some limitations, including insufficient shear stress during flow for nanosheet orientation, and limitation on the size and shape of the substrate.

To overcome these issues, other methods of application, including rotational coating (Chapter 2) and spray coating (Chapter 3) are investigated. Rotational coating allows one to apply centripetal acceleration to the nanocoating while drying over a broad range. This can help better investigate how such forces can affect the orientation of the nanosheets while drying. Spray coating uses droplets to apply coating to various substrates regardless of size and shape, and thus potentially broadening applications. By introducing different coating methods, a closer examination of how flow affects the orientation of the nanosheets is possible.

While PVA is an ideal polymer binder, it is desirable to introduce other binders with specific functionalities for new application development and to create more sustainable materials. As such, chitosan is selected to introduce antimicrobial properties to nanocoatings, which could particularly be used for food packaging application (Chapter 4). During early explorations, the nanocoatings were mainly applied onto synthetic polymer substrates such as polyethylene terephthalate, polypropylene, and polyethylene,[ref?] while natural polymers are largely ignored. In this dissertation, the exploration is extended to paper, composed of the most abundant natural polymer, cellulose (Chapter 5). The goal is to investigate whether nanocoatings with a high concentration of well-aligned nanosheets can also help impart barrier and flame retardant properties to paper for broader applications.

In addition to continuously develop and optimize the one-step coassembly process to fabricate nanocoatings, another method is developed to further extend the scope of nanocoatings.

Compared to the conventional methods, which can typically include up to 20 wt. % nanofillers into polymer matrices, one-step coassembly can help incorporate up to 70 wt. % nanosheets into the final nanocoatings. However, further increasing the loading of nanosheets remains a challenge via the one-step coassembly method, while some special applications such fire insulation do require nanocoatings with even higher inorganic concentrations. As such, a novel impregnation method is explored to prepare nanocoatings containing up to 87.5 wt. % inorganic nanosheets (Chapter 6), which demonstrates very unique properties.

References

1. Ebina, T.; Mizukami, F., Flexible Transparent Clay Films with Heat-Resistant and High Gas-Barrier Properties. *Advanced Materials* **2007,** *19* (18), 2450-2453.

2. Zhao, H.; Yang, Z.; Guo, L., Nacre-inspired composites with different macroscopic dimensions: strategies for improved mechanical performance and applications. *NPG Asia Materials* **2018,** *10* (4), 1-22.

3. Shchukin, D. G.; Zheludkevich, M.; Yasakau, K.; Lamaka, S.; Ferreira, M. G. S.; Möhwald, H., Layer-by-Layer Assembled Nanocontainers for Self-Healing Corrosion Protection. *Advanced Materials* **2006,** *18* (13), 1672-1678.

4. Ding, F.; Liu, J.; Zeng, S.; Xia, Y.; Wells, K. M.; Nieh, M.-P.; Sun, L., Biomimetic nanocoatings with exceptional mechanical, barrier, and flame-retardant properties from large-scale one-step coassembly. *Science Advances* **2017,** *3*, 7.

5. Chang, S.; Slopek, R. P.; Condon, B.; Grunlan, J. C., Surface Coating for Flame-Retardant Behavior of Cotton Fabric Using a Continuous Layer-by-Layer Process. *Industrial & Engineering Chemistry Research* **2014,** *53* (10), 3805-3812.

6. Liang, S.; Neisius, N. M.; Gaan, S., Recent developments in flame retardant polymeric coatings. *Progress in Organic Coatings* **2013,** *76* (11), 1642-1665.

7. Sinha Ray, S.; Okamoto, M., Polymer/layered silicate nanocomposites: a review from preparation to processing. *Progress in Polymer Science* **2003,** *28* (11), 1539-1641.

8. Kharlampieva, E.; Kozlovskaya, V.; Sukhishvili, S. A., Layer-by-Layer Hydrogen-Bonded Polymer Films: From Fundamentals to Applications. *Advanced Materials* **2009,** *21* (30), 3053-3065.

9. Pornea, A. M.; Puguan, J. M. C.; Deonikar, V. G.; Kim, H., Fabrication of multifunctional wax infused porous PVDF film with switchable temperature response surface and anti corrosion property. *Journal of Industrial and Engineering Chemistry* **2019**.

10. Yeh, J.-M.; Liou, S.-J.; Lai, S.-J.; Wu, P.-C., Enhancement of Corrosion Protection Effect in Polyaniline via the formation of Polyaniline-Clay Nanocomposite Materials. *Chem. Mater.* **201,** *13*, 1131-1136.

11. Laufer, G.; Kirkland, C.; Cain, A. A.; Grunlan, J. C., Clay-chitosan nanobrick walls: completely renewable gas barrier and flame-retardant nanocoatings. *ACS Appl Mater Interfaces* **2012,** *4* (3), 1643-9.

12. Walther, A.; Bjurhager, I.; Malho, J. M.; Pere, J.; Ruokolainen, J.; Berglund, L. A.; Ikkala, O., Large-area, lightweight and thick biomimetic composites with superior material properties via fast, economic, and green pathways. *Nano Lett* **2010,** *10* (8), 2742-8.

13. Liu, A.; Berglund, L. A., Clay nanopaper composites of nacre-like structure based on montmorrilonite and cellulose nanofibers—Improvements due to chitosan addition. *Carbohydrate Polymers* **2012,** *87* (1), 53-60.

14. Priolo, M. A.; Holder, K. M.; Greenlee, S. M.; Stevens, B. E.; Grunlan, J. C., Precisely Tuning the Clay Spacing in Nanobrick Wall Gas Barrier Thin Films. *Chemistry of Materials* **2013,** *25* (9), 1649-1655.

15. Priolo, M. A.; Holder, K. M.; Gamboa, D.; Grunlan, J. C., Influence of clay concentration on the gas barrier of clay-polymer nanobrick wall thin film assemblies. *Langmuir* **2011,** *27* (19), 12106-14.

16. Guin, T.; Krecker, M.; Hagen, D. A.; Grunlan, J. C., Thick growing multilayer nanobrick wall thin films: super gas barrier with very few layers. *Langmuir* **2014,** *30* (24), 7057-60.

17. Mittal, V., Polymer Layered Silicate Nanocomposites: A Review. *Materials* **2009,** *2* (3), 992-1057.

18. Liu, J.; Boo, W. J.; Clearfield, A.; Sue, H. J., Intercalation and Exfoliation A Review on Morphology of Polymer Nanocomposites Reinforced by Inorganic Layer Structures. *Materials and Manufacturing Processes* **2006,** *20*, 143-151.

19. Pavlidou, S.; Papaspyrides, C. D., A review on polymer–layered silicate nanocomposites. *Progress in Polymer Science* **2008,** *33* (12), 1119-1198.

20. Kim, H.; Macosko, C. W., Processing-property relationships of polycarbonate/graphene composites. *Polymer* **2009,** *50* (15), 3797-3809.

21. Muller, K.; Bugnicourt, E.; Latorre, M.; Jorda, M.; Echegoyen Sanz, Y.; Lagaron, J. M.; Miesbauer, O.; Bianchin, A.; Hankin, S.; Bolz, U.; Perez, G.; Jesdinszki, M.; Lindner, M.; Scheuerer, Z.; Castello, S.; Schmid, M., Review on the Processing and Properties of Polymer Nanocomposites and Nanocoatings and Their Applications in the Packaging, Automotive and Solar Energy Fields. *Nanomaterials (Basel)* **2017,** *7* (4).

22. Guan, Y.; Yang, S.; Zhang, Y.; Xu, J.; Han, C. C.; Kotov, N. A., Fabry-Perot Fringes and Their Application To Study the Film Growth, Chain Rearrangement, and Erosion of Hydrogen-Bonded PVPON/PNN Films. *Journal of Physical Chemistry B* **2006,** *110*, 13484-13490.

23. Zou, J.-F.; Yu, Z.-Z.; Pan, Y.-X.; Fang, X.-P.; Ou, Y.-C., Conductive mechanism of polymer/graphite conducting composites with low percolation threshold. *Journal of Polymer Science Part B: Polymer Physics* **2002,** *40* (10), 954-963.

24. Li, B.; Zhong, W.-H., Review on polymer/graphite nanoplatelet nanocomposites. *Journal of Materials Science* **2011,** *46* (17), 5595-5614.

25. Gross, B. C.; Erkal, J. L.; Lockwood, S. Y.; Chen, C.; Spence, D. M., Evaluation of 3D printing and its potential impact on biotechnology and the chemical sciences. *Anal Chem* **2014,** *86* (7), 3240-53.

26. Mannoor, M. S.; Jiang, Z.; James, T.; Kong, Y. L.; Malatesta, K. A.; Soboyejo, W. O.; Verma, N.; Gracias, D. H.; McAlpine, M. C., 3D printed bionic ears. *Nano Lett* **2013,** *13* (6), 2634-9.

27. Yeh, S.-R.; Seul, M.; Shraiman, B. I., Assembly of ordered colloidal aggregrated by electric-field-induced fluid flow. *Nature* **1990,** *386* (6), 57-59.

28. Gorelikov, I.; Kumacheva, E., Electrodeposition of Polymer-Semiconductor Nanocomposite Films. *Chem. Mater.* **2004,** *16* (21), 4122-4127.

29. Ammam, M., Electrophoretic deposition under modulated electric fields: a review. *RSC Advances* **2012,** *2* (20).

30. Li, Y. C.; Mannen, S.; Morgan, A. B.; Chang, S.; Yang, Y. H.; Condon, B.; Grunlan, J. C., Intumescent all-polymer multilayer nanocoating capable of extinguishing flame on fabric. *Adv Mater* **2011,** *23* (34), 3926-31.

31. Wei, X.; Li, D.; Jiang, W.; Gu, Z.; Wang, X.; Zhang, Z.; Sun, Z., 3D Printable Graphene Composite. *Sci Rep* **2015,** *5*, 11181.

32. Priolo, M. A.; Gamboa, D.; Grunlan, J. C., Transparent Clay−Polymer Nano Brick Wall Assemblies with Tailorable Oxygen Barrier. *ACS Applied Materials & Interfaces* **2009,** *2* (1), 312-320.

33. Cooper, T. M.; Campbell, A. L.; Crane, R. L., Formation of polypeptide-dye multilayers by electrostatic self-assembly technique. *Langmuir* **1995,** *11* (7), 2713-2718.

34. Denis-Rohr, A.; Bastarrachea, L. J.; Goddard, J. M., Antimicrobial efficacy of N -halamine coatings prepared via dip and spray layer-by-layer deposition. *Food and Bioproducts Processing* **2015,** *96*, 12-19.

35. Ding, F.; Liu, J.; Zeng, S.; Xia, Y.; Wells, K. M.; Nieh, M.-P.; Sun, L., Biomimetic nanocoatings with exceptional mechanical, barrier, and flame-retardant properties from large-scale one-stemp coassembly. *Science Advances* **2017,** *3*.

36. Podsiadlo, P.; Kaushik, A. K.; Arruda, e. M.; Waas, A. M.; Shim, b. S.; Xu, J.; Nandivada, H.; Pumplin, B. G.; Lahann, J.; Ramamoorthy, A.; Kotov, N. A., Ultrastrong and Stiff Layered Polymer Nanocomposites. *Science* **2007,** *318* (59847), 80-8.

37. Chen, T.; Zhao, Y.; Song, S., Comparison of colloidal stability of montmorillonite dispersion in aqueous NaCl solution with in alcohol-water mixture. *Powder Technology* **2017,** *322*, 378-385.

38. Lu, Y.; Ganguli, R.; Drewien, C. A.; Anderson, M. T.; Brinker, C. J.; Gong, W.; Guo, Y.; Soyex, H.; Dunn, B.; Huang, M. H.; Zink, J. I., Continuous formation of supported cubic and hexagonal mesoporous films by sole-gel dip-coating. *Nature* **1997,** *389*, 364-368.

39. Brinker, C. J., Dip Coating. In *Chemical Solution Deposition of Functional Oxide Thin Films*, 2013; pp 233-261.

40. Kakaei, K.; Esrafili, M. D.; Ehsani, A., Graphene and Anticorrosive Properties. In *Graphene Surfaces - Particles and Catalysts*, 2019; pp 303-337.

41. Bindini, E.; Naudin, G.; Faustini, M.; Grosso, D.; Boissière, C., Critical Role of the Atmosphere in Dip-Coating Process. *The Journal of Physical Chemistry C* **2017,** *121* (27), 14572-14580.

42. Gans, A.; Dressaire, E.; Colnet, B.; Saingier, G.; Bazant, M. Z.; Sauret, A., Dip-coating of suspensions. *Soft Matter* **2019,** *15* (2), 252-261.

Chapter 2. **Spray coating method for preparing PVA/MMT nanocoatings**

2.1 Introduction

From the previous chapter, it can be seen that the nanocoatings produced through one-step coassembly exhibit excellent features: highly ordered structures,[1] excellent mechanical,[2] barrier,[3-5] and flame retardant[6-8] properties, and scalable processing.[9, 10] Dip coating was the first one-step coassembly method developed to fabricate nanocoatings. Following that, rotational coating was developed but mainly for fundamental exploration.

For large scale manufacturing, spray coating might be a more desirable processing method because it's a versatile and low-cost technique.[11] The spray coating gun works by forcing air through a nozzle to disperse the dispersion as a collection of droplets covering the surface of the substrate. The droplets produced are affected by the surface energy, dispersion viscosity, and capillarity and intertie forces.[12-15] Spray coating has virtually no limitation on substrate size and can utilize a broad range of fluids (with various rheological characteristics)[11, 16] by adjusting spraying parameters. In addition, spray deposition time is faster compared to other methods,[17, 18] and spray coating can easily generate desirable coating thickness by altering dispersion concentration and/or coating cycles.[16, 19]

However, to prepare nanocoatings via spray coating, there are a few key challenges to address: achieving coating uniformity and maintaining a high degree of nanosheet orientation at a high production rate. For spray coating, water is surely the best solvent candidate considering cost, health, and the environment, and thus the polyvinyl alcohol (PVA)/montmorillonite (MMT) aqueous dispersion developed for dip coating is still adopted.

PVA/MMT nanocoatings are of great interest due to their ability to improve multiple properties and their waterborne nature; thus, they are particularly suitable as the dispersion for spray coating. This is mainly due to the ability of MMT to exfoliate into single-layer nanosheets in an aqueous system under sonication.[20] Also, the weak hydrogen bonding and van der Waals interactions allow the PVA chains to attach to the MMT sheet surface,[21, 22] facilitating the following coassembly and orientation process. The orientation process is also affected by the specific processing method.

This chapter aims to address the above challenges and develop a spray coating method for preparing nanocoatings at a high speed and scale. It will also be compared with the results from other coating methods.

2.2 Experimental

2.2.1 Materials

PVA [Mowiol 8-88; M_w (weight average molecular weight): 67,000, 86.7 to 88.7 mole percent hydrolysis; Kuraray)], Sodium montmorillonite (PGN nanoclay, Minerals Technologies Inc., USA), GA (50% aqueous solution; Sigma-Aldrich), and HCl (37%; Sigma-Aldrich) were used as received without further purification. The PET films were obtained from Toray Plastics (America) Inc. with a thickness of 24 μm.

2.2.2 Preparation of MMT/PVA dispersion

PVA was dissolved in deionized (DI) water at 80 °C and stirred for three hours. MMT was uniformly dispersed in DI water under stirring for one hour and ultrasonicated in a sonication bath (Branson 8510R-MT, 250 W, 44kHz) for another hour. A predetermined amount of PVA solution was added to the MMT aqueous dispersion to form a dispersion system containing 1.5 wt. % total of solids (MMT + PVA). The mixture was stirred for one hour and ultrasonicated for one hour to

ensure uniformity of the dispersion. Once the mixture was cooled in an ice bath, a predetermined amount of cross-linking agent GA was added to the mixture. The mole ratio of GA to the total mole number of hydroxyl groups on the PVA chains was 1:20 and HCl was used as the catalyst with a mole ratio of 1:5 to GA.

2.2.3 Preparation of nanocoatings via spray coating

A PET film (ca. 14 cm × 17 cm) was washed with DI water and dried in an oven for 30 minutes; these procedures were repeated with ethanol. The film was then adhered to a glass plate with the assistance of a thin layer of water in between the plate and the film. The glass plate with the PET film was mounted onto a linear actuator. To control the actuator, a stepper motor (Model J-5718HB3401, Shanghai Zhengji Company, Shanghai, China) paired with a controller (Arduino Mega 2560, Italy) was used. The spray gun (G444; 0.2 mm nozzle; Master Airbrush, USA) was set at 16 cm from the nozzle to the glass plate and 24 cm from the nozzle to the bench (Figure 6). The actuator was set to operate at 1.2 cm/s, and the flow on the spray gun was set at 5 μL/s. The PET film was sprayed coated with the following time intervals: 15, 30, or 45 s. Also, each film was spray coated for 1, 2, or 3 cycles.

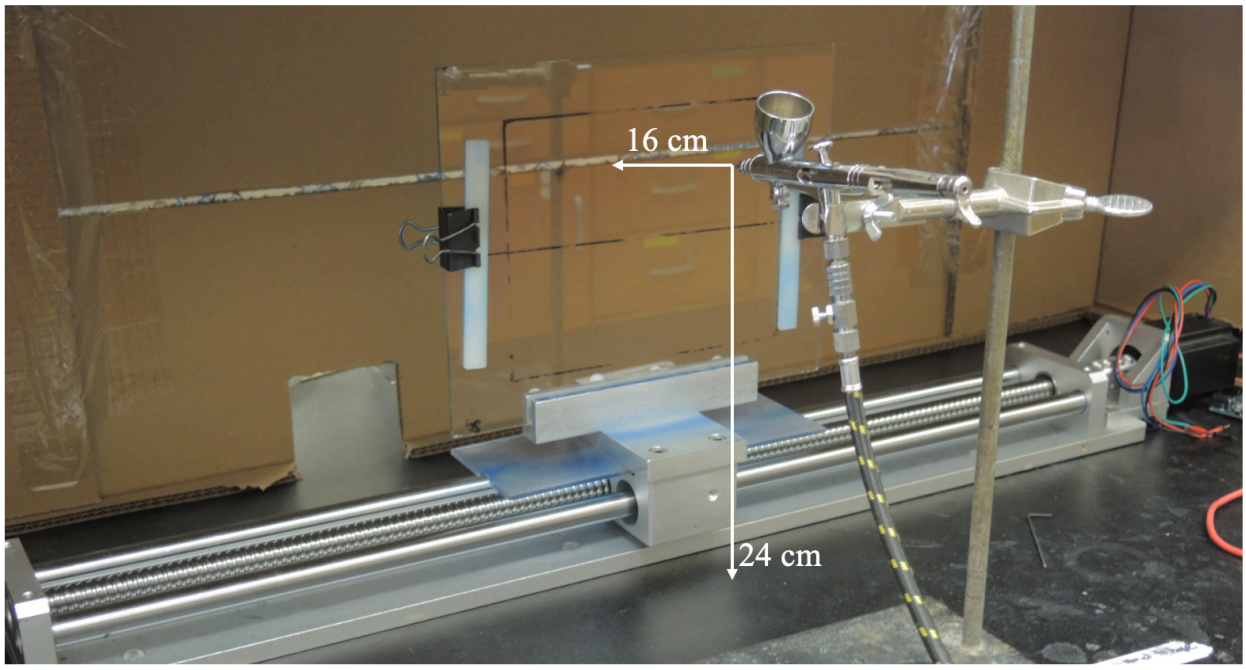

Figure 6. Spray Coating experimental set up.

2.2.4 Characterization

The nanocoatings were characterized by an ultraviolet-visible (UV-Vis) spectrophotometer (Lambada 900, Perkin Elmer) to evaluate their transparency and turbidity. A Bruker D2 X-ray diffractometer with a Bragg-Brentano fixed sample geometry and a LynxEye linear detector was used to record the X-ray diffraction (XRD) patterns of the coated PET films. Turbidity was calculated using the following equation:

$$Turbidity = \frac{-\ln\left(I/I_{\circ}\right)}{L} \qquad \text{Equation 1}$$

where, I is the transmittance of coated PET film, $I_{\circ}$ is the transmittance of uncoated PET film, and L is thickness of the nanocoating.

Small angle X-ray scattering (SAXS) characterization was conducted using a Bruker NanoStar instrument with a Turbo (rotating anode) X-ray source. The Göbel mirror and Cu Kα

were used to choose a wavelength of 1.5418 Å. To collimate the beam, a pair of scatterless pinholes were used with the following diameters: 500 and 350 μm. A MikroGap VÅNTEC-2000 detector was used to collect the 2D data. A sample-to-detector distance of 67 cm to cover a scattering vector, $\mathbf{q}$ [$|q| \equiv \frac{4\pi}{\lambda}\sin\left(\frac{\theta}{2}\right)$, where θ is the scattering angle], and ranged from 0.015 to 0.37 $Å^{-1}$. Examination of the lamellar alignment for the different samples was completed by conducting a rocking curve experiment that shows the distribution of deviation from the perfect orientation, with Bragg angle (θ_2) being equal to the angle between the incident beam and the sample (φ). This was completed by collecting 2D scattering patterns at different φ values by manually rotating the sample. The data were corrected for background and reduced to 1D data, with the same sector integration completed on each φ value.

To capture the cross-section of the nanocoatings, the coated film samples were embedded into epoxy, which was microtomed into 80 to 100 nm thin sections on a Reichert-Jung Ultracut E ultramicrotome. The sections were deposited onto a 400-mesh copper grid and imaged on an FEI Talos F200X scanning transmission electron microscope with an accelerating voltage of 120 kV.

The oxygen transmission rates (OTRs) of the nanocoatings were tested on a MOCON (Minneapolis, MN) OX-TRAN 1/50 OTR tester at 23 °C and 0% RH using ASTM D3985 standard method. To calculate the O_2 permeability and to account for the thickness of the nanocoating, the following equation was used:[23]

$$P = \left(\frac{\phi_p}{P_p} + \frac{\phi_g}{P_g}\right)^{-1}, \phi_p = \frac{d_p}{d_p + d_g}, \phi_g = \frac{d_p}{d_p + d_g} \qquad \text{Equation 2}$$

where d_p, ϕ_p, and P_p are the thickness, volume fraction, and permeability of the substrate, respectively. The variable with subscript *g* corresponds to the values of the nanocoating.

The thickness of the nanocoatings was obtained by removing a portion of the nanocoating from the substrate with a Scotch® tape, then measured by a Dektak 150 surface profiler from Veeco Instruments (Mannheim, Germany).

2.3 Results and Discussion

Figure 7 illustrates the experimental procedures to prepare PVA/MMT nanocoatings on PET films. The coassembly is facilitated due to (1) the weak van der Waals force and hydrogen bonding between the MMT and the PVA[22, 24, 25] when they were uniformly dispersed in water; (2) flow of the dispersion on the PET film after spraying.

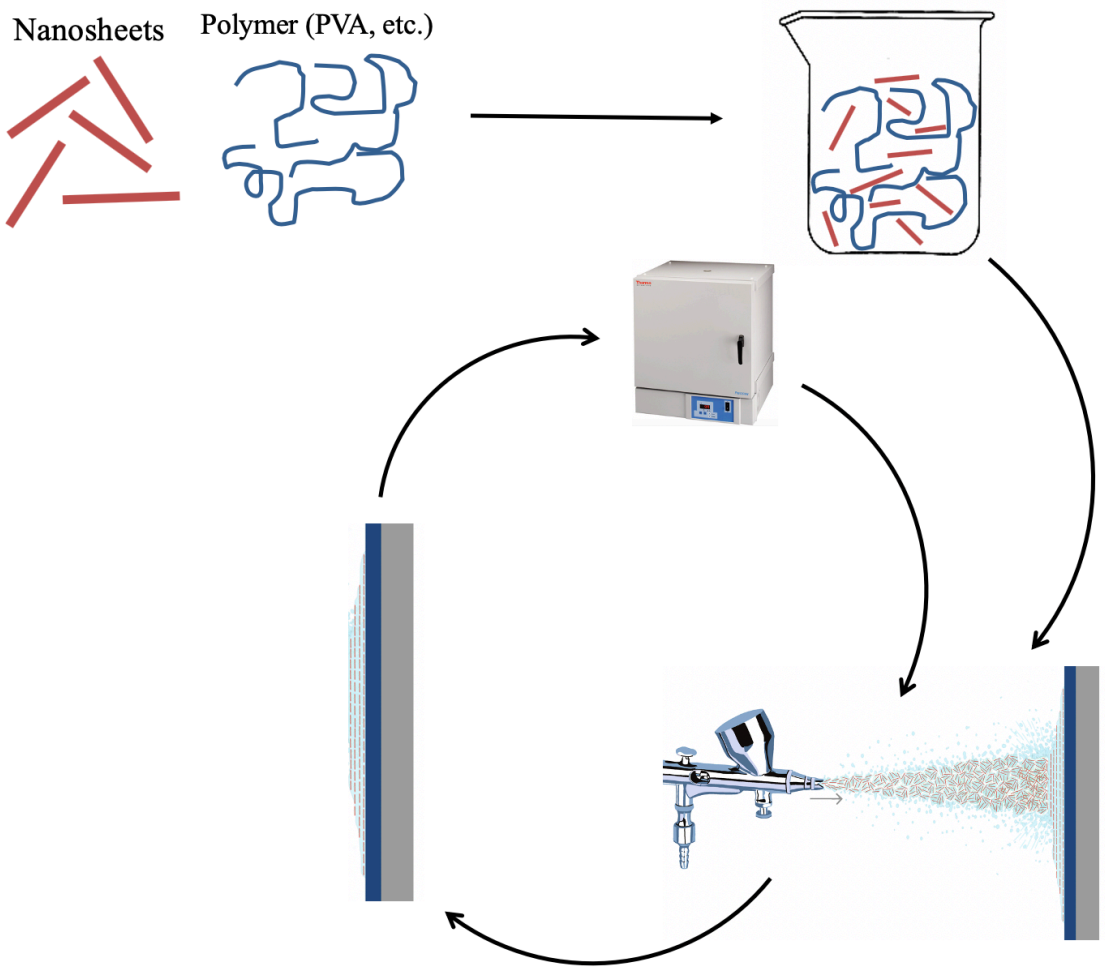

Figure 7. Schematic and experimental set up for spray coating a polymer film.

The optical microscopy images of the spray coated samples depict that the nanocoatings do not cover the entire surface of the substrate after 1 or 2 cycles of coating (45 s each cycle), as shown in Figure 8. After 3 cycles of spray coating, virtually the entire surface was covered by the formed PVA/MMT nanocoating, but the presence of iridescence (Figure 8C) indicates that the thickness of the formed nanocoating is not uniform. This is probably because of the limited flow of the sprayed droplets on the PET film. To systematically examine the quality of the spray coated samples, their transmittance and turbidity were investigated.

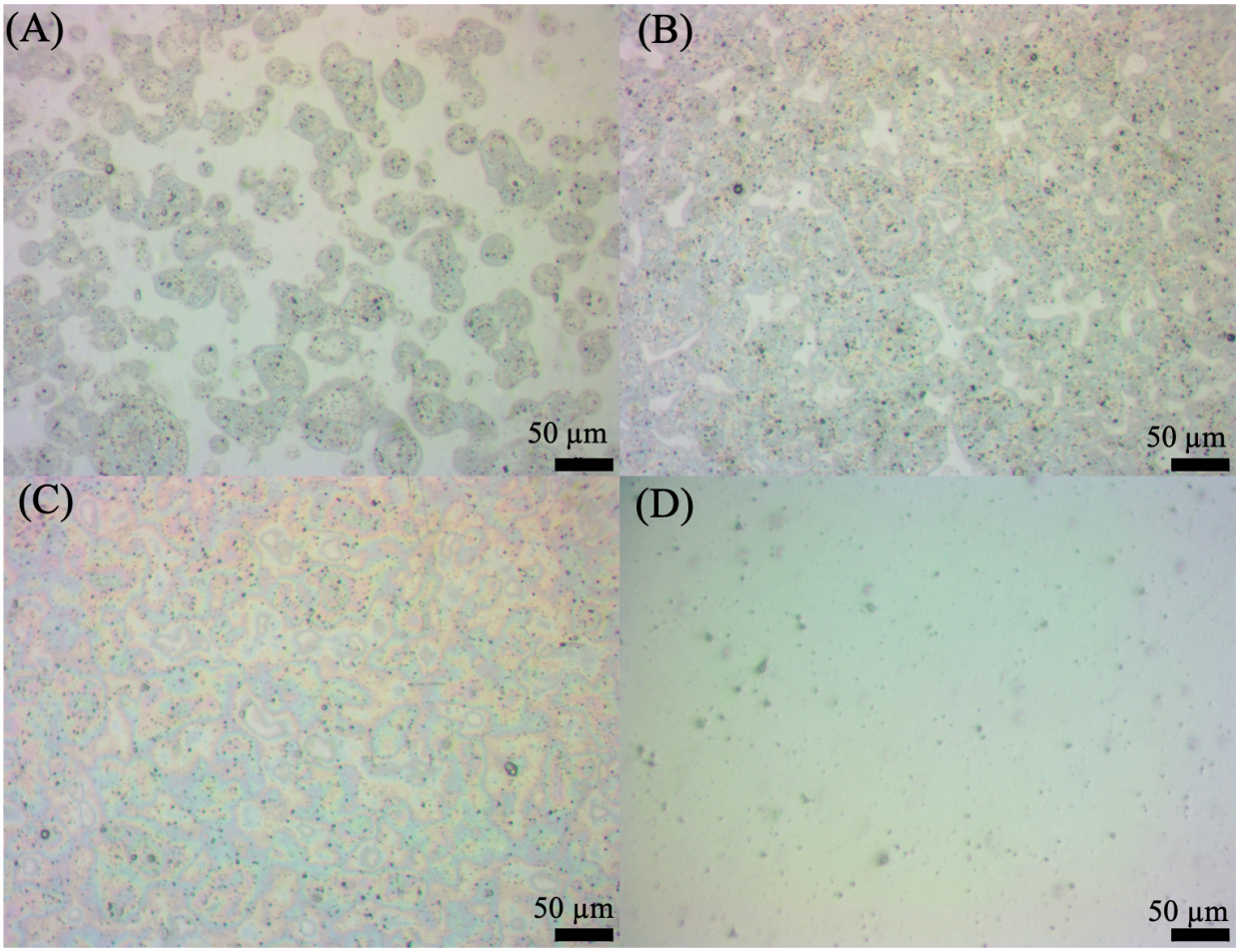

Figure 8. Optical microscopy images of PET-PVA/MMT-50-1.5-C samples spray coated for 45 s for 1 (A), 2 (B), or (C) 3 cycles, and (D) optical microscopy image of a pristine PET film.

The transmittance of the coated PET films gives a preliminary indication of the quality and uniformity of the formed nanocoatings. Figure 9 displays high transparency for all of the spray coated PET films, but all films are slightly inferior to the uncoated PET film. In previous work and Chapter 3, the dip coated and rotationally coated samples exhibit virtually the same transparency as the uncoated films due to the high level of nanosheet orientation and uniform thickness. The difference in transparency of the spray coated samples from the dip coated and rotationally coated samples is probably due to the lower level of nanosheet orientation and less uniform coating thickness. This difference is verified by the optical images shown in Figure 3. Similar trends were

observed in their turbidities (Figure 9 and Figure 10) which were calculated from Equation Equation 1 and can be explained by the same reasons. Figure 10 shows that the turbidity of the samples spray coated 45 s for 3 cycles is lower than other samples coated at 45s. This could be attributed to the possibility that each layer covers up the defects of the previous nanocoating.

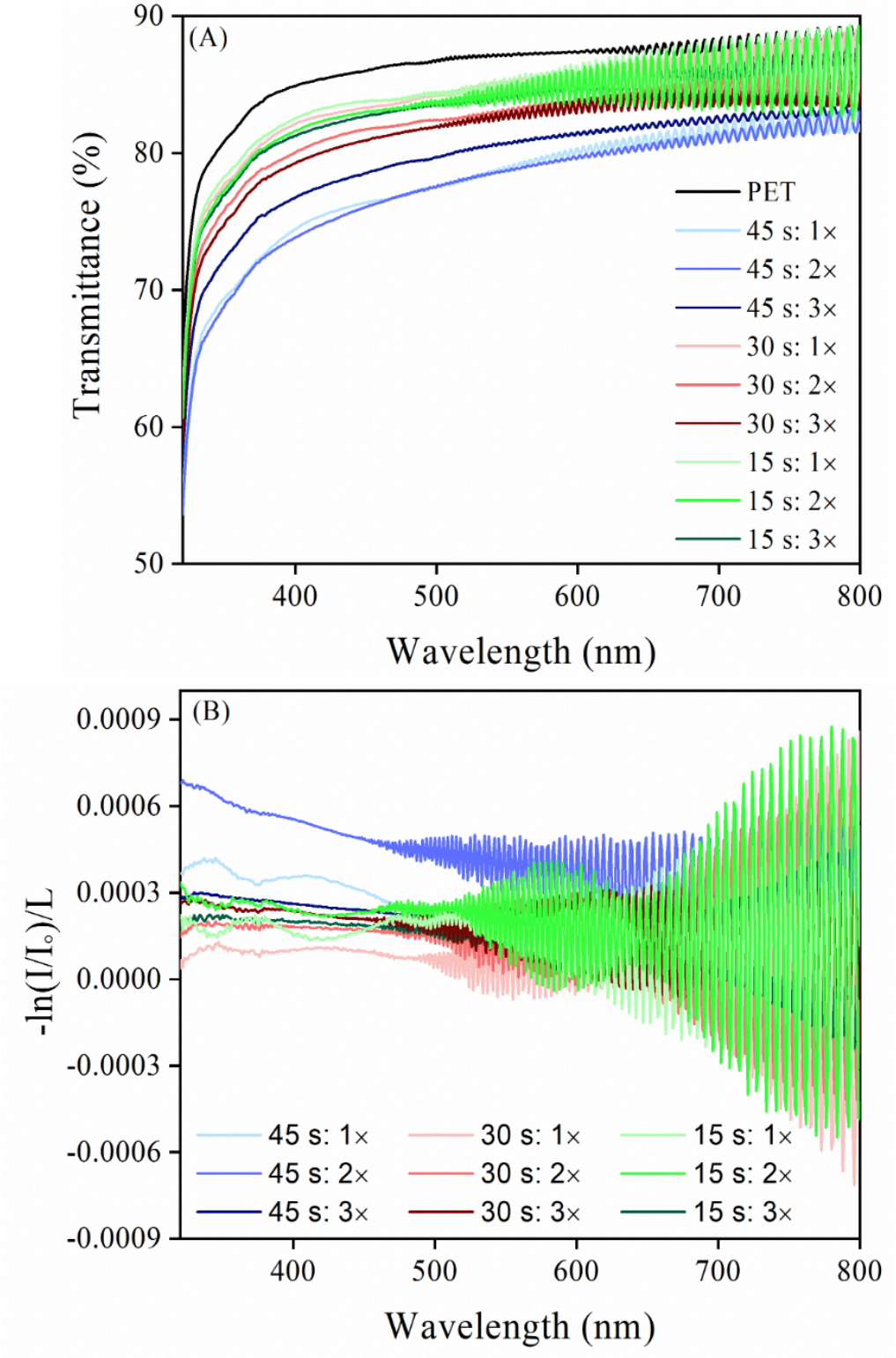

Figure 9. (A) Transmittance of the spray coated PET films and (B) turbidity of the spray coated nanocoatings.

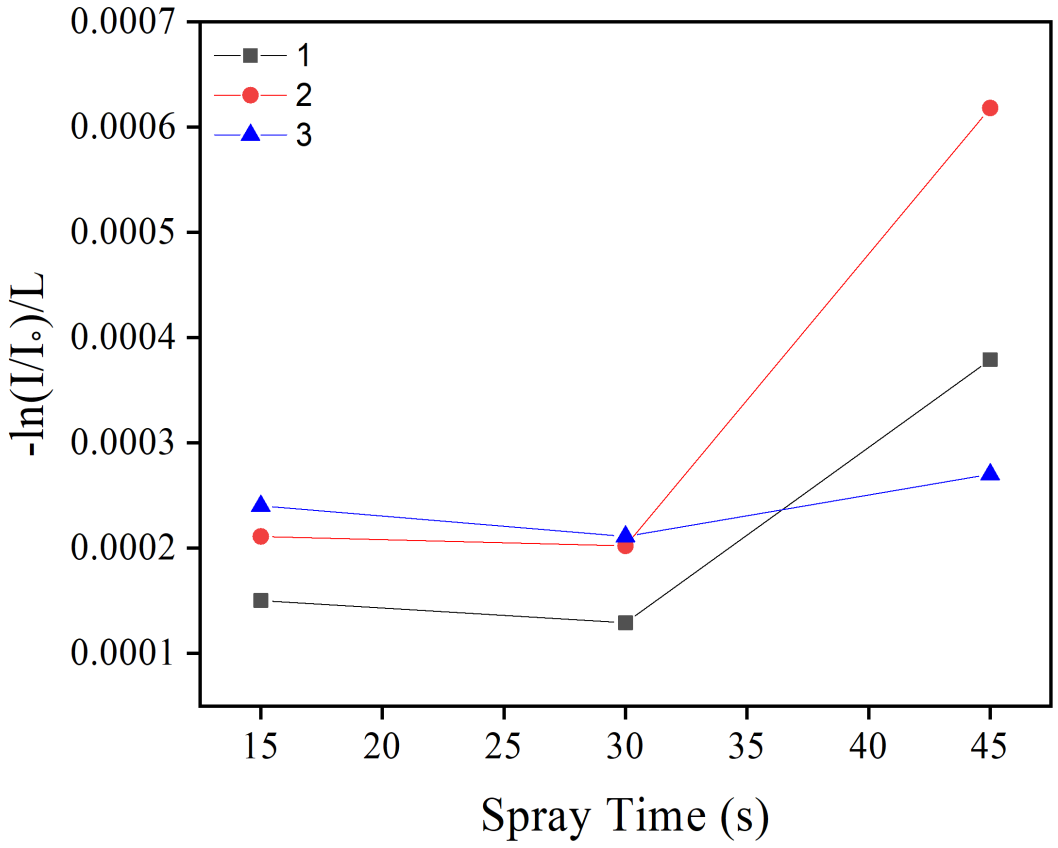

Figure 10. Turbidity of the spray coated nanocoatings at 400 nm.

The structure of the coassembled MMT nanosheets in the spray coated samples was examined using XRD. The XRD patterns show an increase in intensity with increasing spray time and number of cycles (Figure 11), which is expected. Initial evaluation of the film quality can be made through the XRD patterns. In Figure 11, the film sprayed for 45 s and 3 cycles exhibited the most intensive peak, from the collected data, which suggests a most ordered aligned layered structure. Meanwhile, all the diffraction peaks are at virtually the same location, suggesting the formed nanocoatings have a similar interlayer distance. This is expected as all the nanocoatings contain the same concentration of inorganic MMT nanosheets and PVA binder. Further investigation was completed through TEM microscopy and SAXS analysis to more comprehensively examine the overall orientation of the MMT nanosheets.

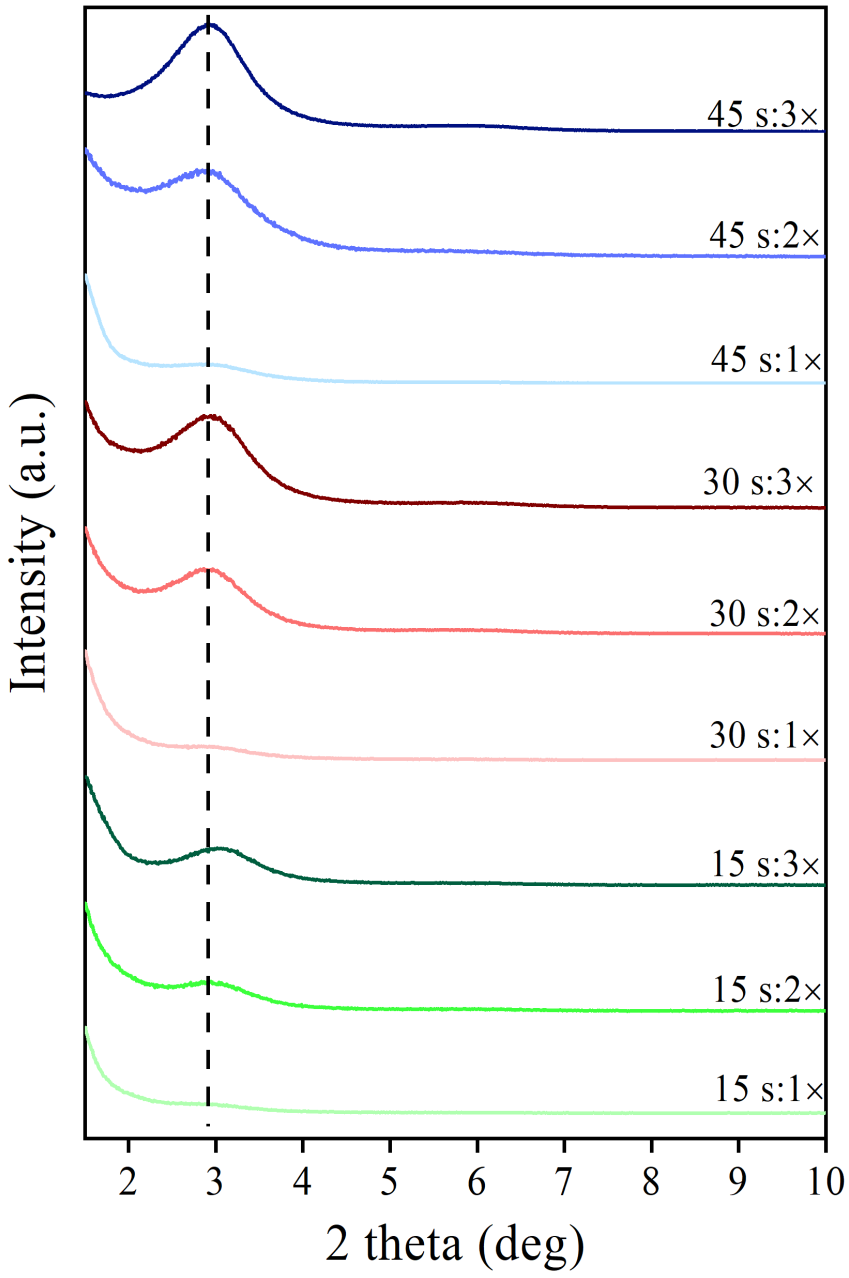

Figure 11. XRD patterns of the formed nanocoatings.

Even though XRD gives an initial examination of the layered structure of the formed nanocoatings, a closer inspection was completed through TEM imagining. Figure 12 depicts the cross-sectional TEM image of the formed nanocoating, which shows well-aligned nanosheets. To further investigate the microstructure, sample PVA/MMT-50-1.5-C-45s:3× was characterized by

SAXS. The 2D and 1D SAXS patterns are shown in Figure 13 with the background in the 1D patterns normalized with the collected data at φ = 90°. The sample was perpendicular to the beam at φ = 90°, when the pattern showed no alignment. But as the sample moved towards the Bragg's angle (black arrow), the intensity at θ_B increases. By plotting the intensity of $2\theta_B$ as a function of φ, one is able to examine the alignment. To do this, the data were fitted with the Gaussian distribution:

$$f(x) = \frac{1}{\sigma\sqrt{2\pi}} e^{-(x-\mu)^2/2\sigma^2} \qquad \text{Equation 3}$$

where μ is the mean and σ^2 is the variance. The following equation can obtain the full width half max (FWHM) of the peak:

$$FWHM = 2\sqrt{2\ln 2}\,\sigma \qquad \text{Equation 4}$$

The FWHM from the fitting of PVA/MMT-50-1.5-C-45s:3× is 14.4° ± 0.2°.

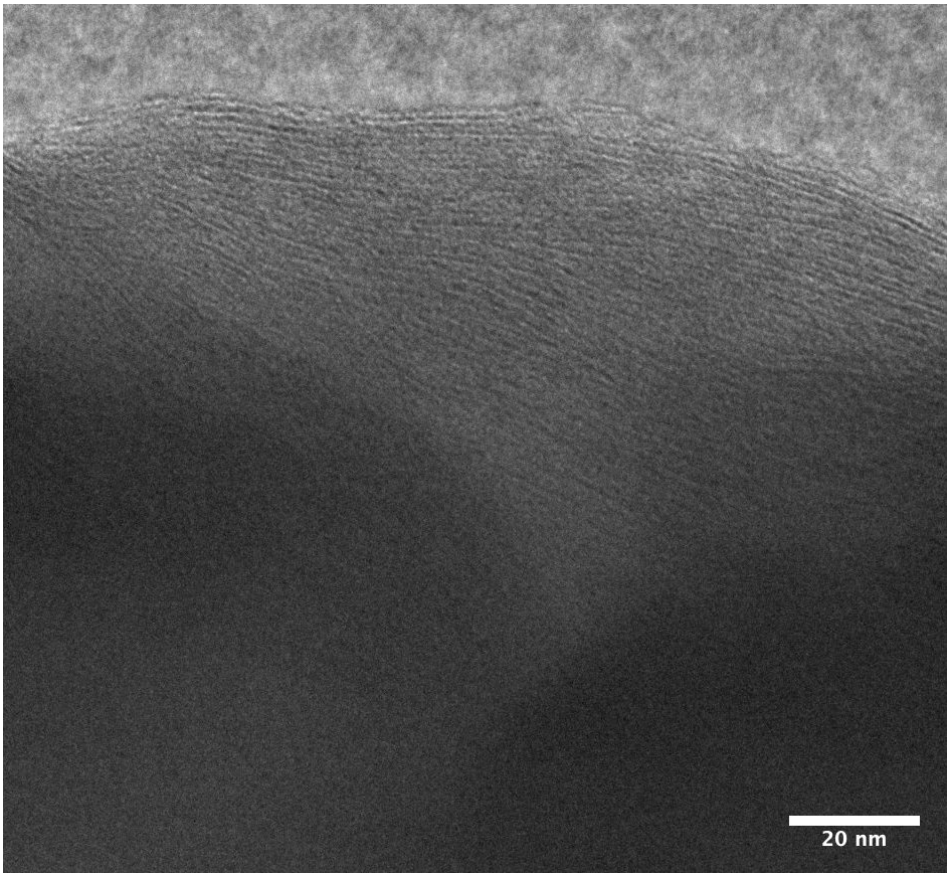

Figure 12. TEM image of the cross section of the nanocoating spray coated for 45 s and 3 cycles.

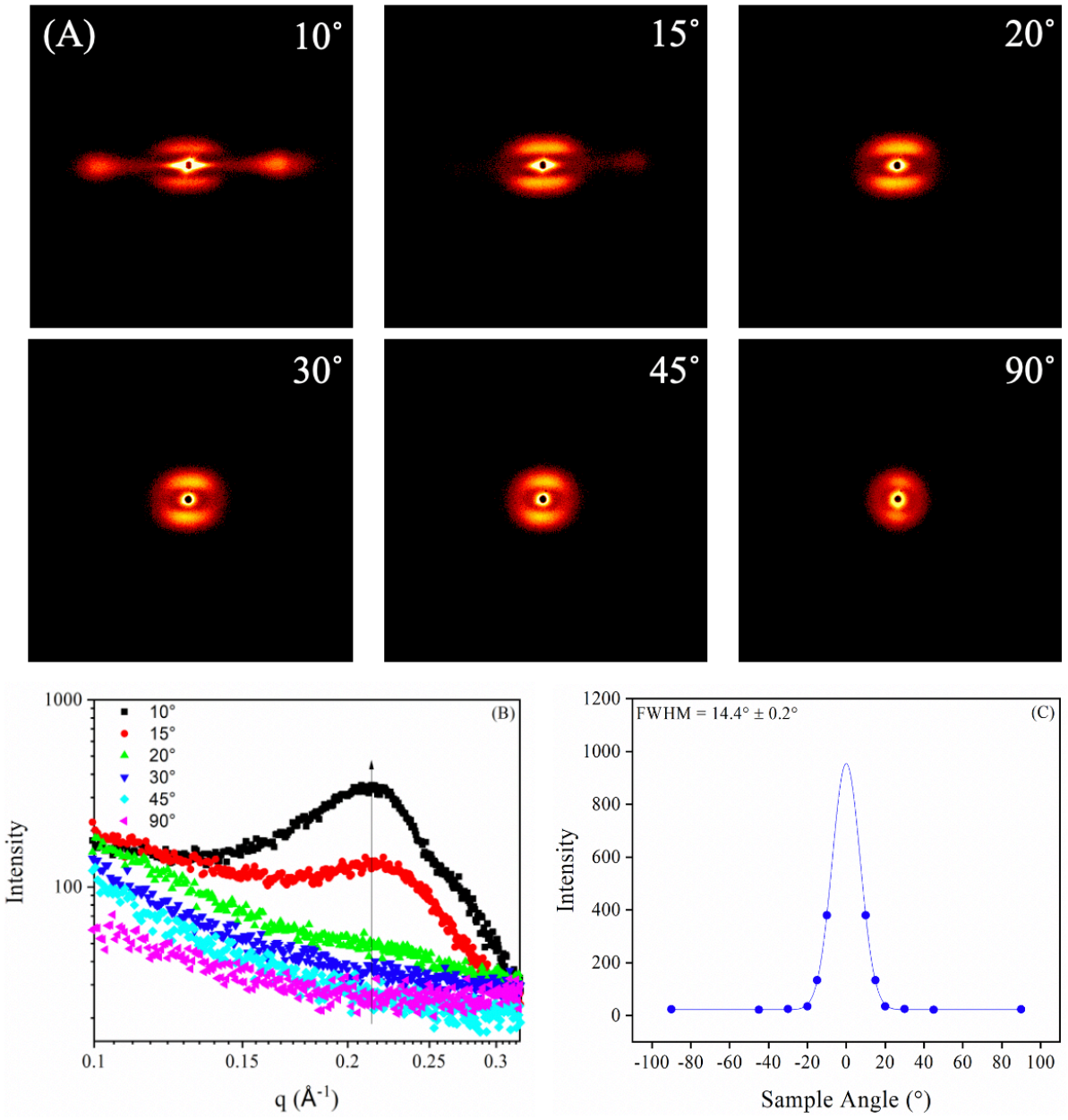

Figure 13. SAXS characterization of the spray coated PET-PVA/MMT-50-1.5-C-45s:3×. (A) 2D SAXS patterns of the coated film, (B) Bragg's patterns of the coated film, and (C) scattered intensity as a function of incident beam to the sample angle; the solid line represents the best fitting line of the Gaussian fit with the R^2 equal to 0.999.

A comprehensive examination of the overall quality of the produced nanocoatings was completed through testing the OTR of the spray coated films. As shown in Table 1, the OTRs of the coated films improved as compared to the uncoated PET, which has an OTR of 64 $cm^3/m^2 \cdot day \cdot atm$. The oxygen barrier properties were normalized to adjust for the coating thickness and eliminate the effect of the PET substrate. The normalized oxygen permeability data of the nanocoatings are summarized in Table 1 and the permeability data were calculated using Equation 2. Overall, the oxygen permeability remained high for most of the samples, but a remarkable improvement was achieved in sample PVA/MMT-50-1.5-C-45s:3× (Figure 14). This is because the PET films were not completely covered even after 3 cycles of 15 or 30 s spray coating, but were well covered after 3 cycles of 45 s spray coating as discussed before.

Table 1. Barrier properties of various coated PET films.

	Thickness (nm)	OTR testing [cm^3/m^2•day• atm]	O_2 Permeability of coated film in total [10^{-16} cm^3(STP)cm/cm^2•s• Pa]	O_2 Permeability of coating layer [10^{-16} cm^3(STP)cm/cm^2•s• Pa]
PET (24 m)		64	16.08	
PET-PVA-C	596 ±29	14.8	3.82	0.1311
15 s:1×	64 ±10	59.3	16.30	0.58825
15 s:2×	81 ± 11	56.8	15.62	0.46956
15 s:3×	115 ± 13	51.6	14.21	0.35047
30 s:1×	100 ± 16	53.6	14.76	0.37844
30 s:2×	139 ± 33	45.9	12.66	0.25943
30 s:3×	208 ± 46	31.2	8.63	0.14482
45 s:1×	140 ± 28	44.7	12.32	0.23653
45 s:2×	219 ± 70	30.2	8.35	0.14325
45 s:3×	309 ± 84	1.7	0.47	0.00615

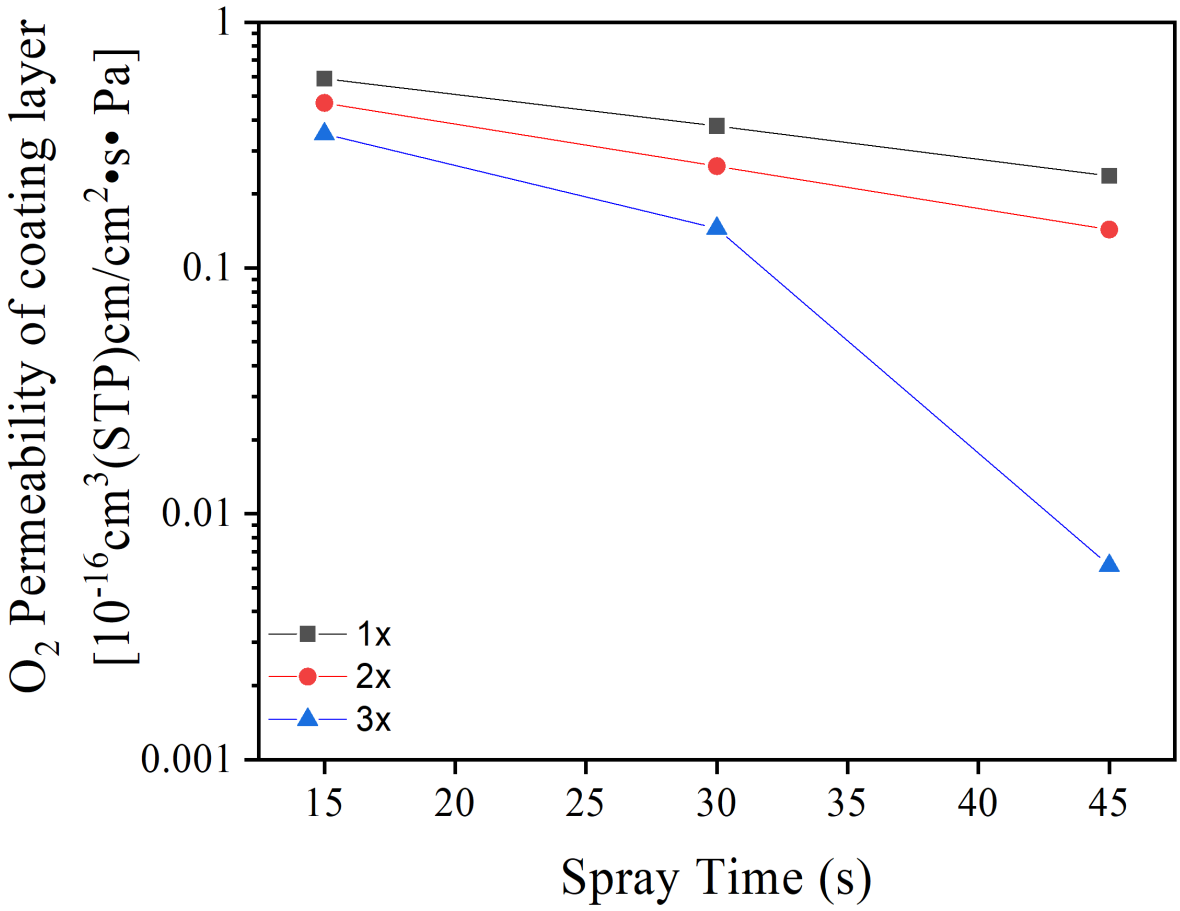

Figure 14. O_2 Permeability of PVA/MMT-50-1.5-C nanocoatings.

While PET is used in this study, the spray coating method is versatile, and many other plastic films can serve as substrates for spray coating. However, for some plastic films with a relatively low surface energy, such as BOPP, HDPE, LDPE, etc., a corona treatment may be necessary to improve the surface hydrophobicity for better coating quality with a waterborne coating.

2.4 Conclusion

Spray coating is an effective coating method as it has no shape or size limitation on substrate. Based on the above characterization results, it can be seen that spray coating can form nanocoatings with an ordered layered structure, but the overall quality of the spray coated samples is not as high as that of the ones from dip coating or rotational coating. Proper spray coating can form a nanocoating layer to effectively lower the permeability of the coated substrate, but care must be exercised to minimize defects (uncovered surface).

References

1. Choudalakis, G.; Gotsis, A. D., Permeability of polymer/clay nanocomposites: A review. *European Polymer Journal* **2009,** *45* (4), 967-984.

2. Chen, H.; Müller, M. B.; Gilmore, K. J.; Wallace, G. G.; Li, D., Mechanically Strong, Electrically Conductive, and Biocompatible Graphene Paper. *Advanced Materials* **2008,** *20* (18), 3557-3561.

3. Guin, T.; Krecker, M.; Hagen, D. A.; Grunlan, J. C., Thick growing multilayer nanobrick wall thin films: super gas barrier with very few layers. *Langmuir* **2014,** *30* (24), 7057-60.

4. Priolo, M. A.; Holder, K. M.; Gamboa, D.; Grunlan, J. C., Influence of clay concentration on the gas barrier of clay-polymer nanobrick wall thin film assemblies. *Langmuir* **2011,** *27* (19), 12106-14.

5. Priolo, M. A.; Holder, K. M.; Greenlee, S. M.; Stevens, B. E.; Grunlan, J. C., Precisely Tuning the Clay Spacing in Nanobrick Wall Gas Barrier Thin Films. *Chemistry of Materials* **2013,** *25* (9), 1649-1655.

6. Ebina, T.; Mizukami, F., Flexible Transparent Clay Films with Heat-Resistant and High Gas-Barrier Properties. *Advanced Materials* **2007,** *19* (18), 2450-2453.

7. Watanabe, I., Environmental release and behavior of brominated flame retardants. *Environment International* **2003,** *29* (6), 665-682.

8. Sun, L.; Boo, W. J.; Clearfield, A.; Sue, H. J.; Pham, H. Q., Barrier properties of model epoxy nanocomposites. *Journal of Membrane Science* **2008,** *318* (1-2), 129-136.

9. Srivastava, S.; Kotov, N. A., Composite Layer-by-Layer (LbL) Assembly with Inorganic Nanoparticles and Nanowires. *Accounts of Chemical Research* **2008,** *41*, 1831-1841.

10. Das, P.; Schipmann, S.; Malho, J. M.; Zhu, B.; Klemradt, U.; Walther, A., Facile access to large-scale, self-assembled, nacre-inspired, high-performance materials with tunable nanoscale periodicities. *ACS Appl Mater Interfaces* **2013,** *5* (9), 3738-47.

11. Aziz, F.; Ismail, A. F., Spray coating methods for polymer solar cells fabrication: A review. *Materials Science in Semiconductor Processing* **2015,** *39*, 416-425.

12. Huang, J.; Yuan, Z.; Gao, S.; Liao, J.; Eslamian, M., Understanding Spray Coating Process: Visual Observation of Impingement of Multiple Droplets on a Substrate. *Journal of Shanghai Jiaotong University (Science)* **2018,** *23* (1), 97-105.

13. Yarin, A. L., Drop Impact Dynamics: Splashing, Spreading, Receeding, Bouncing…. *Annu. Rev. Fluid Mech.* **2006,** *38*, 159-192.

14. Roisman, I. V.; Rioboo, R.; Tropea, C., Normal impact of a liquid drop on a dry surfac: model for spreading and receding. *Proc. R. Soc. Lond. A* **2002,** *458*, 1411-1430.

15. Pasandideh-Fard, M.; Qiao, Y. M.; Chandra, S.; Mostaghimi, J., Capillary effects during droplet impact on a solid surface. *Physl Fluids* **1996,** *8*, 650-659.

16. Sung, C.; Hearn, K.; Reid, D. K.; Vidyasagar, A.; Lutkenhaus, J. L., A comparison of thermal transitions in dip- and spray-assisted layer-by-layer assemblies. *Langmuir* **2013,** *29* (28), 8907-13.

17. Nogueira, G. M.; Banerjee, D.; Cohen, R. E.; Rubner, M. F., Spray-layer-by-layer assembly can more rapidly produce optical-quality multistack heterostructures. *Langmuir* **2011,** *27* (12), 7860-7.

18. Bose, S.; Keller, S. S.; Alstrom, T. S.; Boisen, A.; Almdal, K., Process optimization of ultrasonic spray coating of polymer films. *Langmuir* **2013,** *29* (23), 6911-9.

19. Schaaf, P.; Voegel, J. C.; Jierry, L.; Boulmedais, F., Spray-assisted polyelectrolyte multilayer buildup: from step-by-step to single-step polyelectrolyte film constructions. *Adv Mater* **2012,** *24* (8), 1001-16.

20. Gans, A.; Dressaire, E.; Colnet, B.; Saingier, G.; Bazant, M. Z.; Sauret, A., Dip-coating of suspensions. *Soft Matter* **2019,** *15* (2), 252-261.

21. Podsiadlo, P.; Kaushik, A. K.; Arruda, e. M.; Waas, A. M.; Shim, b. S.; Xu, J.; Nandivada, H.; Pumplin, B. G.; Lahann, J.; Ramamoorthy, A.; Kotov, N. A., Ultrastrong and Stiff Layered Polymer Nanocomposites. *Science* **2007,** *318* (59847), 80-8.

22. Ding, F.; Liu, J.; Zeng, S.; Xia, Y.; Wells, K. M.; Nieh, M.-P.; Sun, L., Biomimetic nanocoatings with exceptional mechanical, barrier, and flame-retardant properties from large-scale one-stemp coassembly. *Science Advances* **2017,** *3*.

23. Roberts, A. P.; Henry, B. M.; A.P., S.; Grovenor, C. R. M.; Briggs, G. A. D.; Miyamoto, T.; Kano, M.; Tsukahara, Y.; Yanaka, M., Gas permeation in silicon-oxide/polymer (SiOx/PET) barrier films; role of the oxide lattice, nano-defects and macro-defects. *Journal of Membrane Science* **2002,** *208*, 75-88.

24. Lvov, Y.; Decher, G.; Sukhorukov, G., Assembly of Thin Films by Means of Successive Deposition of Alternate Layers of DNA and Poly(allylamine). *Macromolecules* **1993,** *26*, 5396-5399.

25. Cooper, T. M.; Campbell, A. L.; Crane, R. L., Formation of polypeptide-dye multilayers by electrostatic self-assembly technique. *Langmuir* **1995,** *11* (7), 2713-2718.

Chapter 3. **Development of rotational coating as a facile method for one-step coassembly of nanocoatings**

3.1 Introduction

As introduced in the previous chapter, polymer nanocoatings are of significant interest thanks to their superior mechanical,[1, 2] barrier,[3, 4] and flame-retardant[5, 6] properties. Depending on the properties of the nanocoatings, they can be utilized for widespread application in optics,[7, 8] electronics,[9-11] food packaging,[4, 11, 12] and solar cells.[13]

The properties of nanocoatings are highly dependent upon the morphology of their layered structure, especially the overall level of nanosheet orientation,[3] which is highly dependent on the preparation methods. Dip coating is a widely used method to form nanocoatings.[11, 14, 15] This method allows for tunable thickness and quick buildup of a thin coating with a low concentration dispersion.[16] However, dip coating is not ideal for exploring the mechanism of flow-induced nanosheet orientation, because the flow/drain rate of the dispersion can only be varied within a narrow range, which is not beneficial for investigating the mechanism.

To better study the mechanism, a facile rotational coating process was developed, which allows for the control of key processing parameters (i.e., centripetal acceleration) within a very broad range. As a result, one can better investigate how such external factors affect the orientation of nanosheets during coating formation. Besides, rotational coating is typically a much faster coating process than dip coating, and can potentially be developed to be a continuous production process, and thus promising for mass production.

3.2 Experimental

3.2.1 Materials

PVA [Mowiol 8-88; M_w (weight average molecular weight): 67,000, 86.7 to 88.7 mole percent hydrolysis; Kuraray], sodium montmorillonite (MMT) (PGN nanoclay; Minerals Technologies Inc., USA), GA (50% aqueous solution; Sigma-Aldrich), and HCl (37%; Sigma-Aldrich) were used as received without further purification. PET films were obtained from Tory Plastics (America) Inc. with a thickness of 24 μm.

3.2.2 Preparation of PVA/MMT dispersion

PVA pellets were dissolved in deionized (DI) water with the assistance of heating at 80 °C. MMT was uniformly dispersed in DI water for 1 h under vigorous stirring followed by 1 h of ultrasonication (ultrasonication bath; Branson 8510R-MT, 250 W, 44 kHz). A predetermined amount of PVA solution was added to the MMT aqueous dispersion to prepare a 1.5 wt. % total solids MMT/PVA dispersion. The dispersion was stirred for 1 h and ultrasonicated for another hour. A predetermined amount of GA was added to the dispersion while under stirring. The mole ratio of GA to the total mole number of hydroxyl groups on the PVA chains was 1:20. HCl was added to act as the catalyst for cross-linking reaction with the mole ratio to GA being 1:5.

3.2.3 PVA/MMT nanocoating preparation

The PET film was first cleaned with deionized (DI) water and ethanol, and then dried in an oven at 60 °C. The dried PET film was adhered to the internal wall of the cylinder using a thin layer of water. Then, 30 mL of dispersion was added to the cylinder, which was spun for four full revolutions at the corresponding speed. The excessive dispersion was removed, and the film was

rotated for about 30 minutes for the film to dry with a heating lamp applied near the cylinder. The procedures are briefly illustrated in Figure 15.

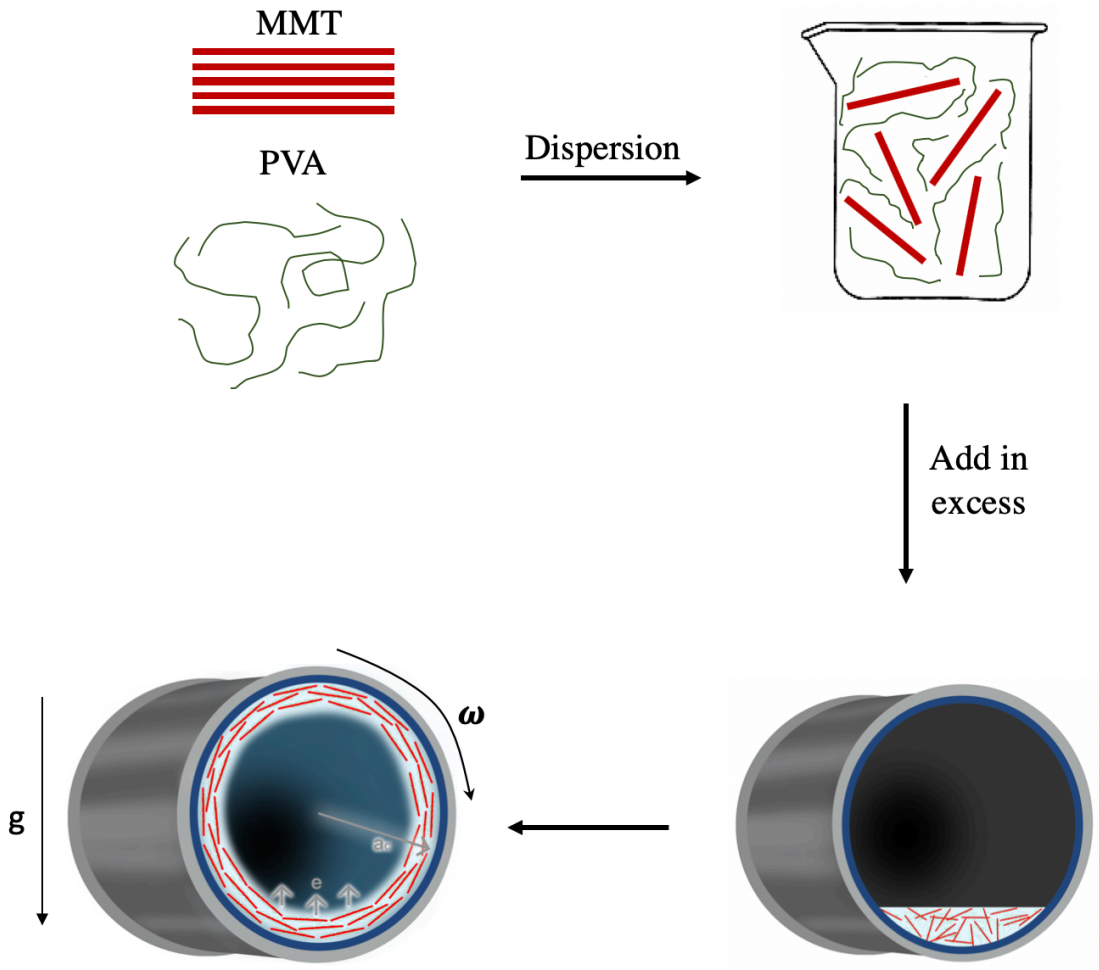

Figure 15. Schematic of the experimental procedures to fabricate nanocoatings via rotational coating.

3.3 Characterization

UV-Vis spectra of the coated PET samples were recorded using a UV-Vis spectrophotometer (Lambda 900, PerkinElmer) to determine their transparency and turbidity. Also, XRD patterns were recorded on a Bruker D2 Phaser with a LynxEye linear detector. Oxygen transmission rates (OTRs) of the coated PET films were tested on a MOCON OX-TRAN 1/50 OTR tester at 0%

relative humidity (RH) and 23 °C following ASTM D3985. Thickness of the nanocoatings was measured by using a Dektak 150 surface profiler from Veeco Instruments (Mannheim, Germany). To examine the thickness, a portion of the nanocoating was removed with a Scotch® tape.

3.4 Results and Discussion

To determine the quality of the nanocoatings an initial examination was completed by evaluating the transparency of the coated PET film. As shown in Figure 16, most of the prepared nanocoatings exhibited higher transparency than the neat substrate. Further assessment of the nanocoatings without the influence of the substrate and nanocoating thickness was completed through turbidity examination (Equation 1). In Figure 16B and Figure 17, the turbidity data are plotted, which shows an apparent reduction as a function of increasing centripetal acceleration. This further suggests that a high centripetal acceleration is beneficial for nanosheet orientation.[17, 18]

Also, it is observed that the coated PET films exhibited an even higher transmittance than the uncoated substrate, which is rarely achieved in the field. This is probably due to the very high level of nanosheet orientation (as supported by the presence of the Fabry-Pérot pattern[19, 20]) and the anti-reflective properties (due to the refractive index of the materials[21, 22]) of the coating.

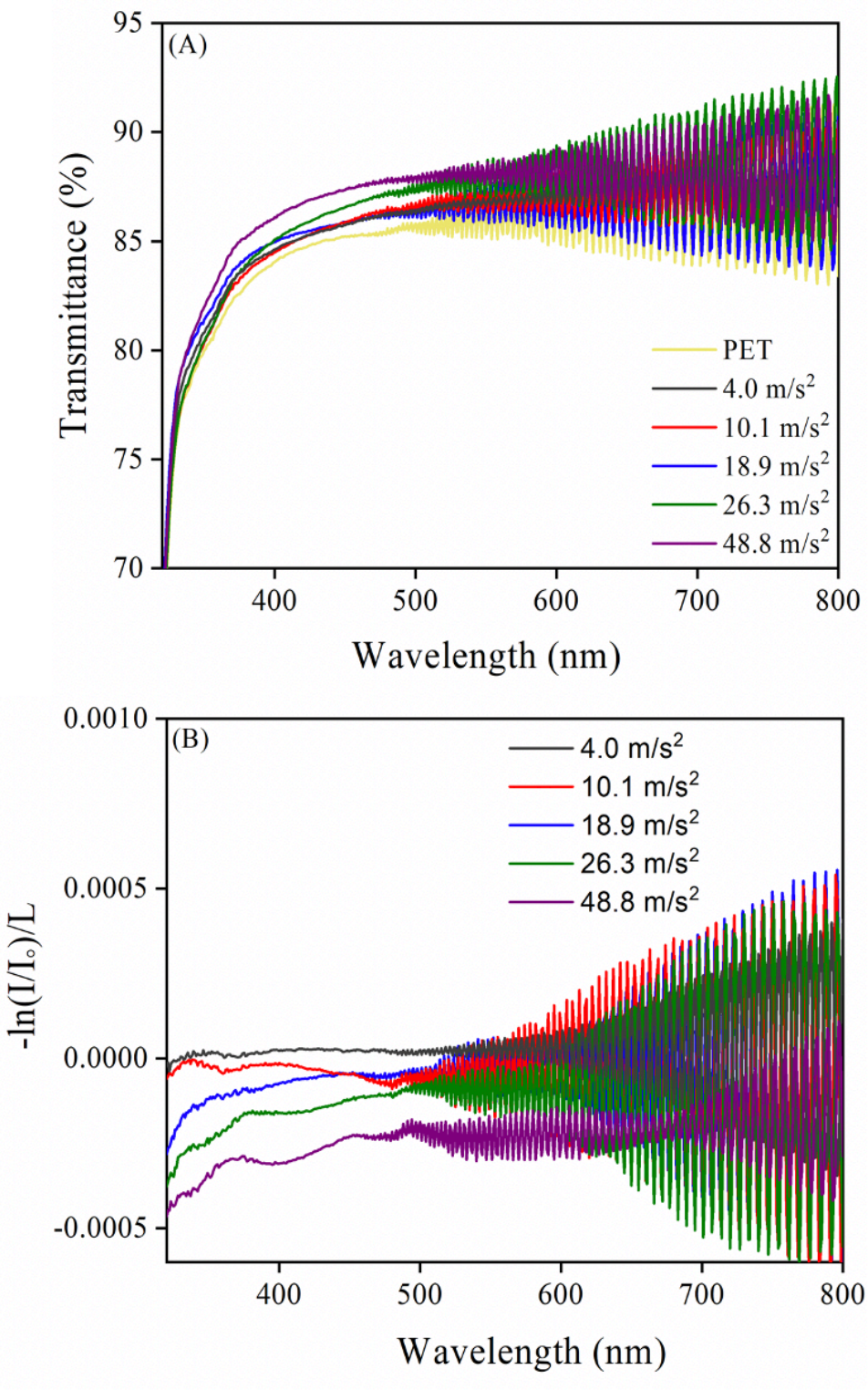

Figure 16. (A) Transmittance of the coated PET films and (b) turbidity of the PVA/MMT nanocoatings prepared at various centripetal accelerations.

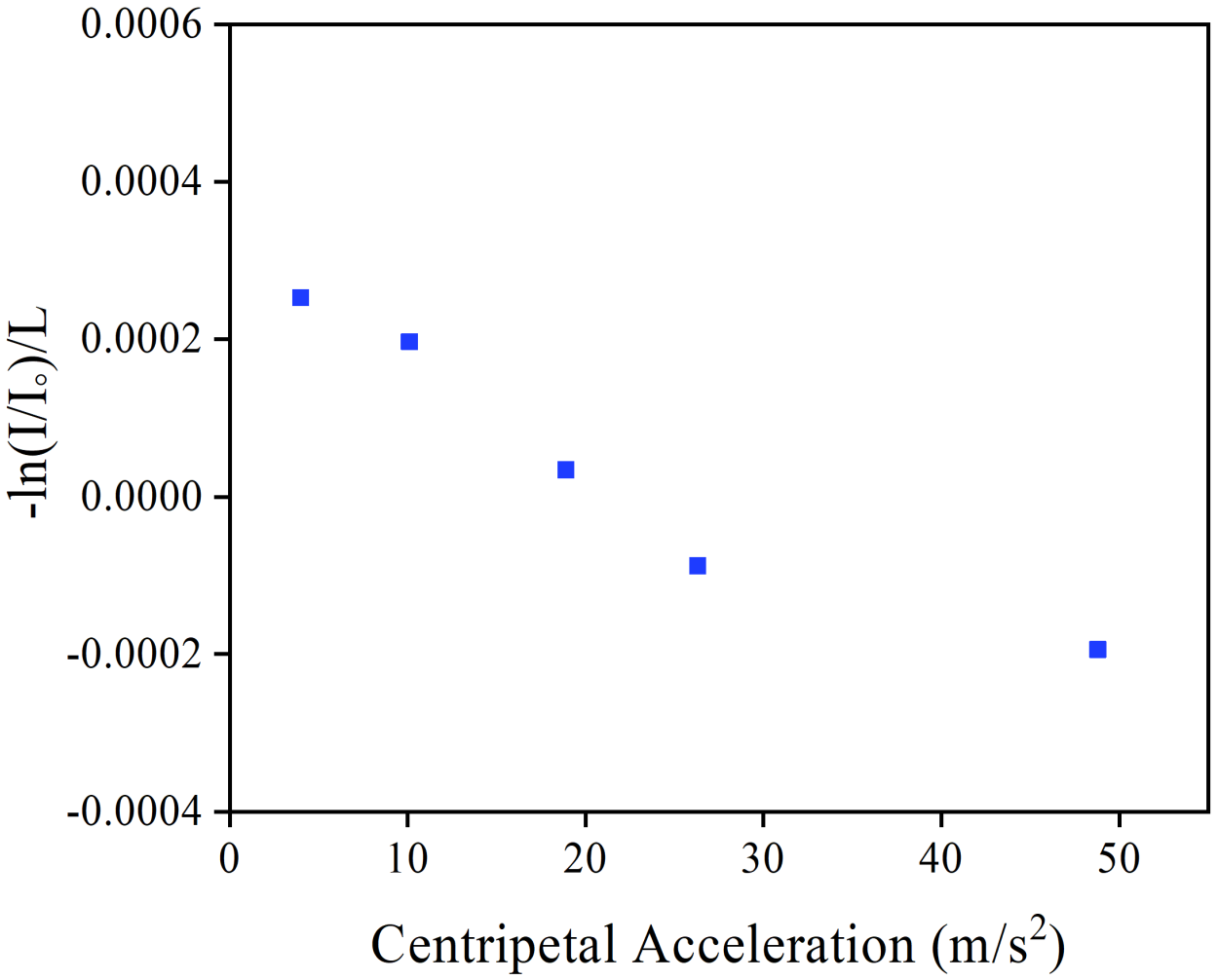

Figure 17. Turbidity at 400 nm of the PVA/MMT nanocoatings prepared at various centripetal accelerations.

To examine further the orientation of the nanosheets, XRD characterization was carried out. Figure 18 depicts the XRD patterns of the coated PET films at various centripetal accelerations. All the diffraction peaks are at virtually the same 2θ position of 2.86°, corresponding to an interlayer distance of 30.8 Å of the formed layered structure. This result is expected, as the interlayer distance is mainly determined by the ratio of MMT and PVA binder, which was maintained constant in this project. A slight increase in basal diffraction peak intensity is observed when the centripetal acceleration increases, which is consistent with the turbidity result. The

increased peak intensity is attributed to a high level of orientation of MMT nanosheets because of the higher centripetal acceleration, which helped to align better the nanosheets.

Even though both the transmittance and XRD results are consistent and expected, they only examined a specific and tiny region of the film. To assess better the overall alignment of the MMT nanosheets in the formed nanocoatings, gas barrier properties were examined, which tests a much larger nanocoating area than UV-Vis and XRD, and thus is more reliable and able to show the overall level of nanosheet orientation. Since barrier properties are dependent on both nanocoating material and microstructure, instead of choosing water vapor permeability that is highly dependent on the coating material hydrophobicity, we chose to test oxygen permeability of the nanocoatings as oxygen has no specific affinity with any coating component here.[3] The tested oxygen transmission rates of the coated PET films are listed in Table 2. To account for thickness and the substrate, the oxygen permeability was calculated (Table 2 and Figure 19) using Equation 2. As shown in Figure 19, the oxygen permeabilities of the nanocoatings significantly decrease with an increase in centripetal acceleration. This result, highly consistent with the turbidity and XRD characterization data, further confirms that an increase in centripetal acceleration improves the orientation of the nanosheets in the formed nanocoatings.

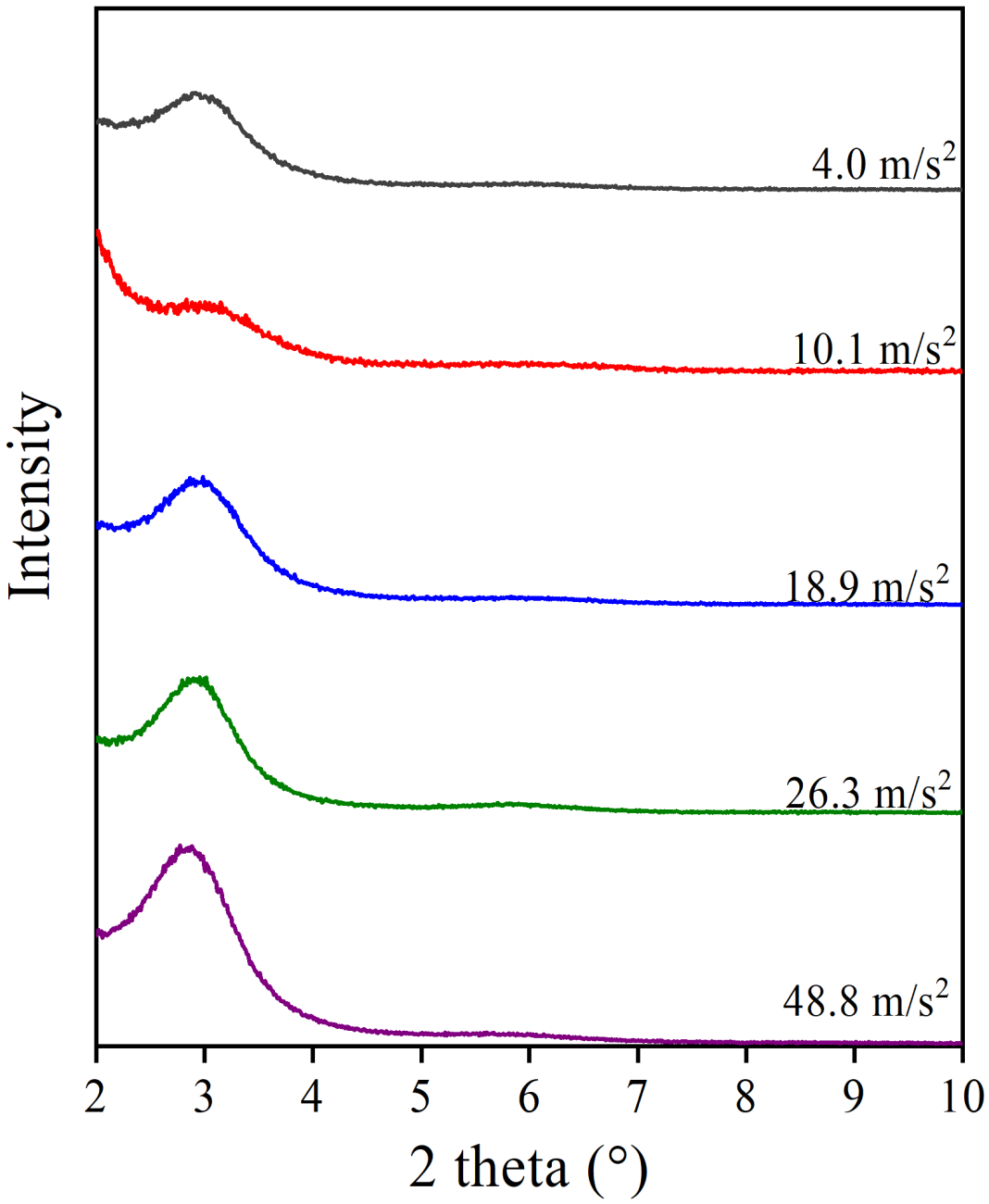

Figure 18. XRD patterns of the coated PET films at various centripetal accelerations.

Table 2. Barrier properties of the coated PET films at various centripetal accelerations.

Centripetal Acceleration (m/s^2)	Thickness (nm)	OTR [cm^3/m^2•day• atm]	O2 Permeability of coated film in total [$10^{-16}cm^3$(STP)cm/cm^2•s• Pa]	O2 Permeability of coating layer [10-$^{16}cm^3$(STP)cm/cm^2•s• Pa]
48.8	112 ± 26	1.6	0.44	0.0021
26.3	114 ± 10	2.2	0.61	0.0030
18.9	118 ± 8	2.6	0.73	0.0038
10.1	123 ± 10	3.0	0.82	0.0044
4.0	123 ± 23	5.1	1.41	0.0079

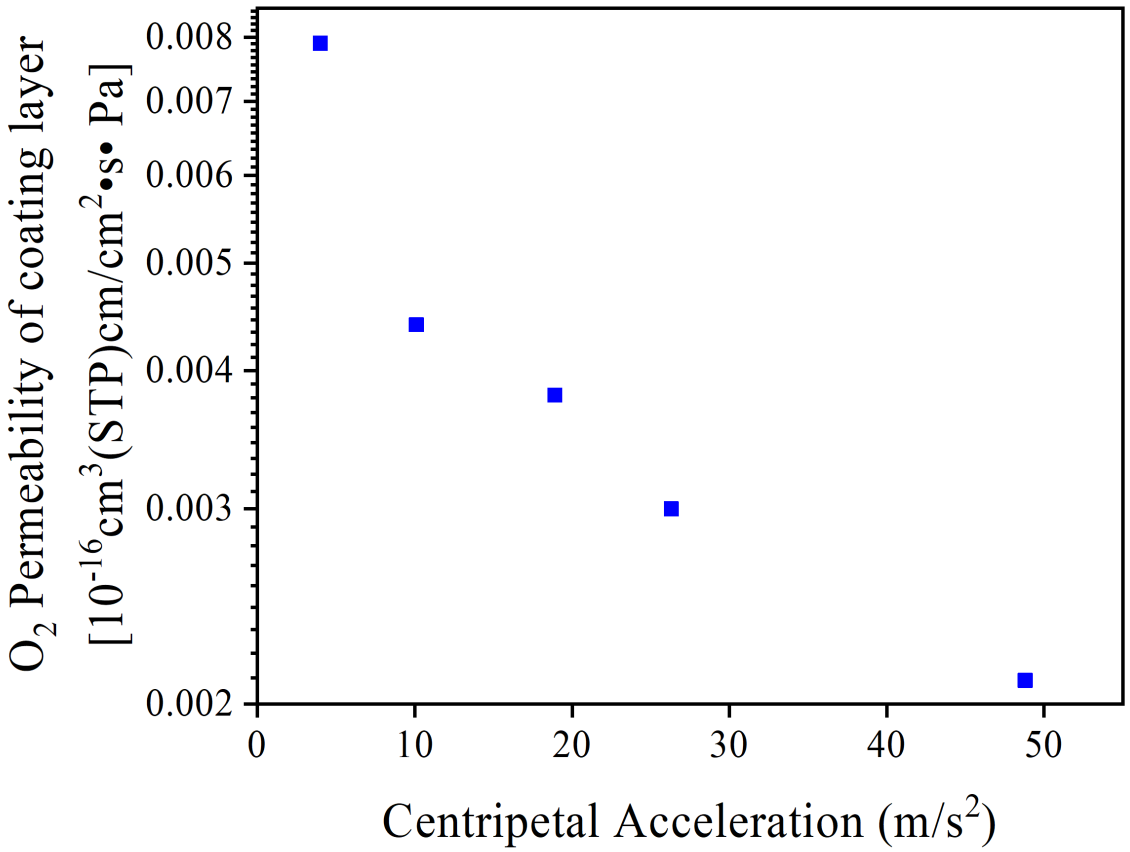

Figure 19. Permeability of the formed nanocoatings at various centripetal accelerations.

3.5 Conclusion

Rotational coating has proven to be an effective method to prepare PVA/MMT nanocoatings, as well as for the investigation of the mechanism of nanosheet orientation. Our results have consistently shown that a higher centripetal acceleration force is beneficial to align and compress the MMT nanosheets to fabricate nanocoatings with high barrier properties. Further work is needed to examine the effect of dispersion viscosity and further increasing the centripetal acceleration to determine if the current trend will continue. Meanwhile, the current rotational coating reported in this chapter is carried out as a batch operation. It is necessary to revise it to be incorporated into a continuous coating line for potential mass production.

References

1. Ebina, T.; Mizukami, F., Flexible Transparent Clay Films with Heat-Resistant and High Gas-Barrier Properties. *Advanced Materials* **2007,** *19* (18), 2450-2453.

2. Chen, H.; Müller, M. B.; Gilmore, K. J.; Wallace, G. G.; Li, D., Mechanically Strong, Electrically Conductive, and Biocompatible Graphene Paper. *Advanced Materials* **2008,** *20* (18), 3557-3561.

3. Ding, F.; Liu, J.; Zeng, S.; Xia, Y.; Wells, K. M.; Nieh, M.-P.; Sun, L., Biomimetic nanocoatings with exceptional mechanical, barrier, and flame-retardant properties from large-scale one-stemp coassembly. *Science Advances* **2017,** *3*.

4. Priolo, M. A.; Holder, K. M.; Greenlee, S. M.; Stevens, B. E.; Grunlan, J. C., Precisely Tuning the Clay Spacing in Nanobrick Wall Gas Barrier Thin Films. *Chemistry of Materials* **2013,** *25* (9), 1649-1655.

5. Chang, S.; Slopek, R. P.; Condon, B.; Grunlan, J. C., Surface Coating for Flame-Retardant Behavior of Cotton Fabric Using a Continuous Layer-by-Layer Process. *Industrial & Engineering Chemistry Research* **2014,** *53* (10), 3805-3812.

6. Mateos, A. J.; Cain, A. A.; Grunlan, J. C., Large-Scale Continuous Immersion System for Layer-by-Layer Deposition of Flame Retardant and Conductive Nanocoatings on Fabric. *Industrial & Engineering Chemistry Research* **2014,** *53* (15), 6409-6416.

7. Srivastava, S.; Kotov, N. A., Composite Layer-by-Layer (LbL) Assembly with Inorganic Nanoparticles and Nanowires. *Accounts of Chemical Research* **2008,** *41*, 1831-1841.

8. Liang, S.; Neisius, N. M.; Gaan, S., Recent developments in flame retardant polymeric coatings. *Progress in Organic Coatings* **2013,** *76* (11), 1642-1665.

9. Wong, M.; Ishige, R.; White, K. L.; Li, P.; Kim, D.; Krishnamoorti, R.; Gunther, R.; Higuchi, T.; Jinnai, H.; Takahara, A.; Nishimura, R.; Sue, H. J., Large-scale self-assembled zirconium phosphate smectic layers via a simple spray-coating process. *Nat Commun* **2014,** *5*, 3589.

10. Walther, A.; Bjurhager, I.; Malho, J. M.; Pere, J.; Ruokolainen, J.; Berglund, L. A.; Ikkala, O., Large-area, lightweight and thick biomimetic composites with superior material properties via fast, economic, and green pathways. *Nano Lett* **2010,** *10* (8), 2742-8.

11. Priolo, M. A.; Holder, K. M.; Gamboa, D.; Grunlan, J. C., Influence of clay concentration on the gas barrier of clay-polymer nanobrick wall thin film assemblies. *Langmuir* **2011,** *27* (19), 12106-14.

12. Marsh, K.; Bugusu, B., Food packaging--roles, materials, and environmental issues. *J Food Sci* **2007,** *72* (3), R39-55.

13. Aziz, F.; Ismail, A. F., Spray coating methods for polymer solar cells fabrication: A review. *Materials Science in Semiconductor Processing* **2015,** *39*, 416-425.

14. Gans, A.; Dressaire, E.; Colnet, B.; Saingier, G.; Bazant, M. Z.; Sauret, A., Dip-coating of suspensions. *Soft Matter* **2019,** *15* (2), 252-261.

15. Bindini, E.; Naudin, G.; Faustini, M.; Grosso, D.; Boissière, C., Critical Role of the Atmosphere in Dip-Coating Process. *The Journal of Physical Chemistry C* **2017,** *121* (27), 14572-14580.

16. Podsiadlo, P.; Kaushik, A. K.; Arruda, e. M.; Waas, A. M.; Shim, b. S.; Xu, J.; Nandivada, H.; Pumplin, B. G.; Lahann, J.; Ramamoorthy, A.; Kotov, N. A., Ultrastrong and Stiff Layered Polymer Nanocomposites. *Science* **2007,** *318* (59847), 80-8.

17. J., F.; Winnik, M. A., Polymer Blend Latex Films: Morphology and Transparency. *Macromolecules* **1995,** *28*, 7671-7682.

18. Santilli, C. V.; Pulcinelli, S. H.; Tokumoto, M. S.; Briois, V., In situ UV–vis and EXAFS studies of ZnO quantum-sized nanocrystals and Zn-HDS formations from sol–gel route. *Journal of the European Ceramic Society* **2007,** *27* (13-15), 3691-3695.

19. Mamedov, A.; Ostrander, J.; Aliev, F.; Kotov, N. A., Stratified Assemblies of Magnetite Nanoparticles and Montmorillonite Prepared by the Layer-by-Layer Assembly. *Langmuir* **2000,** *16* (16), 3941-3949.

20. Guan, Y.; Yang, S.; Zhang, Y.; Xu, J.; Han, C. C.; Kotov, N. A., Fabry-Perot Fringes and Their Application To Study the Film Growth, Chain Rearrangement, and Erosion of Hydrogen-Bonded PVPON/PAA Films. *J. Phys. Chem. B* **2006,** *110* (13484-13490).

21. Hattori, H., Anti-Reflection Surface with Particle Coating Deposited by Electrostatic Attraction. *Advanced Materials* **2001,** *1*, 51-54.

22. Hiller, J.; Mendelsohn, J. D.; Rubner, M. F., Reversibly erasable nanoporous anti-reflection coatings from polyelectrolyte multilayers. *Nat Mater* **2002,** *1* (1), 59-63.

Chapter 4. **Sustainable multifunctional nanocoatings from one-step coassembly**

4.1 Introduction

The increasing sustainability requirements for food packaging have set higher demands to use degradable polymers.[1-3] To improve degradability, polylactic acid (PLA) can serve an ideal candidate for food packaging, but it has poor barrier properties.[4] Improvement of barrier properties in PLA traditionally is completed through metallization.[5-7] However, metallization has a high cost and is not beneficial for sustainability.[6]

From previous work, polyvinyl alcohol/montmorillonite (PVA/MMT) nanocoatings have proven to effectively improve the barrier properties of coated plastic films, which are ideal for food packaging applications.[4] To improve sustainability, it would be ideal to replace PVA with a bio-derived polymer that is also biodegradable. Chitosan (CH) could be an ideal candidate for this application since it is both bio-derived and bio-degradable.[8, 9] Chitosan is an amino polysaccharide biopolymer that is derived from chitin, which is readily available from food waste or nature.[10, 11] Also, chitosan can add extra benefits, particularly for food packaging, because it is known to be antimicrobial, so it can prevent the growth of bacteria, fungus, and yeast.[3, 12-14]

This study aims to fabricate CH/MMT nanocoatings to improve the barrier properties and antimicrobial performance of PLA films for food packaging applications. Considering the poor processability of chitosan, a mixture of CH and PVA was used as the organic components to prepare nanocoatings. The one-step coassembly method will still be adopted to prepare the nanocoatings due to its high versatility and scalability. The goal is to prepare ecofriendly

nanocoatings with high barrier properties and antimicrobial performance for potential food packaging applications.

4.2 Experimental

4.2.1 Materials

PVA [Mowiol 8-88; M_w (weight average molecular weight): 67,000, 86.7 to 88.7 mole percent hydrolysis; Kuraray)], sodium montmorillonite (PGN nanoclay, Minerals Technologies Inc., USA), chitosan (85% deacetylated; Alfa Aesar), and HCl (37%; Sigma-Aldrich) were used as received without further purification. PLA films were obtained from BI-AX International Inc. (Tiverton Ontario, Canada) with a thickness of 20 μm.

4.2.2 Preparation of CH/PVA/MMT dispersions

PVA was dissolved in deionized (DI) water with the assistance of stirring and heating at 90 °C. A 2.0 wt. % chitosan solution was prepared by dissolving chitosan in a 2.0 wt. % solution of acetic acid at 50 °C for three hours and allowing it to stir for 24 hours. MMT was uniformly dispersed in DI water for one hour with the assistance of stirring followed by one hour of ultrasonication (ultrasonication bath; Branson 8510R-MT, 250 W, 44 kHz). Predetermined amounts of PVA and CH solutions were added to the MMT aqueous dispersion to prepare dispersions containing 0.5, 1.0, and 1.5 wt. % total solids (MMT+PVA+CH). The dispersion was stirred for one hour and ultrasonicated for another hour. A small amount of GA was added to the dispersion while under stirring. The mole ratio of GA to the total mole number of hydroxyl groups on the PVA and CH chains was 1:20. HCl was added to act as the catalyst for cross-linking reaction with the mole ratio to GA being 1:5.

4.2.3 Preparation of nanocoatings on PLA Films

The PLA films with dimensions of 15 × 20 cm were cleaned with DI water and subsequently dried in an oven at 60 °C for 30 minutes. The cleaning process of the films was repeated with ethanol. To facilely coat the films, they were dipped into the above aqueous dispersions and then vertically hung in an oven to be dried and cross-linked at 60 °C. The coating process was repeated four times, and to maintain an even coating thickness, the films were rotated 180° before every cycle. The compositions of the dispersions used to prepare the nanocoatings on the PLA substrates are listed in Table 3.

Table 3. Compositions of the dispersions to prepare nanocoatings on PLA films.

Sample	Composition of solids (CH+PVA+MMT)			Concentration of total solids in dispersions (wt. %)
	CH/total solids (wt. %)	PVA/total solids (wt. %)	MMT/total solids (wt. %)	
PLA- CH(3)/PVA(7)/MMT-50-1.5-C	0.225	0.525	0.750	1.5
PLA- CH(5)/PVA(5)/MMT-50-1.5-C	0.375	0.375	0.750	1.5
PLA- CH(7)/PVA(3)/MMT-50-1.5-C	0.525	0.225	0.750	1.5
PLA- CH(7)/PVA(3)/MMT-50-1.0-C	0.350	0.150	0.500	1.0
PLA- CH(7)/PVA(3)/MMT-70-0.5-C	0.105	0.045	0.350	0.5
PLA- CH(7)/PVA(3)/MMT-50-0.5-C	0.175	0.075	0.250	0.5
PLA- CH(7)/PVA(3)/MMT-30-0.5-C	0.245	0.105	0.150	0.5

4.2.4 Characterization

The nanocoatings were characterized by an ultraviolet-visible (UV-Vis) spectrophotometer (Lambada 900, Perkin Elmer) to evaluate their transparency. A Bruker D2 X-ray diffractometer with a Bragg-Brentano fixed sample geometry and a LynxEye liear detector was used to record the X-ray diffraction (XRD) patterns of the coated PLA samples.

Small angle x-ray scattering (SAXS) characterizations were conducted using a Bruker NanoStar instrument with a Turbo (rotating anode) X-ray source. A Göbel mirror and Cu K_α were used to choose a wavelength of 1.5418 Å. To collimate the beam, a pair of scatterless pinholes were used with the following diameters: 500 and 350 μm. A MikroGap VÅNTEC-2000 detector was used to collect the 2D Data. A sample-to-detector distance of 67 cm was used to cover a scattering vector, $\mathbf{q}$ [$|q| \equiv \frac{4\pi}{\lambda}\sin\left(\frac{\theta}{2}\right)$, where θ is the scattering angle], was used and ranged from 0.015 to 0.370 $Å^{-1}$. Examination of the lamellar alignment for the different samples was completed by conducting a rocking curve experiment that shows the distribution of deviation from the perfect orientation, with Bragg angle (θ_2) being equal to the angle between the incident beam and the sample (φ). This was completed by collecting 2D scattering patterns at different φ values by manually rotating the sample. The data were corrected for background and reduced to 1D data with the same sector integration completed on each φ value.

To capture the cross section of the nanocoating layers, the samples were embedded into epoxy, which was microtomed into 80 to 100 nm thin sections on a Reichert-Jung Ultracut E ultramicrotome. The sections were deposited onto a 400-mesh copper grid and imaged on an FEI Talos F200X scanning transmission electron microscope with an accelerating voltage of 120 kV.

The oxygen transmission rates (OTRs) of the coated samples were tested on a MOCON (Minneapolis, MN) OX-TRAN 1/50 OTR tester at 23 °C and 0% RH following the ASTM D3985

standard method. The thicknesses of the nanocoatings were obtained by first removing a portion of the coating from the substrate with a Scotch® tape and then using a surface profiler [Dektak 150, Veeco Instruments (Mannheim, Germany)]. The antimicrobial properties of the coated films were examined using an anti-biofilm test. 1 × 1 cm films were placed in separate wells and inoculated with Pseudomonas aeruginosa using glass coverslips for control. The biofilms were allowed to grow for 36 h, rinsed with buffer, and sonicated to disperse bacteria. Then dilutions of the bacteria were plated on solid media, and the colonies were examined.

4.3 Results and Discussion

CH showed poor film formability during our preliminary exploration; it failed to form CH/MMT nanocoatings through one-step coassembly. To improve the film formability of the dispersions, PVA was mixed with CH since the former possesses a very high film formability, has a high compatibility with CH because they both contain hydroxyl groups, and is cost-effective. Figure 20 illustrates the experimental procedures to fabricate CH/PVA/MMT nanocoatings on PLA films using dip coating to achieve a highly ordered layered structure.[15, 16] MMT, in an aqueous dispersion, is exfoliated into individual single-layer nanosheets under sonication.[4, 17, 18] This allows PVA and CH to attach to the surface of MMT nanosheets due to the weak hydrogen bonding and van der Waals force interactions.[16]

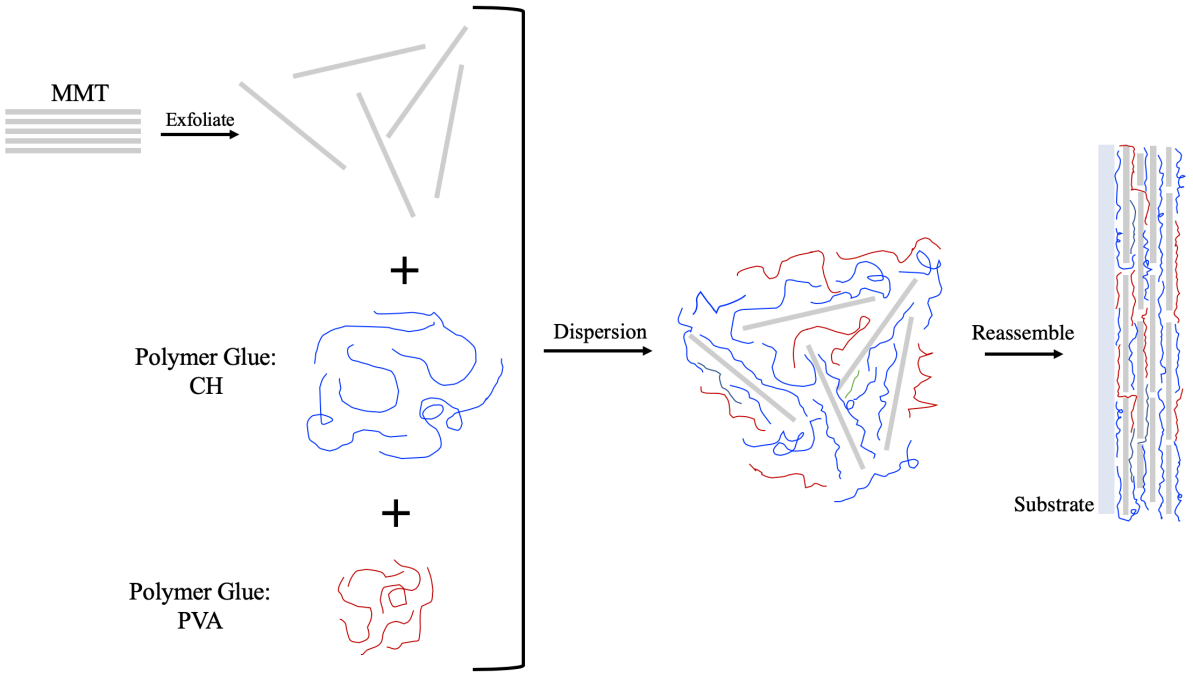

Figure 20. Schematic of the fabrication of CH/PVA/MMT nanocoatings via one-step coassembly.

Overall, the coated PLA films maintained high transparency, but transparency reduction was observed when higher concentrations of MMT were used in the nanocoatings (Figure 21). The high transparency of the coated PLA films suggested that a highly ordered structure was achieved in the formed nanocoatings. The orientation of the nanosheets was also indicated by the presence of the Fabry-Pérot pattern in the UV-Vis spectra.[16, 19] The UV-Vis characterization allows for an initial examination of the orientation of the MMT nanosheets, which is the most critical factor in the quality of the formed nanocoatings. To further assess the orientation, XRD, TEM, and SAXS were utilized.

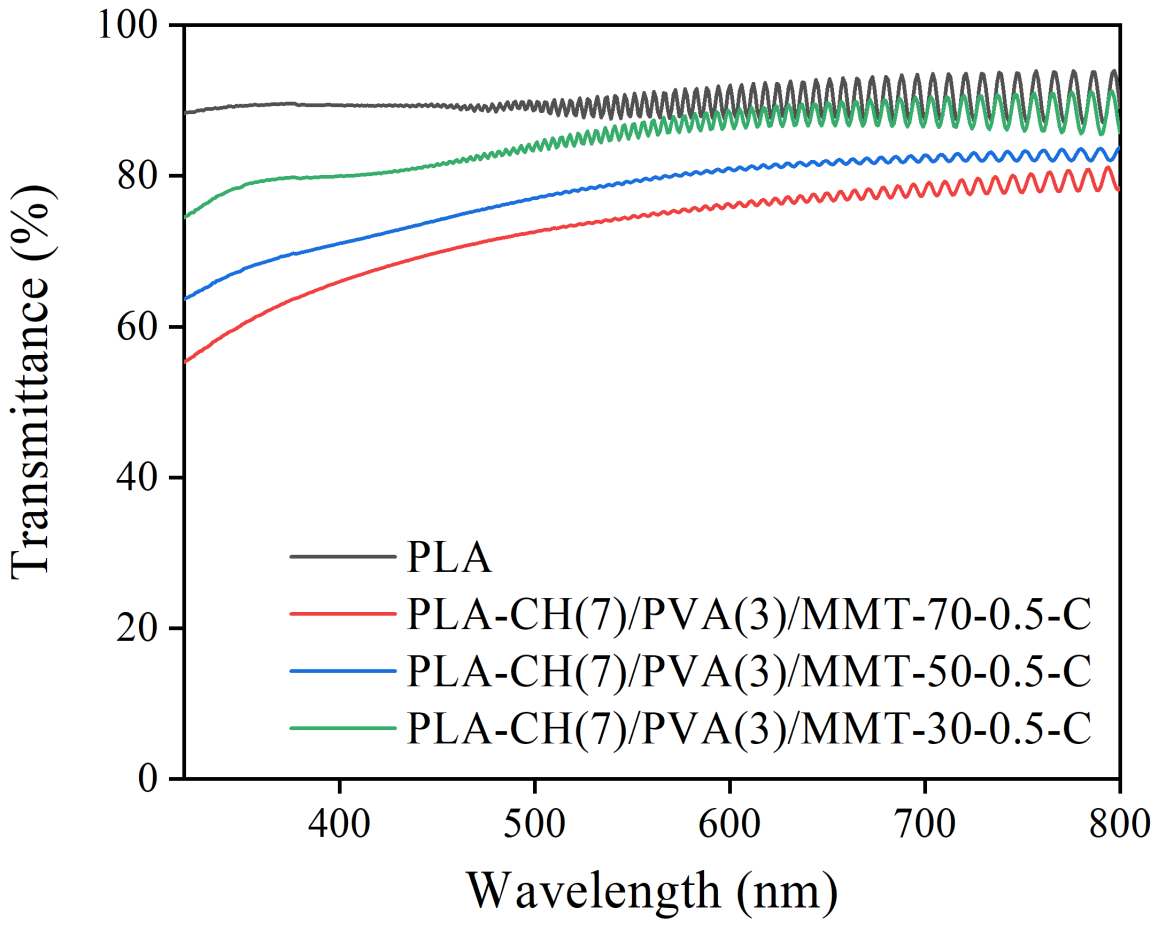

Figure 21. UV-Vis spectra of the coated PLA films.

Further confirmation of MMT nanosheets' high level of orientation was established through XRD. In the XRD patterns shown in Figure 22, basal diffraction peaks were observed for the nanocoatings, with the one containing 50 wt. % of MMT the most intensive, 70 wt. % second, and 30 wt. % the lowest. This is because, at a lower concentration, the MMT nanosheets can have more space to rotate during and after the initial flow-induced orientation process.[20-22] On the other end, too high a concentration of MMT nanosheets will lead to significantly enhanced viscosity, which will decrease the ability for the nanosheets to rotate and align and thus not beneficial for orientation either.[22] Our experimental results showed that at 70 wt. %, MMT nanosheets can still form an ordered structure, but at an even higher concentration, significant structural deterioration

was observed. As such, the nanocoatings with higher concentrations of MMT were not prepared in this project.

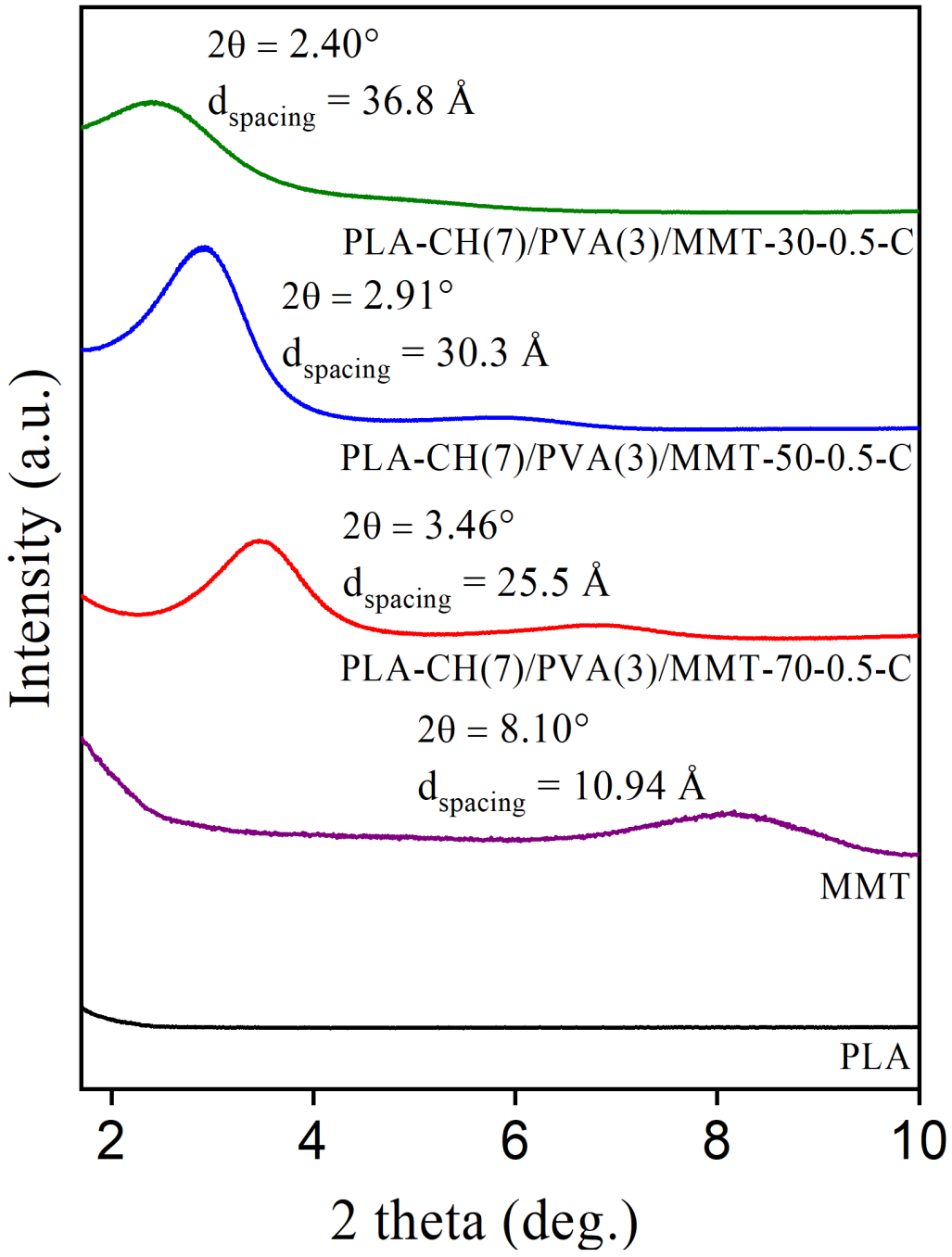

Figure 22. XRD patterns of the coated PLA films and MMT control.

Even though XRD gives an initial examination of the layered structure of the formed nanocoatings, a closer inspection was completed through TEM imagining. Figure 23 depicts the cross-sectional images of the formed nanocoatings, and the results are consistent with the XRD patterns. In Figure 23A, it is observed that the MMT nanosheets in CH(7)/PVA(3)/MMT-30-0.5-C nanocoating are not well aligned. This inconsistency in structure could be attributed to the fact that MMT nanosheets have space to rotate during drying at a relatively low concentration. But in Figure 23B, a well-aligned structure can be observed for CH(7)/PVA(3)/MMT-50-0.5-C, which could be attributed to the MMTs not having enough space to rotate during the drying process. For CH(7)/PVA(3)/MMT-70-0.5-C in Figure 23C, a rather high level of alignment of the MMT nanosheets is observed. However, the overall uniformity is not as high as that of CH(7)/PVA(3)/MMT-50-0.5-C, which is probably because of the high viscosity resulting from the very high MMT concentration, which prevents the MMT nanosheets from aligning perfectly during flow induced orientation. This phenomenon will be further discussed in the SAXS characterization below.

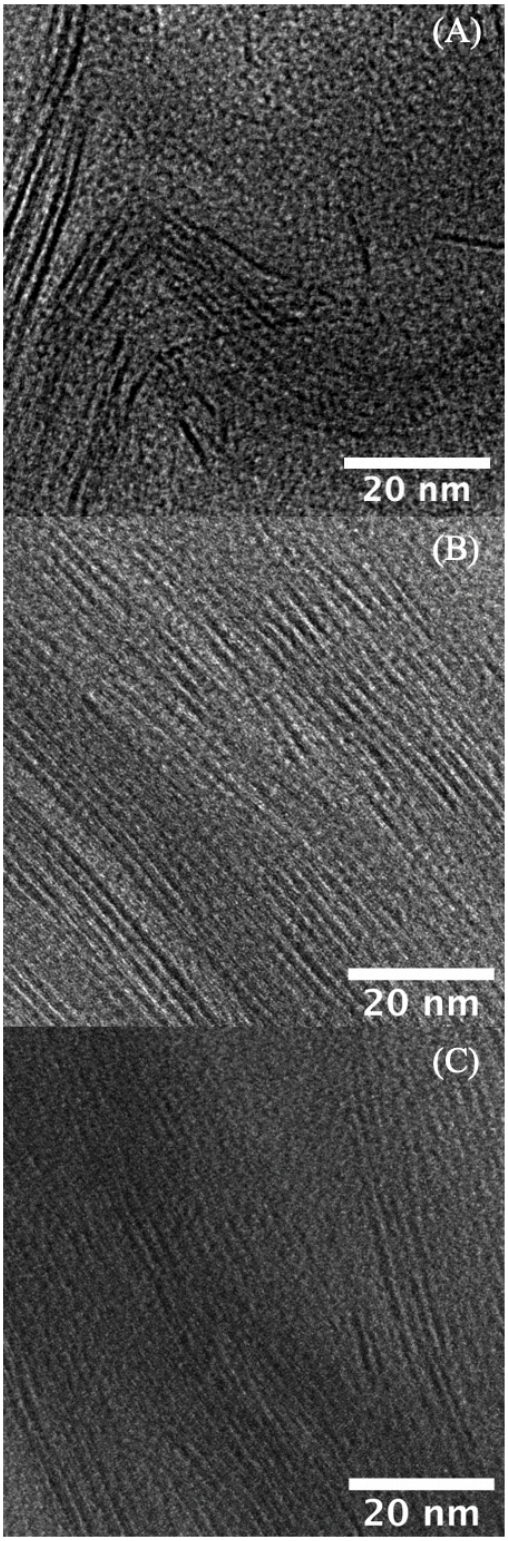

Figure 23. TEM images of the cross section of the nanocoatings. (A) CH(7)/PVA(C)/MMT-30-0.5-C, (B) CH(7)/PVA(C)/MMT-50-0.5-C, and (C) CH(7)/PVA(C)/MMT-70-0.5-C.

Since TEM only covers a small region, SAXS was used to examine the quality of the nanocoating structure statistically. Figure 24 shows the 2D SAXS patterns of the coated samples. For all samples, the intensity of the signal decreases as it is moved closer to φ = 90° (the sample being perpendicular to the beam), but sample CH(3)/PVA(7)/MMT-50-0.5-C shows the highest intensity and strongest signal throughout φ. Statistical examination of the patterns was completed to determine the uniformity throughout the coating. 1D SAXS patterns are shown in Figure 25 for the three coated samples with the background normalized by the collected data. At φ = 90°, the sample is perpendicular to the beam, and the pattern will show no alignment, but as the sample moves towards the Bragg's angle, the intensity at θ_B increases. By plotting the intensity of $2\theta_B$ as a function of φ, examination of the alignment was possible. To do this, the data were fitted with the Gaussian distribution:

$$f(x) = \frac{1}{\sigma\sqrt{2\pi}} e^{-(x-\mu)^2/2\sigma^2} \qquad \text{Equation 3}$$

where μ is the mean and σ^2 is the variance. The full width half max (FWHM) can be obtained by the following equation:

$$FWHM = 2\sigma\sqrt{2\ln 2} \qquad \text{Equation 4}$$

The FWHMs from the fitting of CH(3)/PVA(7)/MMT-50-0.5-C, CH(7)/PVA(3)/MMT-30-0.5-C, and CH(3)/PVA(7)/MMT-70-0.5-C are 10.44° ± 0.08°, 11.00° ± 0.30°, and 12.03° ± 0.06°, respectively. This indicates that the orientation in CH(3)/PVA(7)/MMT-50-0.5-C is the highest, which is consistent with both the XRD and TEM characterization results.

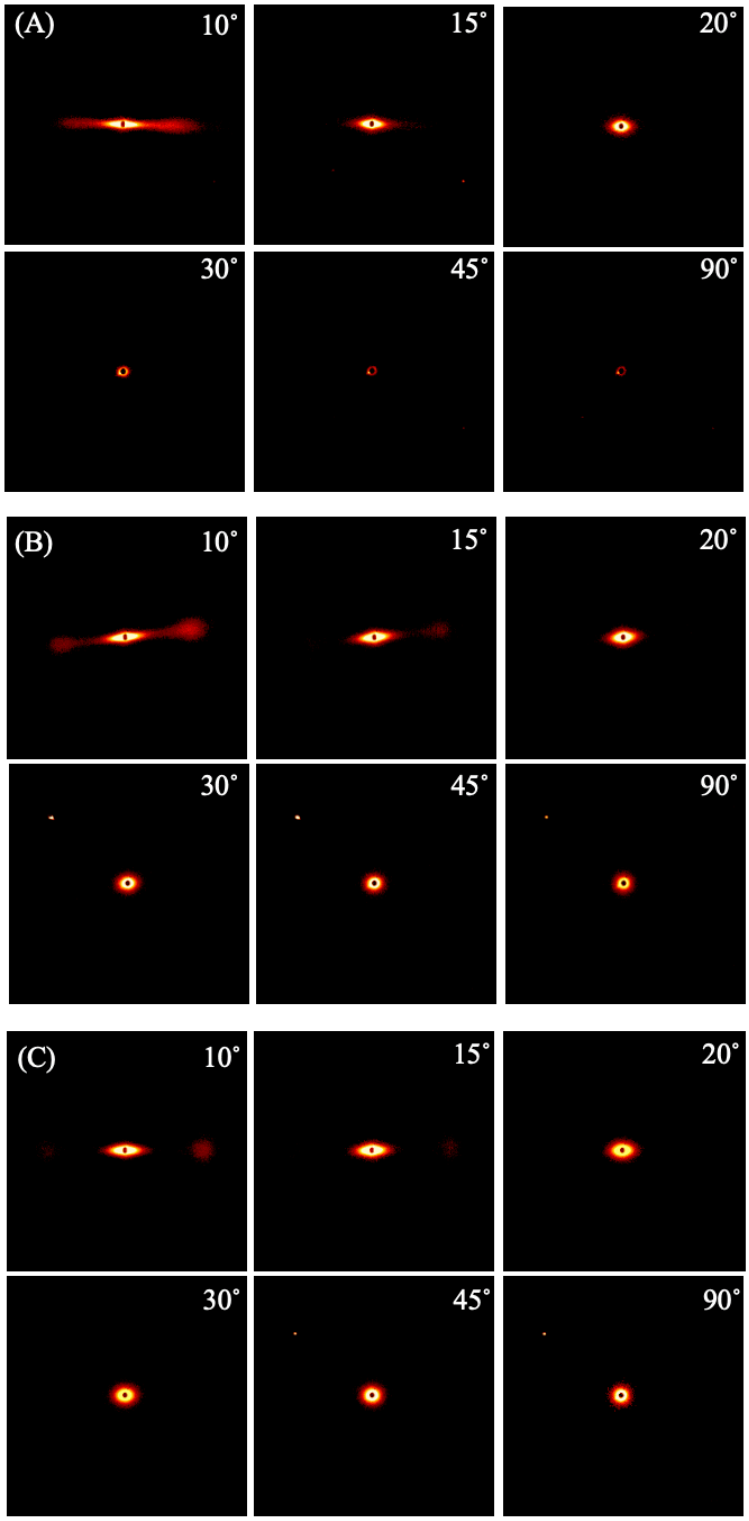

Figure 24. 2D SAXS patterns of (A) CH(7)/PVA(3)/MMT-30-0.5-C, (B) CH(7)/PVA(3)/MMT-50-0.5-C, (C) CH(7)/PVA(3)/MMT-70-0.5-C samples at various φ.

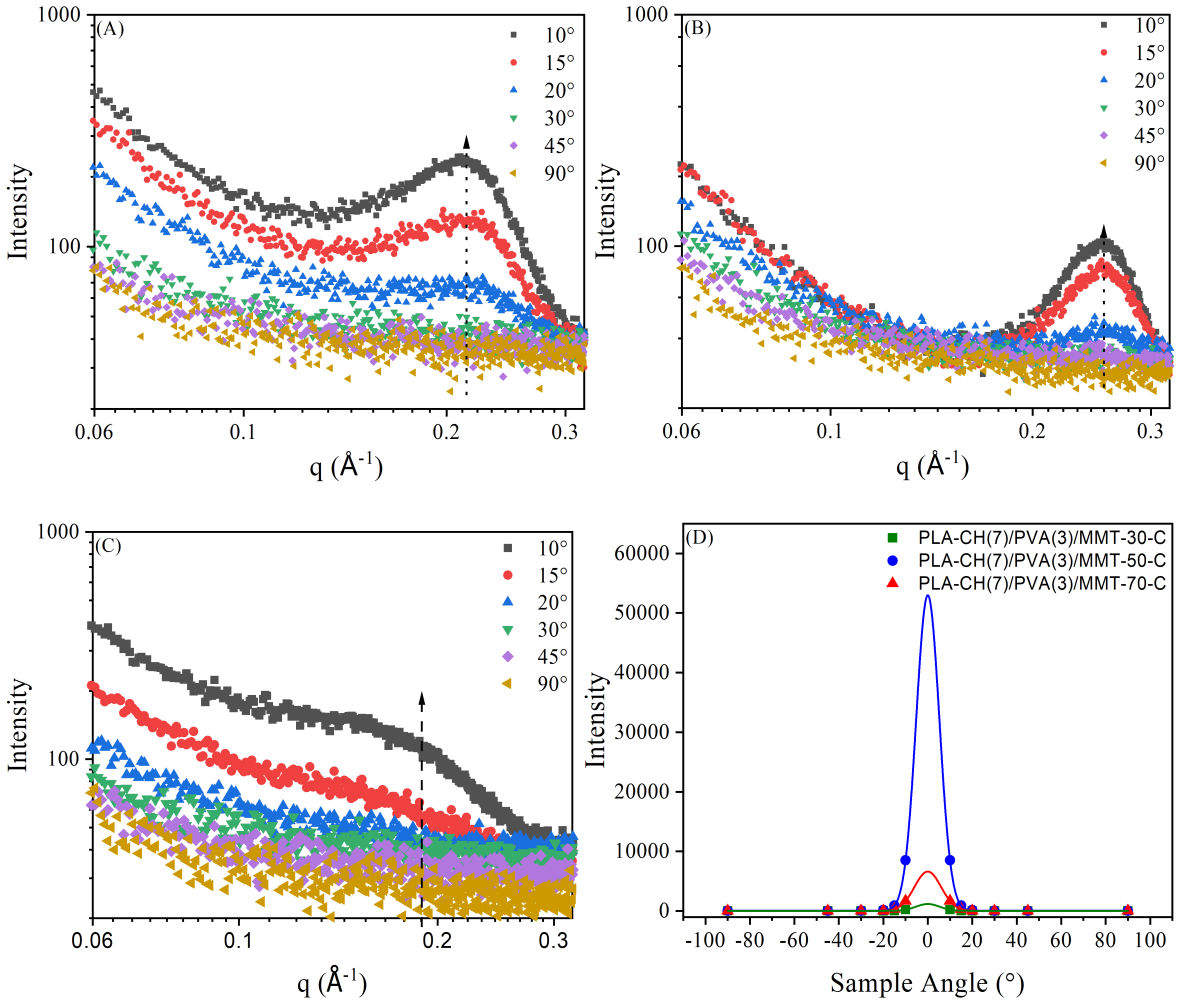

Figure 25. SAXS patterns of the formed nanocoatings. (A) CH(7)/PVA(3)/MMT-50-0.5-C, (B) CH(7)/PVA(3)/MMT-70-0.5-C, (C) CH(7)/PVA(3)/MMT-30-0.5-C, and (D) scattering intensity as a function of incident beam to the sample angle with the solid line representing the Gaussian fit. The R^2 values from the fitting for CH(7)/PVA(3)/MMT-50-0.5-C, CH(7)/PVA(3)/MMT-30-0.5-C, and CH(7)/PVA(3)/MMT-70-0.5-C are 0.9998, 0.9980, and 0.9999, respectively.

To evaluate various factors that affect the morphology and microstructure of the formed nanocoatings, total solids concentration and ratio of CH/PVA was varied. The total dispersion concentration (CH+PVA+MMT) in the dispersion was increased from 0.5 wt. % to 1.0 and 1.5 wt. %, and the ratio of CH/PVA was changed from 7:3 to 5:5 and 3:7. The OTRs of the above coated samples were tested and summarized in Table 4. Overall, the barrier properties of the PLA films

(Table 4) were significantly improved after coating as a result of the highly packed MMT nanosheets and their high level of orientation. The uncoated PLA film has an OTR of 1205.0 mL/(m^2·day) but decreases to 0.1 mL/(m^2·day) for PLA-CH(7)/PVA(3)/MMT-50-0.5-C. To normalize the effects from the thickness and the substrate, the permeability of the nanocoatings with different formulations were calculated (Equation 2) and are summarized in Table 4 and plotted in Figure 26. As shown in Figure 7A, when MMT concentration was increased from 30 to 50 wt. %, a significant oxygen permeability reduction was achieved. This is owning to a higher concentration of MMT nanosheets and a higher level of nanosheet orientation, leading to a more tortuous pathway and thus a lower oxygen permeability. However, when MMT nanosheet concentration was increased from 50 to 70 wt. %, the oxygen permeability increased. This suggests a less ordered structure in PLA-CH(7)/PVA(3)/MMT-70-0.5-C, as verified by the XRD, TEM, and SAXS characterizations above. Meanwhile, as shown in Figure 7B, a lower concentration of dispersion [PLA-CH(7)/PVA(3)/MMT-50-0.5-C] is beneficial for forming a more ordered structure. This can be attributed to its lower viscosity, and thus the MMT nanosheets can be better aligned during one-step coassembly.

It was also observed that at a higher CH/PVA ratio, the formed nanocoating exhibited a slightly lower permeability (Figure 26C). This could be contributed by the weak miscibility between CH and PVA, which might be partially resolved through crosslinking.[23-25] By incorporating more CH, the miscibility issue can be minimized, allowing the nanosheets to better align, and thus a higher barrier property.

Table 4. Oxygen barrier properties of the coated PLA films.

Sample	Thickness (nm)	OTR [mL/(m²·day)]	O_2 Permeability of coated film in total [10^{-16}cm³(STP)cm/cm²·s·Pa]	O_2 Permeability of coating layer [10^{-16}cm³(STP)cm/cm²·s·Pa]
PLA (20 μm)	-	1205.0	-	-
PLA-PVA-C	510 ± 26	7.4	1.73	0.0433
PLA-CH/PVA-C	877 ± 82	8.7	2.03	0.0438
PLA- CH(3)/PVA(7)/MMT-50-1.5-C	491± 25	1.1	0.26	0.00625
PLA- CH(5)/PVA(5)/MMT-50-1.5-C	524 ± 41	0.9	0.20	0.00512
PLA- CH(7)/PVA(3)/MMT-50-1.5-C	491 ± 26	0.6	0.15	0.00346
PLA- CH(7)/PVA(3)/MMT-50-1.0-C	276 ± 18	0.8	0.17	0.00232
PLA- CH(7)/PVA(3)/MMT-70-0.5-C	328 ± 14	0.2	0.04	0.00065
PLA- CH(7)/PVA(3)/MMT-50-0.5-C	318 ± 12	0.1	0.02	0.00031
PLA- CH(7)/PVA(3)/MMT-30-0.5-C	311 ± 6	0.2	0.05	0.00077

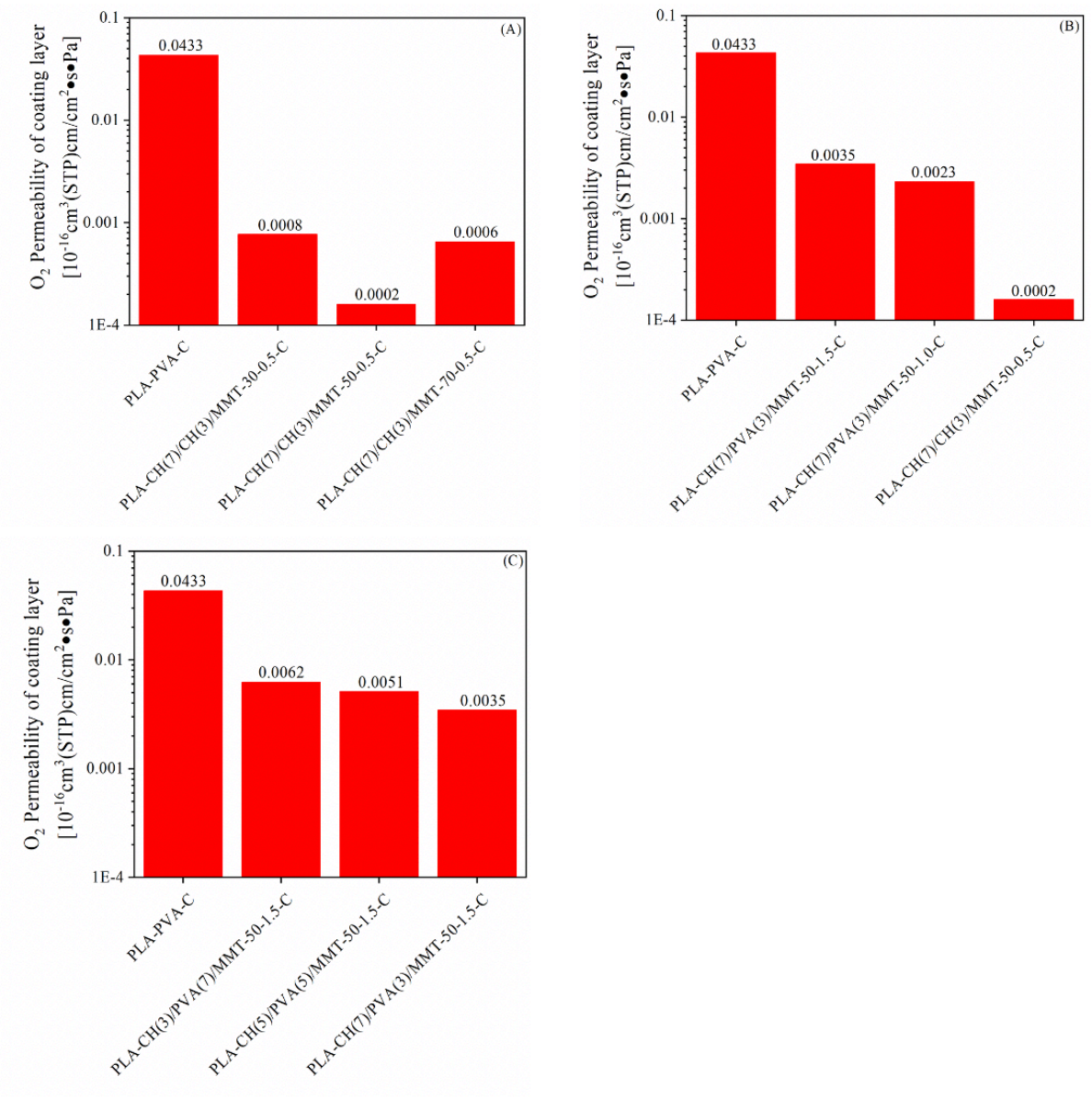

Figure 26. Permeability of various nanocoatings. (A) nanocoatings with various MMT %, (B) nanocoatings with various wt. %, and (C) nanocoatings with various CH/PVA ratios.

The antimicrobial property of the nanocoatings was evaluated, and the results are shown in Figure 27. Partially replacing PVA with CH led to an improvement in the antimicrobial performance of the coated PLA films. When a lower concentration dispersion was used to make

nanocoatings on PLA films [PLA- CH(7)/PVA(3)/MMT-50-0.5-C], the coated PLA films still maintain a decent antimicrobial performance, although the coating thickness was only 328 nm (in comparison to 491 nm for PLA- CH(7)/PVA(3)/MMT-50-1.5-C). More systematic evaluations are needed to give a comprehensive assessment of the antimicrobial properties of the coated PLA films for potential food packaging applications.

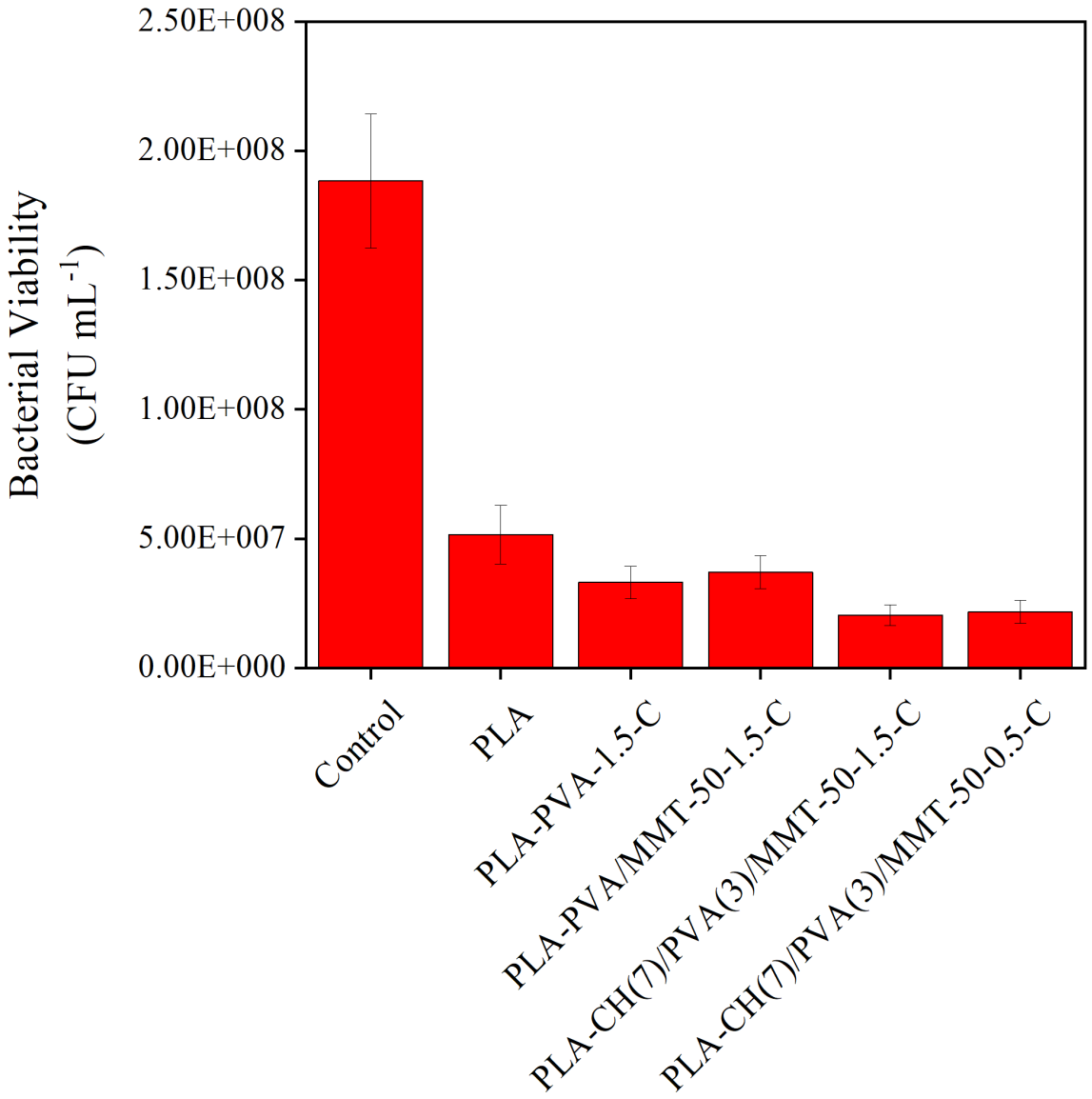

Figure 27. Bacterial viability of the coated PLA films with various formulations.

4.4 Conclusion

A facile and effective one-step coassembly process was used to form a nacre-like structure on PLA films using CH, PVA, and MMT. A highly ordered layered structure has been achieved, which led to dramatically decreased oxygen permeability relative to MMT coatings and appreciably enhanced antibacterial performance of the coated PLA films, promising for food packaging applications.

References

1. Casariego, A.; Souza, B. W. S.; Cerqueira, M. A.; Teixeira, J. A.; Cruz, L.; Díaz, R.; Vicente, A. A., Chitosan/clay films' properties as affected by biopolymer and clay micro/nanoparticles' concentrations. *Food Hydrocolloids* **2009,** *23* (7), 1895-1902.

2. Abdollahi, M.; Rezaei, M.; Farzi, G., A novel active bionanocomposite film incorporating rosemary essential oil and nanoclay into chitosan. *Journal of Food Engineering* **2012,** *111* (2), 343-350.

3. Pal, A. K.; Katiyar, V., Nanoamphiphilic Chitosan Dispersed Poly(lactic acid) Bionanocomposite Films with Improved Thermal, Mechanical, and Gas Barrier Properties. *Biomacromolecules* **2016,** *17* (8), 2603-18.

4. Ding, F.; Liu, J.; Zeng, S.; Xia, Y.; Wells, K. M.; Nieh, M.-P.; Sun, L., Biomimetic nanocoatings with exceptional mechanical, barrier, and flame-retardant properties from large-scale one-stemp coassembly. *Science Advances* **2017,** *3*.

5. Siracusa, V.; Dalla Rosa, M.; Iordanskii, A. L., Performance of Poly(lactic acid) Surface Modified Films for Food Packaging Application. *Materials (Basel)* **2017,** *10* (8).

6. Mangaraj, S.; Goswami, T. K.; Mahajan, P. V., Applications of Plastic Films for Modified Atmosphere Packaging of Fruits and Vegetables: A Review. *Food Engineering Reviews* **2009,** *1* (2), 133-158.

7. Burgess, S. K.; Kriegel, R. M.; Koros, W. J., Carbon Dioxide Sorption and Transport in Amorphous Poly(ethylene furanoate). *Macromolecules* **2015,** *48* (7), 2184-2193.

8. Liu, A.; Berglund, L. A., Clay nanopaper composites of nacre-like structure based on montmorrilonite and cellulose nanofibers—Improvements due to chitosan addition. *Carbohydrate Polymers* **2012,** *87* (1), 53-60.

9. Laufer, G.; Kirkland, C.; Cain, A. A.; Grunlan, J. C., Clay-chitosan nanobrick walls: completely renewable gas barrier and flame-retardant nanocoatings. *ACS Appl Mater Interfaces* **2012,** *4* (3), 1643-9.

10. Svagan, A. J.; Akesson, A.; Cardenas, M.; Bulut, S.; Knudsen, J. C.; Risbo, J.; Plackett, D., Transparent films based on PLA and montmorillonite with tunable oxygen barrier properties. *Biomacromolecules* **2012,** *13* (2), 397-405.

11. Wang, S.; Jing, Y., Effects of a Chitosan Coating Layer on the Surface Properties and Barrier Properties of Kraft Paper. *BioResources* **2016,** *11*, 1868-1881.

12. de Azeredo, H. M. C., Antimicrobial nanostructures in food packaging. *Trends in Food Science & Technology* **2013,** *30* (1), 56-69.

13. Tang, Y.; Hu, X.; Zhang, X.; Guo, D.; Zhang, J.; Kong, F., Chitosan/titanium dioxide nanocomposite coatings: Rheological behavior and surface application to cellulosic paper. *Carbohydr Polym* **2016,** *151*, 752-759.

14. Vasile, C.; Darie, R. N.; Cheaburu-Yilmaz, C. N.; Pricope, G.-M.; Bračič, M.; Pamfil, D.; Hitruc, G. E.; Duraccio, D., Low density polyethylene – Chitosan composites. *Composites Part B: Engineering* **2013,** *55*, 314-323.

15. Srivastava, S.; Kotov, N. A., Composite Layer-by-Layer (LbL) Assembly with Inorganic Nanoparticles and Nanowires. *Accounts of Chemical Research* **2008,** *41*, 1831-1841.

16. Podsiadlo, P.; Kaushik, A. K.; Arruda, e. M.; Waas, A. M.; Shim, b. S.; Xu, J.; Nandivada, H.; Pumplin, B. G.; Lahann, J.; Ramamoorthy, A.; Kotov, N. A., Ultrastrong and Stiff Layered Polymer Nanocomposites. *Science* **2007,** *318* (59847), 80-8.

17. Liu, J.; Boo, Q.-J.; Clearfield, A.; Sue, H.-J., Intercalation and Exfoliation: A Review on Morphology of Polymer Nanocomposites Reinforced by Inorganic Layer Structures. *Materials and Manufacturing Processes* **2006,** *20*, 143-151.

18. Pavlidou, S.; Papaspyrides, C. D., A review on polymer–layered silicate nanocomposites. *Progress in Polymer Science* **2008,** *33* (12), 1119-1198.

19. Guan, Y.; Yang, S.; Zhang, Y.; Xu, J.; Han, C. C.; Kotov, N. A., Fabry-Perot Fringes and Their Application To Study the Film Growth, Chain Rearrangement, and Erosion of Hydrogen-Bonded PVPON/PNN Films. *Journal of Physical Chemistry B* **2006,** *110*, 13484-13490.

20. Sue, H. J.; Gam, K. T., Epoxy Nanocomposties Based on the Synthetic α–Ζιρχονιυμ Πηοσπηατε Λαψερ Στρυχτυρε. *Chem. Mater.* **2004,** *16*, 242-249.

21. Sun, L.; Boo, W. J.; Clearfield, A.; Sue, H. J.; Pham, H. Q., Barrier properties of model epoxy nanocomposites. *Journal of Membrane Science* **2008,** *318* (1-2), 129-136.

22. Sun, L.; Boo, W.-J.; Liu, J.; Clearfield, A.; Sue, H.-J.; Verghese, N. E.; Pham, H. Q.; Bicerano, J., Effect of Nanoplatelets on the Rheological Behavior of Epoxy Monomers. *Macromolecular Materials and Engineering* **2009,** *294* (2), 103-113.

23. Costa-Júnior, E. S.; Barbosa-Stancioli, E. F.; Mansur, A. A. P.; Vasconcelos, W. L.; Mansur, H. S., Preparation and characterization of chitosan/poly(vinyl alcohol) chemically crosslinked blends for biomedical applications. *Carbohydrate Polymers* **2009,** *76* (3), 472-481.

24. Don, T.; King, C.; Chiu, W.; Peng, C., Preparation and characterization of chitosan-g-poly(vinyl alcohol)/poly(vinyl alcohol) blends used for the evaluation of blood-contacting compatibility. *Carbohydrate Polymers* **2006,** *63* (3), 331-339.

25. Shagholani, H.; Ghoreishi, S. M.; Mousazadeh, M., Improvement of interaction between PVA and chitosan via magnetite nanoparticles for drug delivery application. *Int J Biol Macromol* **2015,** *78*, 130-6.

Chapter 5. **Improving barrier properties of paper for potential packaging applications**

5.1 Introduction

Paper is a versatile and flexible material that can be used for printing, household products, food packaging, etc.[1, 2] What makes it so versatile are its properties, such as its low density, good mechanical properties, excellent recyclability, and inherent biodegradability.[3-5] Paper is usually composed of plant-based fibers produced in the form of a matted or felted sheet. This is completed by pressing the fibers together to produce paper products with a wide range of thicknesses.[6] Also, paper can be composed of other fibrous materials, including sugar cane, cotton, and linen.[6] A main disadvantage of paper is its fibrous porous structure and thus poor barrier properties.[7]

In contrast to paper, plastic films with much higher barrier properties than paper have replaced paper in many packaging applications and have become an essential part of everyday life.[8, 9] However, its poor degradability has generated significant environmental concerns. In the recent years, there is a renaissance to replace plastic films with paper products.[10, 11] To help reduce the use of plastic films, paper usually needs to be modified to improve its properties to meet specific application requirements. For example, for food packaging applications, the most critical demand is to improve the barrier properties of paper because paper typically has a high porosity and thus a very poor barrier against gas (such as oxygen, water vapor, etc.).[12, 13] A common approach to improve the barrier properties of paper is to coat paper with a thin layer of wax, but this modification adds appreciable cost, causes certain health concerns, and also makes it difficult to recycle the final products.[13-16]

The previous chapters have clearly shown that the nanocoating technology we developed can help significantly improve the barrier properties of the coated substrates, as well as flame

retardancy and mechanical properties, all of which are beneficial for packaging applications.[17] Besides, the thickness of the nanocoatings are significantly lower than the conventional coatings (including the wax coating on paper), and thus a minimal concern on cost.

In this study, we aim to improve two critical properties of paper, i.e., barrier properties and flame retardancy, targeting potential food packaging applications. Both regular recycled paper and cotton paper were selected as the substrates. The dip coating method was used because it is well-established, scalable, and most readily to be adopted in papermaking industry. A brief sonication treatment was introduced during dip coating to help better impregnate the coating ingredients, i.e., polyvinyl alcohol (PVA) molecules and montmorillonite (MMT) nanosheets, into the pores of the paper substrate to achieve the best possible surface coverage, but meanwhile minimize potential damage to the paper structure.[18] The PVA/MMT nanocoating developed in the early chapters was selected because of its high versatility.

5.1.1 Materials

Both regular multi-purpose paper (Boise Aspen 30 Premium Recycled Paper, 75 g/m^2) and 100% cotton paper (Southworth, 90 g/m^2) were selected as substrates. PVA [EXCEVAL™ AQ-4104; hydrolysis of 98.0 mol. %], sodium montmorillonite (PGN nanoclay, Minerals Technologies Inc., New York, USA), glutaraldehyde (GA) (50% aqueous solution; Sigma-Aldrich), and HCl (37%; Sigma-Aldrich) were used as received without further purification. In this case, PVA EXCEVAL™ AQ-4104, a different PVA grade was used, because it was specifically developed for coating paper products.[19]

5.1.2 Preparation of PVA/MMT dispersion

PVA was dissolved in deionized (DI) water at 90° C with the assistance of stirring. MMT was uniformly dispersed in DI water under stirring, followed by one hour of ultrasonication in an

ultrasonication bath (Branson 8510R-MT, 250 W, 44 kHz). Predetermined amounts of the MMT dispersion and PVA solution were mixed to obtain a 1.5 wt. % PVA/MMT aqueous dispersion. To ensure uniformity, it was stirred for one hour and ultrasonicated for another hour. The dispersion was then cooled in an ice bath, and a small amount of crosslinking agent GA was added in a mole ratio of 1:20 (GA:PVA-OH groups). Also, HCl was used as a catalyst for the cross-linking reaction, with a 1:5 mole ratio to GA.

5.1.3 Preparation of nanocoatings on paper substrates

Paper substrates (ca. 15 cm × 17 cm) were prepared by dehydrating either regular paper or cotton paper samples in an oven at 60 °C for 24 h. Each paper sample is then submerged in the PVA/MMT dispersion for five minutes under sonication. The paper substrates were allowed to dry vertically for 45 minutes at 60 °C and dip coated four times. Between these coating cycles, they were rotated 180° to ensure a full coverage of the substrate. The final samples were labeled as χ-PVA/MMT-50-1.5-C, with χ representing the type of paper used: CP for cotton paper or P for regular paper. The experimental procedures for fabricating the nanocoating on paper are depicted in Figure 28.

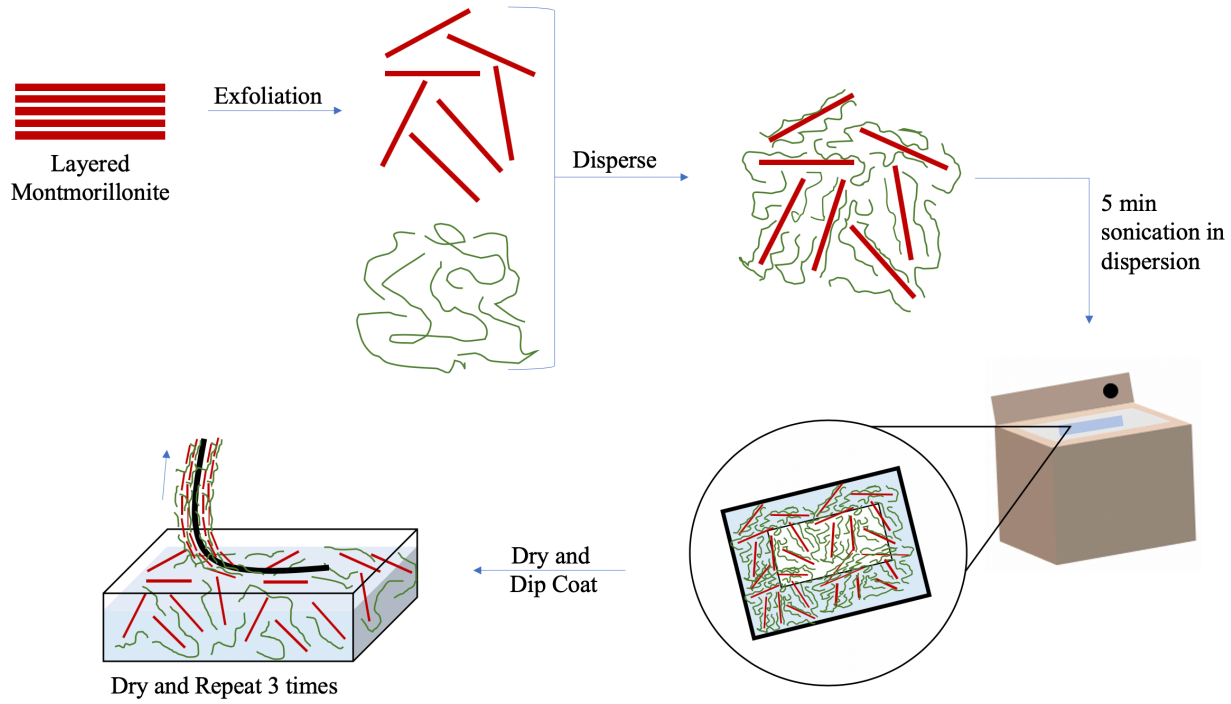

Figure 28. Schematic of the procedures to prepare PVA/MMT nanocoatings on paper substrates (not drawn to scale).

Characterization

The X-ray diffraction (XRD) patterns of the formed nanocoatings were obtained using a Bruker D2 phaser with a fixed Bragg-Brentano θ-2θ geometry and a LynxEye liner detector. An FEI nova NanoSEM 450 scanning electron microscope (SEM) was used to capture surface images of the samples. The samples were sputter-coated with a thin layer (ca. 6 nm) of Au/Pd (80:20) prior to SEM imaging.

Paper is a very poor barrier to water vapor. To better assess the water vapor transmission rate (WVTR) of paper, two different methods were adopted: (1) A bench top method well adopted in industry from ASTM E96/E96M was used for initial assessment, due to the high WVTRs of the paper substrates. The testing procedures are illustrated in Figure 29. First, a 1:1 ratio mixture of

beeswax and rosin is heated to 150 °C. The jars (20.3 cm in diameter and 10.2 cm in height, with a mouth diameter of 7.2 cm) are filled with DI with ca. ¼ inch of headspace. The testing specimens are cut into appropriate dimensions to fit the top of the jars. Once the beeswax/rosin mixture is thoroughly combined, it is applied to the rim of the jars. The testing specimens are then carefully applied to the rim of the jars. The sealed jars are placed in a chamber, in which a fan is set to promote circulation and a saturated sodium chloride solution is set to maintain a 50% relative humidity (RH). The relative humidity was carefully monitored using a humidity sensor. Over the period of 50 hours the jars are weighted every 2 hours to determine the slope of the straight line of the change in mass versus time, i.e., the weight loss rate. The WVTR is then calculated according to Equation 5). The specimens were also tested on a MOCON PERMATRAN-W 1/50 WVTR tester at 23 °C and 50% RH following ASTM E398 (hereafter referred to as MOCON method).

$$WVTR = \frac{slope\ (g/h)}{Test\ area\ (m^2)} \qquad \text{Equation 5}$$

The flammability of the coated regular paper and cotton paper was evaluated following ASTM D7309. All the samples are 12.5 cm in length and 1.5 cm in width, and the flame height is 4 cm. The sample is placed on a wire grid and the flame is placed 2.2 cm from the sample to the base of the flame.

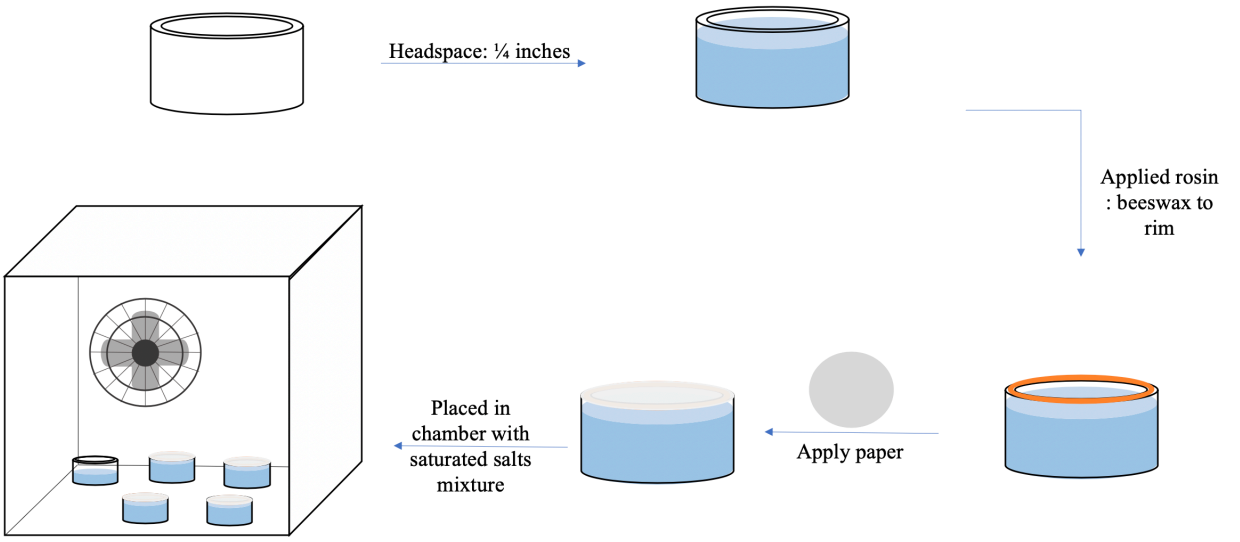

Figure 29. Schematic of the benchtop method to test the WVTR of the coated regular paper and cotton paper.

5.2 Results and Discussion

As discussed in the previous chapters, in an aqueous system, MMT is exfoliated into individual single-layer nanosheets under sonication. In a PVA/MMT dispersion, PVA chains are able to attach to the surface of the MMT nanosheets due to the weak hydrogen bonding and van der Waals interactions.[20] For paper substrates, a brief ultrasonication treatment was adopted to help impregnate the PVA and MMT into their porous structure, as shown in Figure 28. The coated samples were hung vertically in an oven to generate liquid flow on paper surface, which helps induce the alignment of the MMT nanosheets.[17] During the process, MMT nanosheets and PVA chains are able to self-coassemble to form a nanocoating on paper surface, with MMT nanosheets well-aligned along the substrate, leading to significantly improved barrier properties. The dispersion of 1.5 wt. % of solids (PVA + MMT) was chosen to maintain a low viscosity and the success it had on plastic films.

The orientation of MMT nanosheets is of the highest significance since it will dictate the quality of the resultant nanocoating, i.e., the overall performance. Initial evaluation of the MMT

orientation on various substrates was conducted by collecting their XRD patterns. As shown in Figure 30, the diffraction peak of MMT was detected at a 2θ value of 7.32° with a *d*-spacing of 12.1 Å. The uncoated regular paper and cotton paper show no peaks in the low angle range. Once coated, the basal diffraction peaks signified MMT orientation within the nanocoatings. The increase in the interlayer distance of the MMT layers within the nanocoatings on regular paper (25.2 Å) and cotton paper (25.7 Å) supports the presence of the PVA binder within the MMT nanosheet layers.

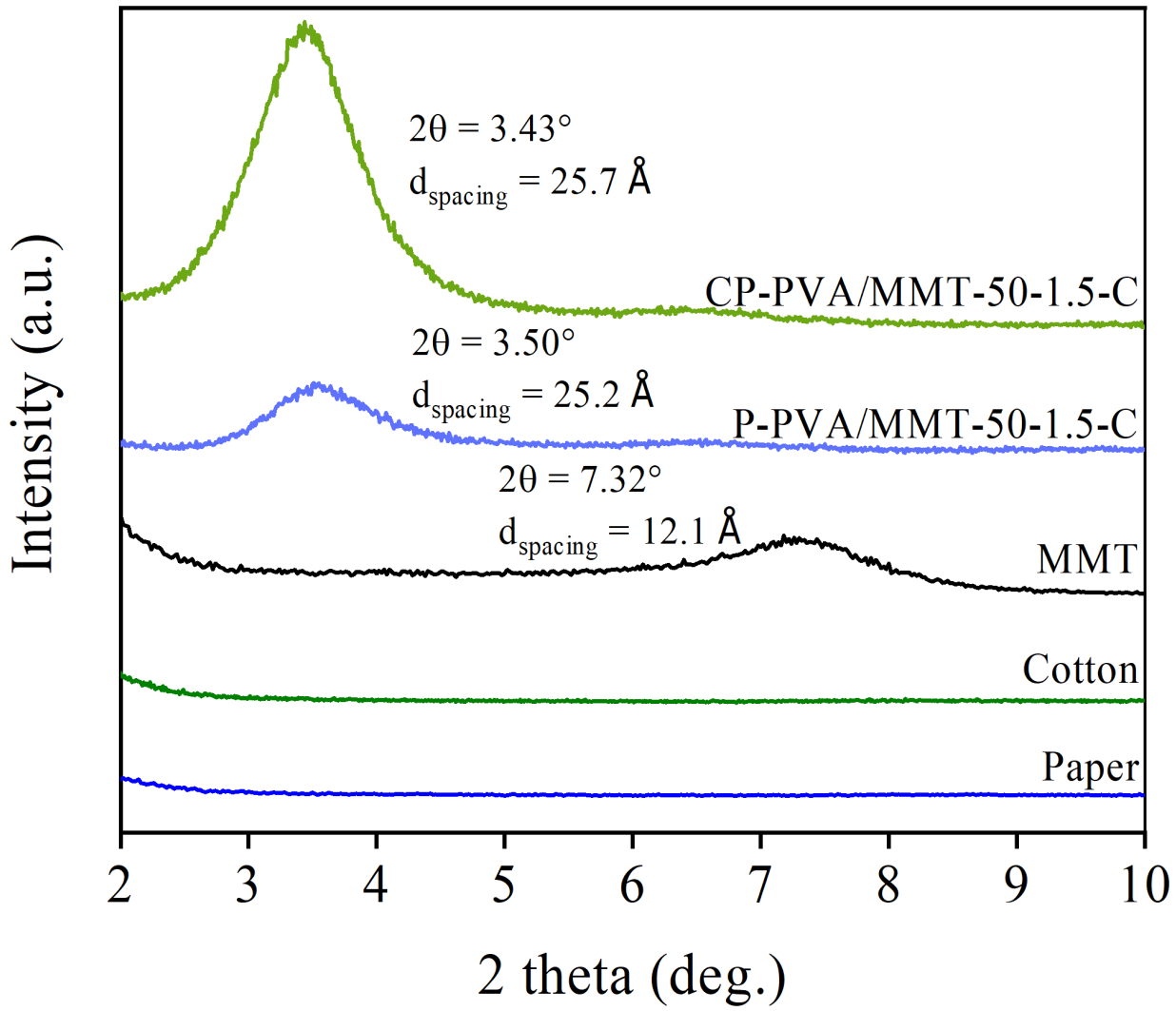

Figure 30. XRD patterns of the coated regular paper and cotton paper.

Due to the porous structure of paper, it exhibits poor barrier properties. The key goals of the sonication and coating treatment are to fill the internal porous structure and to cover surface defects, respectively. SEM imaging was used to observe the surface morphology after coating treatment. As shown in Figure 31, the uncoated paper and cotton paper both contain large pores throughout the structure. By sonication and coating treatment, most pores on paper were well-covered (Figure 31). But it can be observed that the coated paper and cotton paper still contain some small pores. One of the reasons that the pores were not completely covered was probably because limited ultrasonication treatment. Unfortunately, a longer ultrasonication treatment or repetition of ultrasonication cycles may damage the overall structure of paper and thus is not desirable.[11, 18] Also, it was observed during the experiment, when sonicated for over 5 minutes, the paper substrates started to deteriorate. Further work is needed to develop more effective treatments to completely cover the paper surface. This could be potentially completed by adjusting coating dispersion viscosity or introducing different polymer binders and/or inorganic nanosheets.

To further determine the quality of the nanocoatings, the WVTR was examined, since XRD and SEM focus on a very small area of the coated substrates and thus can only determine structural properties at highly localized regions. In contrast, WVTR tests a wide area of sample, so a significant change in WVTR demonstrates consistently high alignment of nanosheets across the coating layer. Two different methods were used to determine the WVTRs and the results are summarized in Table 5. Both regular paper and cotton paper possess a significantly improved battier to water vapor after coating treatment. According to the MOCON method, the WVTRs of the regular paper and cotton paper dropped from 2511.1 to 240.9 $g \bullet day^{-1} \bullet m^{-2}$ and from 1718.3 to 283.5 $g \bullet day^{-1} \bullet m^{-2}$, respectively. Similar trends on the WVTR results were also obtained from the bench top testing method. The above results indicate that the nanocoating has covered the majority

of the paper substrate to reduce the WVTR, which is very beneficial for some applications. Overall, the PVA/MMT coated paper samples have a lower WVTR than the ones coated with beeswax, which were reported to have a WVTR of 396.0 $g \bullet day^{-1} \bullet m^{-2}$.[12]

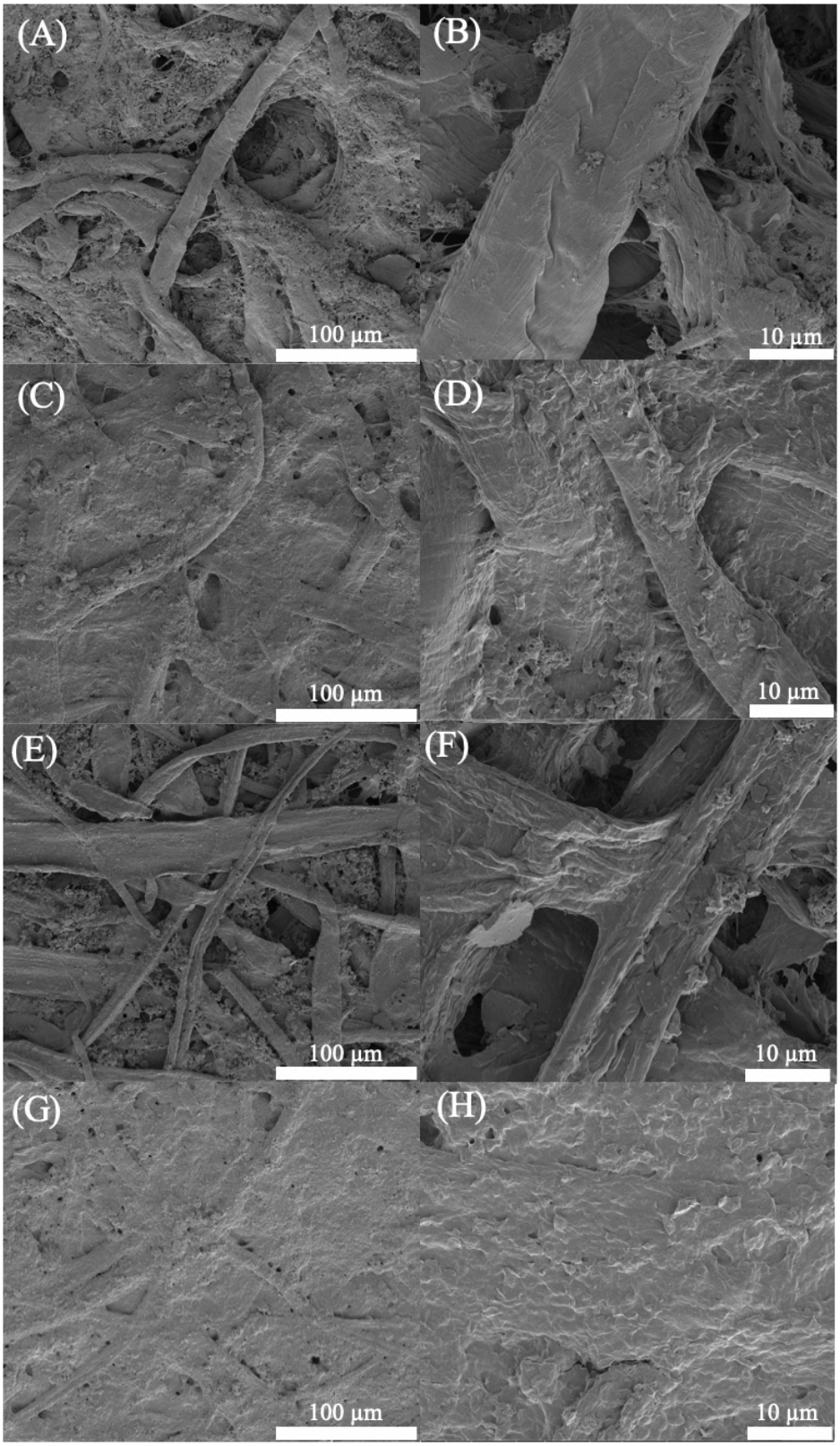

Figure 31. SEM images of the cotton paper (A) and (B), the coated cotton paper (C) and (D), the regular paper (E) and (F), and the coated regular paper (G) and (H).

Table 5. WVTRs of the coated regular paper and cotton paper.

Formulation in graft	$WVTR_{MOCON}$ ($g \bullet day^{-1} \bullet m^{-2}$)	$WVTR_{Bench\ Top}$ ($g \bullet day^{-1} \bullet m^{-2}$)
Paper	2511.1	2323
Cotton Paper	1718.3	2239
P-PVA/MMT-50-1.5-C	240.9	252
CP-PVA/MMT-50-1.5-C	283.5	268

The flammability of the coated paper and cotton paper was also examined and the results are shown in Figure 32 and Figure 33. From Figure 32, it can be observed that the nanocoating did not slow down the rate of the spread of fire. The flame rates of the uncoated and coated cotton paper were 3.4 and 3.9 mm/s, respectively, and 4.4 and 4.2 mm/s, respectively, for the uncoated and coated regular paper. However, it did help promote char formation and thus help maintain the paper structure. After the flammability test, the uncoated samples were almost completely gasified, only leaving behind a small amount of ash, but the coated samples did not fall apart and maintained the overall shape (Figure 33).

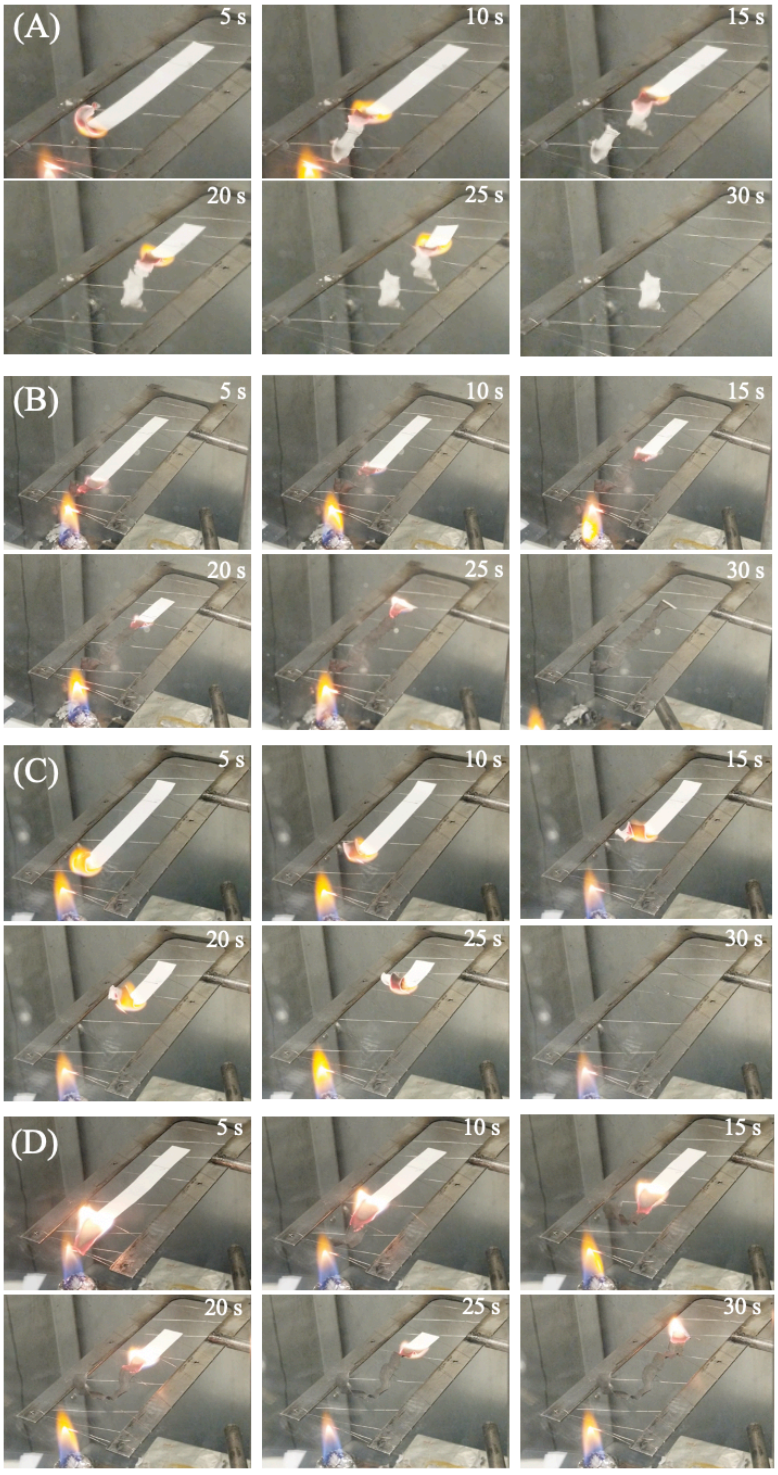

Figure 32. Images of the combustion process of the samples: (A) regular paper, (B) coated regular paper, (C) cotton paper, and (D) coated cotton paper.

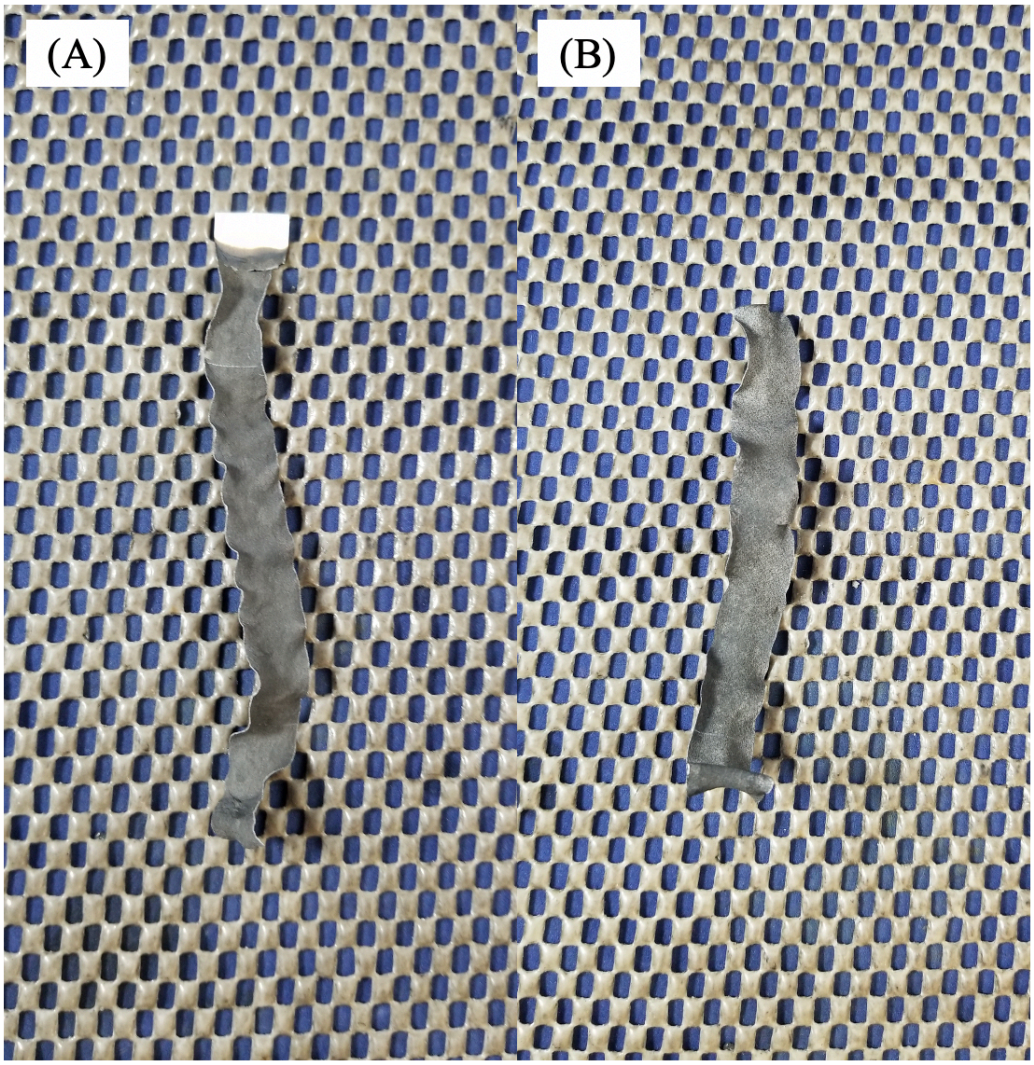

Figure 33. Residues of (A) the coated paper and (B) the coated cotton paper.

5.3 Conclusion

Sonication and dip coating methods were used to deposit a PVA/MMT nanocoating on two different paper substrates. The nanocoatings were characterized by XRD, SEM, and WVTR. The XRD results support the formation of well-aligned MMT nanosheets on paper substrates and the SEM images show that most pores on the substrates were covered by the formed nanocoatings, which leads to a drastic decrease in WVTR of the coated substrates. The nanocoatings also led to a minor improvement in flame retardancy.

References

1. Hu, Z.; Tang, C.; He, Z.; Lin, J.; Ni, Y., 1-Methycyclopropene (MCP)-Containing Cellulose Paper Packaging for Fresh Fruit and Vegetable Preservation: A Reviw. *BioResources* **2017,** *12*.

2. Barhoum, A.; Rahier, H.; Abou-Zaied, R. E.; Rehan, M.; Dufour, T.; Hill, G.; Dufresne, A., Effect of cationic and anionic surfactants on the application of calcium carbonate nanoparticles in paper coating. *ACS Appl Mater Interfaces* **2014,** *6* (4), 2734-44.

3. Rastogi, V.; Samyn, P., Bio-Based Coatings for Paper Applications. *Coatings* **2015,** *5* (4), 887-930.

4. Khwaldia, K.; Arab-Tehrany, E.; Desobry, S., Biopolymer Coatings on Paper Packaging Materials *Comprehensive Reviews In Food Science and Food Safety* **2010,** *9*.

5. Stewart, B., Packaging design and development In *Packaging Technology: Fundamentals, materials and processes*, Emblem, A.; Emblem, H., Eds. Woodhead Publishing Limited: 2012.

6. Riley, A., Paper and paperboard packaging. In *Packaging technology: Fundamentals, materials and processes*, Emblem, A.; Emblem, H., Eds. Woodhead Publishing LImited: 2012.

7. Mahadeva, S. K.; Walus, K.; Stoeber, B., Paper as a platform for sensing applications and other devices: a review. *ACS Appl Mater Interfaces* **2015,** *7* (16), 8345-62.

8. Mangaraj, S.; Goswami, T. K.; Mahajan, P. V., Applications of Plastic Films for Modified Atmosphere Packaging of Fruits and Vegetables: A Review. *Food Engineering Reviews* **2009,** *1* (2), 133-158.

9. Emblem, A., Plastics proerties for packaging materials. In *Packaging technology: Fundamental, materials and processes*, Emblem, A.; Emblem, H., Eds. Woodhead Publishing Limited: 2012; pp 287-309.

10. Amini, E.; Azadfallah, M.; Layeghi, M.; Talaei-Hassanloui, R., Silver-nanoparticle-impregnated cellulose nanofiber coating for packaging paper. *Cellulose* **2016,** *23* (1), 557-570.

11. Ghule, K.; Ghule, A. V.; Chen, B.-J.; Ling, Y.-C., Preparation and characterization of ZnO nanoparticles coated paper and its antibacterial activity study. *Green Chemistry* **2006,** *8* (12).

12. Zhang, D.; Xiao, H., Dual-functional beeswaxes on enhancing antimicrobial activity and water vapor barrier property of paper. *ACS Appl Mater Interfaces* **2013,** *5* (8), 3464-8.

13. Anthony, R.; Xiang, Z.; Runge, T., Paper coating performance of hemicellulose-rich natural polymer from distiller's grains. *Progress in Organic Coatings* **2015,** *89*, 240-245.

14. Zou, Y.; Hsieh, J. S.; Mehnert, E.; Kokoszka, J., The study of PET recyclable polymers as paper coatings. *Progress in Organic Coatings* **2007,** *60* (2), 127-131.

15. Moggridge, G. D.; Lape, N. K.; Yang, C.; Cussler, E. L., Barrier films using flakes and reactive additives. *Progress in Organic Coatings* **2003,** *46* (4), 231-240.

16. Schuman, T.; Adolfsson, B.; Wikström, M.; Rigdahl, M., Surface treatment and printing properties of dispersion-coated paperboard. *Progress in Organic Coatings* **2005,** *54* (3), 188-197.

17. Ding, F.; Liu, J.; Zeng, S.; Xia, Y.; Wells, K. M.; Nieh, M.-P.; Sun, L., Biomimetic nanocoatings with exceptional mechanical, barrier, and flame-retardant properties from large-scale one-stemp coassembly. *Science Advances* **2017,** *3*.

18. Gottesman, R.; Shukla, S.; Perkas, N.; Solovyov, L. A.; Nitzan, Y.; Gedanken, A., Sonochemical coating of paper by microbiocidal silver nanoparticles. *Langmuir* **2011,** *27* (2), 720-6.

19. Kumaki, Y.; Kawagoe, M.; Takada, S.; Garcia, P. J.; Neufeld, L. C., Enhanced Polyvinyl Alcohol as a Barrier Paper Coating for Food Packaging. In *TAPPI PaperCon 2014 Conference Proceedings*, Nashville, April 27-30,, 2014; pp pp 2388-2399.

20. Podsiadlo, P.; Kaushik, A. K.; Arruda, e. M.; Waas, A. M.; Shim, b. S.; Xu, J.; Nandivada, H.; Pumplin, B. G.; Lahann, J.; Ramamoorthy, A.; Kotov, N. A., Ultrastrong and Stiff Layered Polymer Nanocomposites. *Science* **2007,** *318* (59847), 80-8.

Chapter 6. **Polymer/clay nanocomposite films from an impregnation method**

6.1 Introduction

From previous chapters, it can be seen that polymer/montmorillonite (MMT) nanocoatings can introduce improvements in mechanical,[1-3] flame retardant,[4-6] and barrier[7-9] properties of substrates. These property improvements can be attributed to the well-aligned and highly-packed inorganic nanosheets in the nanocoatings.[10, 11] Organic/inorganic nanocoatings can be applied to various substrates using layer-by-layer[1, 12] (LBL) deposition or one-step coassembly[9, 13] as introduced in the previous chapters. In most cases, the coated substrates are used for their various applications. However, in some situations, the nanocoatings need to be delaminated from the substrates. While we have managed to obtain freestanding nanocomposite thin films via delaminating the nanocoating layer from a coated substrate,[13] this method is time consuming and hard to scale up.

Previously, we have been able to prepare nanocoatings with a high concentration of inorganic nanosheets, up to 70 wt. %.[13] However, it is challenging to further enhance nanocoating concentration as the viscosity of the dispersion is already very high. On the other end, it is ideal to achieve extremely high inorganic concentrations for special applications, such as electronic and biomedical applications.[14, 15]

A key characteristic that defines the hybrid nanocoatings is their similarity to the structure of nacre. Nacre has outstanding strength, stiffness, and toughness due to its highly ordered layered structure. Its layered structure is composed of ca. 95 vol. % calcium carbonate and ca. 5 vol. % of organic biopolymers.[16] While calcium carbonate is a very hard and brittle material, the proteins that contribute to the system are soft and tough. The outstanding and balanced mechanical properties of nacre is attributed to this intercalated system, which has inspired material scientists to synthesize materials with a similar structure for practical applications.

The goal of this project is to develop a new processing technique to fabricate free-standing nanocomposite films with an extremely high inorganic concentration for both fundamental and applied research. Instead of assembling organic and inorganic components at the same step, we propose to assemble inorganic nanosheets to form an all-inorganic thin film with a layered structure first. Subsequently, organic components are impregnated into the layered inorganic structure with the assistance of vacuum. In this way, the high viscosity issue of a dispersion containing an extremely high concentration of nanosheets can be avoided.

MMT (average size of individual nanosheets: 260 ± 60 nm)[13] is the material of choice thanks to its ability to easily exfoliate in water, strong mechanical properties, and low cost.[1, 17] Due to the weak van der Waals forces holding the layers together, once dispersed in water, MMT will swell, and exfoliation can occur especially with the assistance of ultrasonication.[1, 18] This is particularly the case when the counter cations of MMT are mainly Na^+. However, MMT itself, as an inorganic compound, is very brittle. A polymer need be impregnated into MMT layers to achieve balanced stiffness, strength, and toughness. Furthermore, a proper selection of polymer may lead to the preparation of functional polymer/MMT nanocomposite films for specific applications.

In this preliminary investigation, polyvinylidene fluoride (PVDF) was selected to be impregnated into MMT layered structure to fabricate PVDF/MMT functional nanocomposite films because PVDF is flexible, biocompatible, piezoelectric, and can form dipole-ion interactions with MMT, which allows for a variety of functional applications.[19]

6.2 Experimental

6.2.1 Materials

Sodium MMT (PGN nanoclay, Minerals Technologies Inc., USA), PVDF (Kynar Flex 2800-00, Arkema Inc., USA), and *N*,*N*-dimethylformamide (anhydrous, 99.8%, Aldrich) were used as received without further purification.

6.2.2 Preparation of PVDF/MMT nanocomposite films

MMT was dispersed in di-ionized (DI) water at room temperature under continuous stirring to prepare a 1.5 wt. % stock dispersion, which was ultrasonicated for an hour to completely exfoliate MMT. A sample of 15.0 mL of MMT aqueous dispersion was cast onto a well-leveled glass petri dish, which was then heated at 60 °C for 12 hours. The dried all-MMT thin film can be easily removed from the petri dish for further processing.

PVDF pellets were dissolved in DMF to prepare a PVDF solution (50 g/L). The prepared all-MMT thin film was then submerged into the PVDF solution for 5 min. Then, vacuum was applied to the sample for 5 minutes. Finally, the PVDF/MMT nanocomposite film was dried in an oven for 2 hours at 60 °C. The procedures are briefly illustrated in Figure 34.

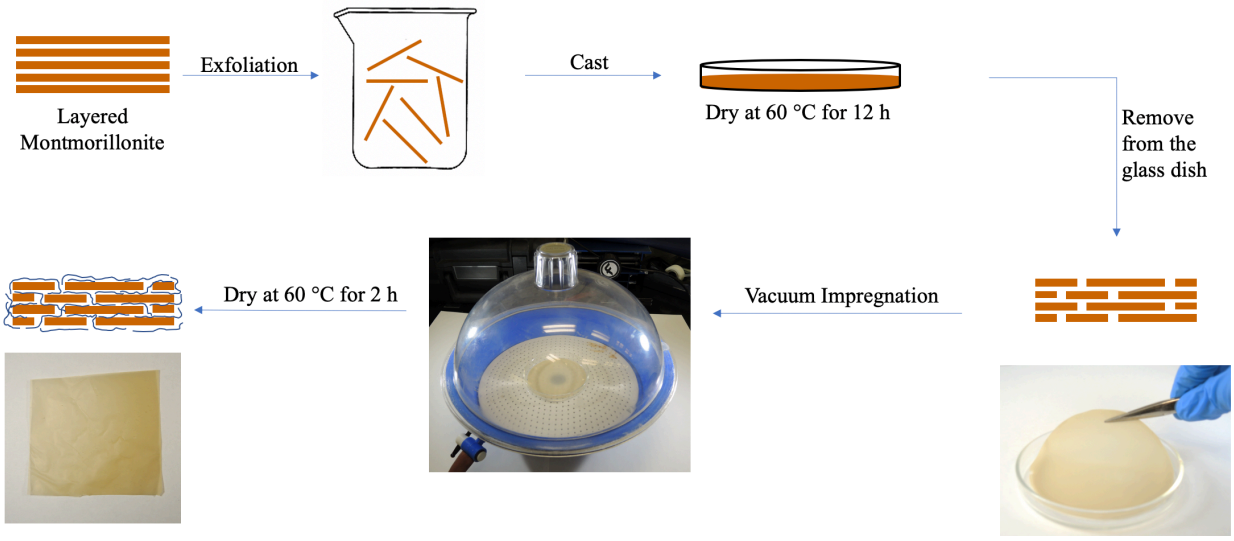

Figure 34. Schematic of the procedures to fabricate a PVDF/MMT nanocomposite film.

6.2.3 Characterization

X-ray diffraction (XRD) patterns of the PVDF/MMT nanocomposite films were recorded on a Bruker D2 Phaser X-ray diffractometer equipped with a LynxEye linear detector and Cu Kα radiation source. A thermogravimetric analyzer (TGA, TA Instruments Q500) was used to determine the composition of the film. The mechanical properties of the free-standing films were tested on a dynamic mechanical analyzer (DMA, TA Instruments Q800). The oxygen transmission rates (OTRs) of the nanocomposite films were tested on a MOCON (Minneapolis, MN) OX-TRAN 1/50 OTR tester at 23 °C and 0% RH using the ASTM D3985 standard method.

6.3 Results and discussion

To confirm the successful impregnation of PVDF into the MMT layers and to investigate the layered structure of the resulting PVDF/MMT nanocomposite films, XRD and TGA characterizations were conducted. The XRD diffraction peaks corresponding to the layered structures of the all-MMT and PVDF/MMT nanocomposite films are shown in Figure 35. The

diffraction peak of the PVDF/MMT nanocomposite film shifted to a lower 2θ angle with an increase in intensity compared to the all-MMT film. The d spacing of free MMT is 12.3 Å and increases to 13.3 Å once impregnated with PVDF. This could be contributed to PVDF impregnating into the layers. Another noticeable feature of the XRD peaks is the change of their full width at half max (FWHM), which is 1.037° ± 0.008° for the all-MMT film and decreased to 0.813° ± 0.004° for the PVDF/MMT nanocomposite film. The above XRD characterization results indicate that PVDF has penetrated into the MMT layers, expanded the interlayer distance, and helped further orient the MMT nanosheets to form a better-aligned layered structure. The possible reason that the impregnation of PVDF can help further improve the level of MMT nanosheet orientation is possibly due to the soft PVDF layer that can better accommodate the rigid MMT nanosheets, leading to a higher degree of alignment, but further investigation is still needed.

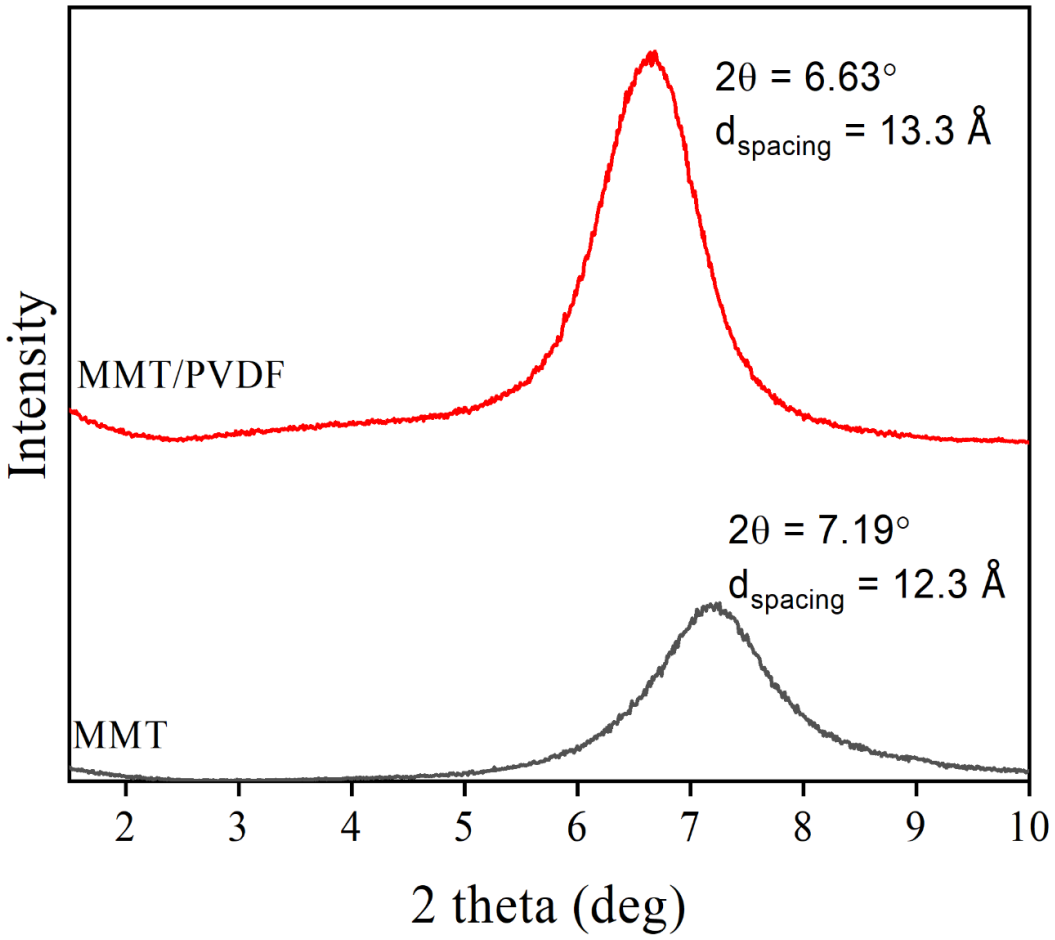

Figure 35. XRD patterns of the formed all-MMT and PVDF/MMT nanocomposite films.

Figure 36 presents the TGA thermograms of the PVDF, all-MMT, and PVDF/MMT nanocomposite freestanding film. The onset of the decomposition for both the MMT and PVDF/MMT freestanding sample is about 30 °C owing to the water loss. Decomposition of the neat PVDF sample occurred between 400 to 460 °C, while the PVDF component in the PVDF/MMT nanocomposite occurred at slightly higher temperatures due to the protection of the inorganic MMT layers. Based on the weight loss of the all-MMT film, PVDF, and PVDF/MMT nanocomposite samples, it was determined that the PVDF/MMT nanocomposite freestanding film contained ca. 12.5 wt. % of PVDF and ca. 87.5 wt. % MMT, a very high concentration of MMT compared to conventional nanocomposites.

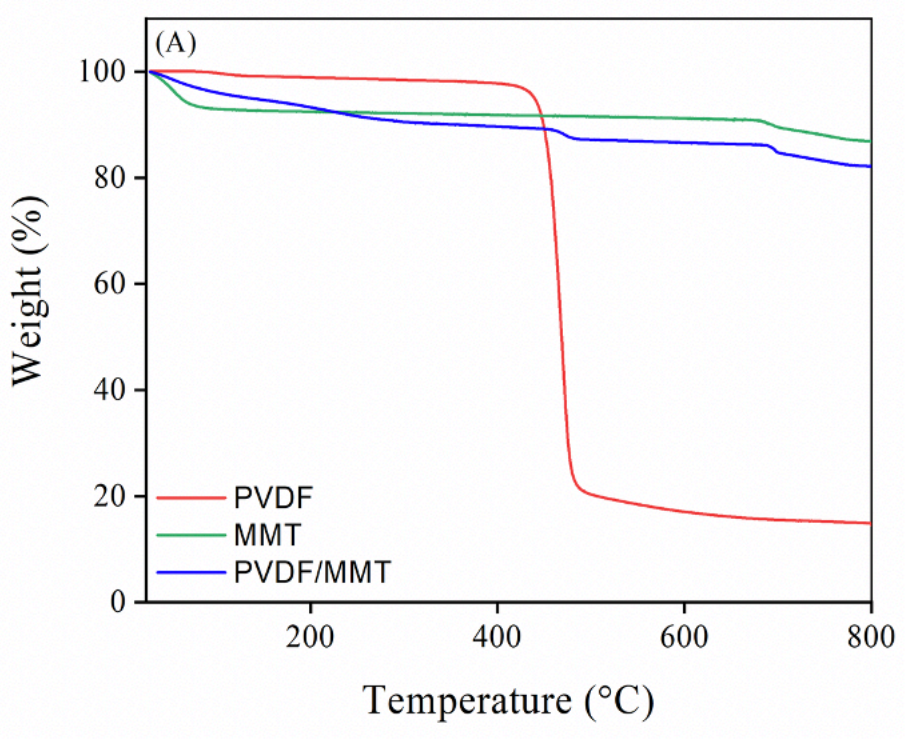

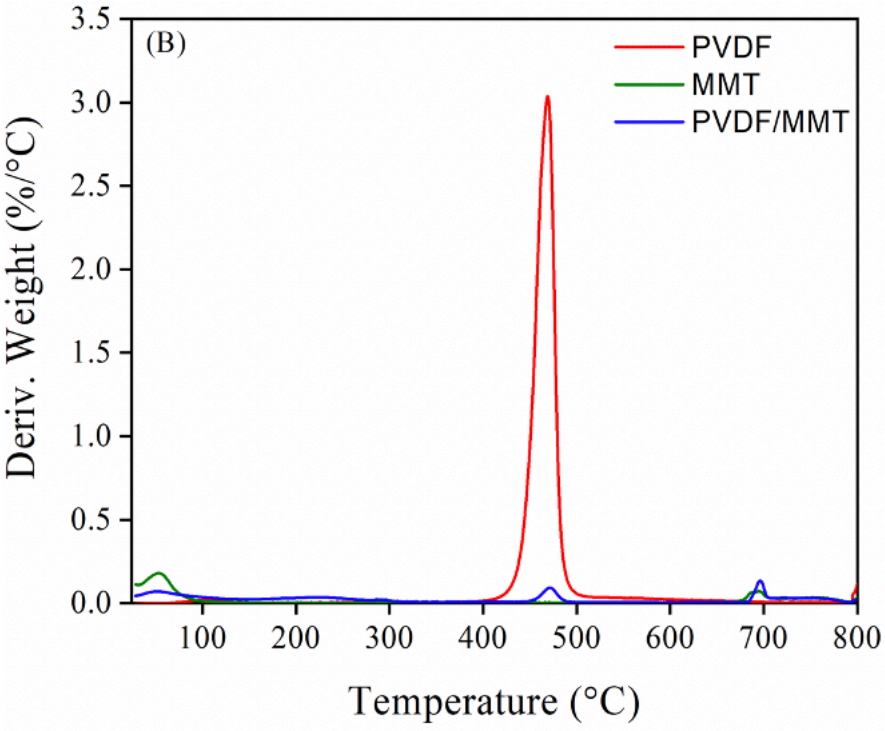

Figure 36. (A) TGA and (B) DTGA thermograms of the PVDF, all-MMT, and PVDF/MMT nanocomposite freestanding film.

Another advantage of the impregnation of soft PVDF into rigid MMT layers is the improvement in mechanical properties, especially toughness. As shown in Figure 37A, the all-MMT film is very brittle and incapable of wrapping around a 1.0 mm rod. With the impregnation of a low concentration of PVDF, the flexibility of the resultant PVDF/MMT nanocomposite film was increased drastically to easily wrap around a 1.0 mm rod (Figure 37B). This is expected, as the impregnated PVDF/MMT nanocomposite film exactly mimics the organic/inorganic hybrid layered structure of nacre,[13] in which the parallel soft PVDF layers help absorb energy and thus significantly improving toughness.[14] Systematic mechanical property testing of the samples was conducted using DMA and the representative stress-strain curves are shown in Figure 38. The tensile strength of the all–MMT film and PVDF was observed to be 9.86 and 24.69 MPa, respectively, while PVDF/MMT nanocomposite film exhibited a much higher tensile strength of 50.73 MPa. The PVDF/MMT film also showed a similar dramatic increase in modulus compared to the all-MMT film and PVDF (Table 6). Moreover, the fracture toughness of the PVDF/MMT composite was much higher than that of the all-MMT film. The simultaneous improvement in stiffness, strength, and fracture toughness of the PVDF/MMT nanocomposite indicates a successful impregnation of PVDF into MMT layers, and also suggests potential promising applications of the PVDF/MMT nanocomposite film.

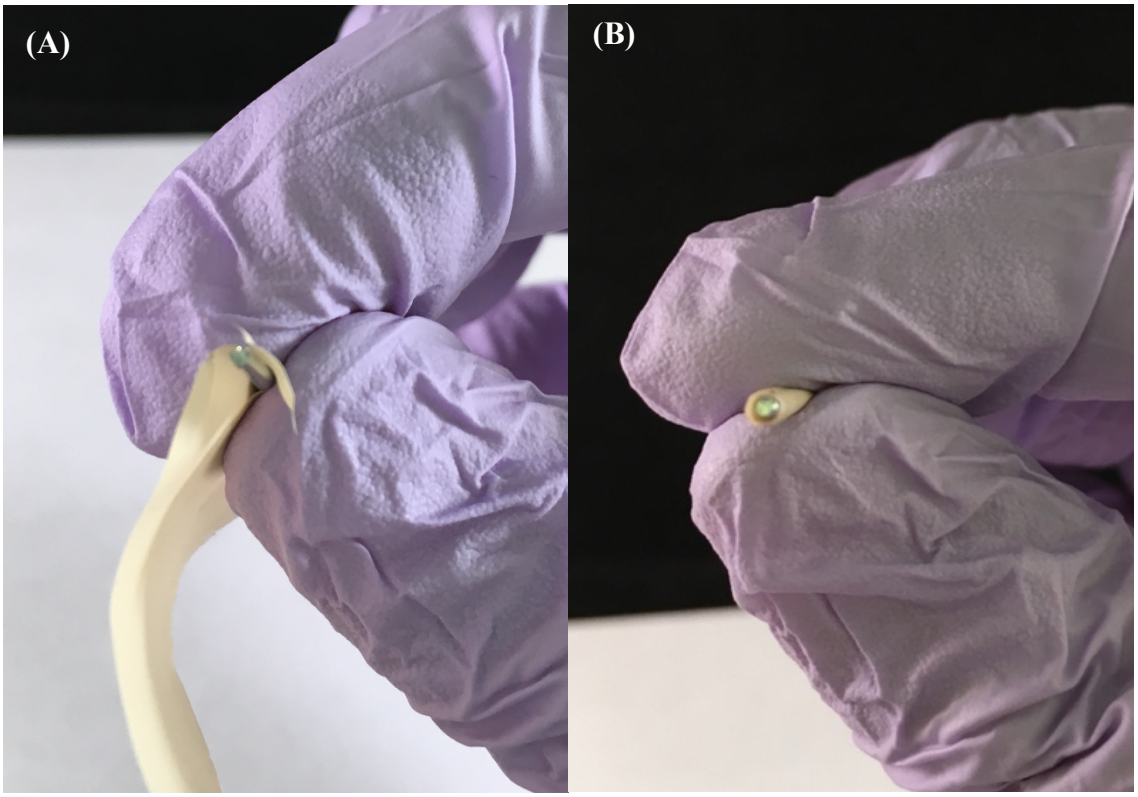

Figure 37. All-MMT (A) and PVDF/MMT (B) nanocomposite freestanding films wrapping around a 1.0 mm rod.

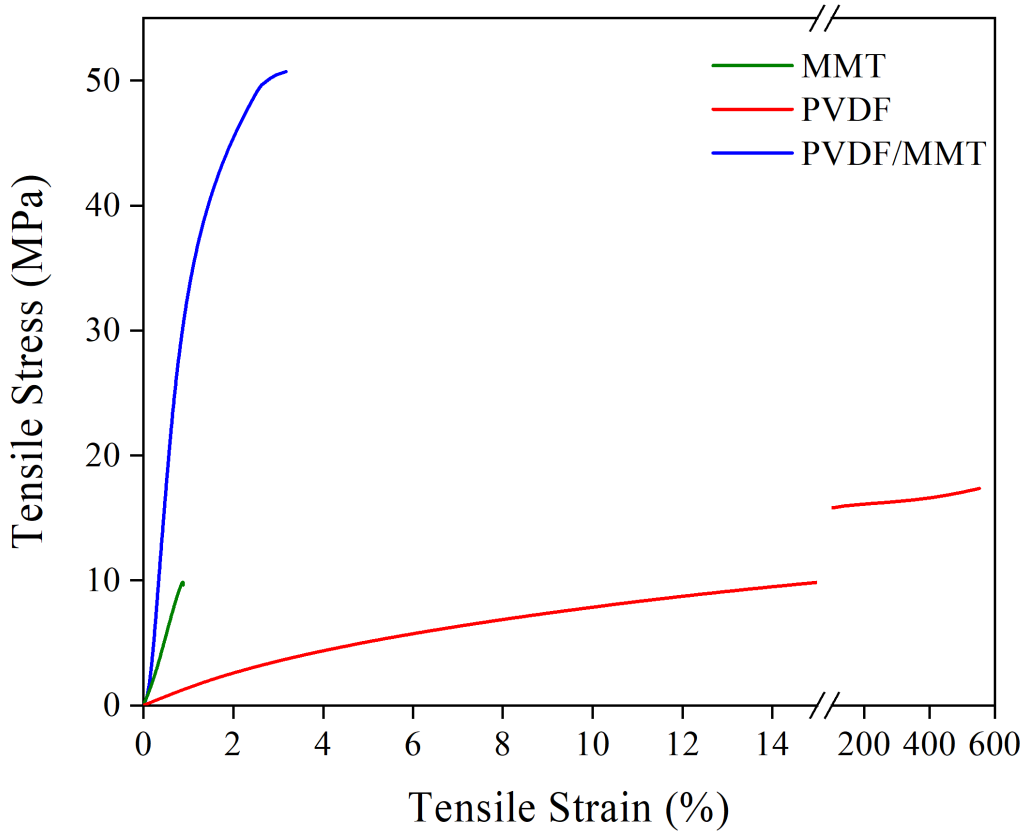

Figure 38. Representative stress-strain curves of the formed free-standing films.

Table 6. Mechanical properties of the formed PVDF/MMT free-standing films.

	Maximum Tensile strength (MPa)	Modulus (MPa)	Ultimate strain (%)	Toughness (MPa)
MMT	10.32 ± 0.93	1072.3 ± 31.3	1.3 ± 0.4	0.05 ± 0.02
PVDF	15.49 ± 2.63	109.3 ± 24.4	547.8 ± 6.8	78.3 ± 13.4
PVDF/MMT	44.98 ± 9.55	2740.0 ± 377.5	3.2 ± 0.02	6.9 ± 0.2

* ± Standard Deviation

Considering the high thermal insulation of inorganic MMT nanosheets, the PVDF/MMT nanocomposite film, which contains a high concentration of well-aligned MMT nanosheets, is expected to exhibit decent flame protection. As shown in Figure 39, the PVDF/MMT nanocomposite film (ca. 27 μm in thickness) was proved to be able to effectively block the heat from a butane torch (1300 °C, 12 s) to protect a cotton ball from ignition. Even though the flammability of PVDF is low,[20] the densely-packed and well-aligned MMT nanosheets serve as framework for effective flame protection. Another benefit of the dense and well-aligned MMT nanosheets is the excellent barrier properties. As shown in Table 2, a significant decrease in oxygen permeability was achieved thanks to the very tortuous pathway created by the well-aligned MMT nanosheets.

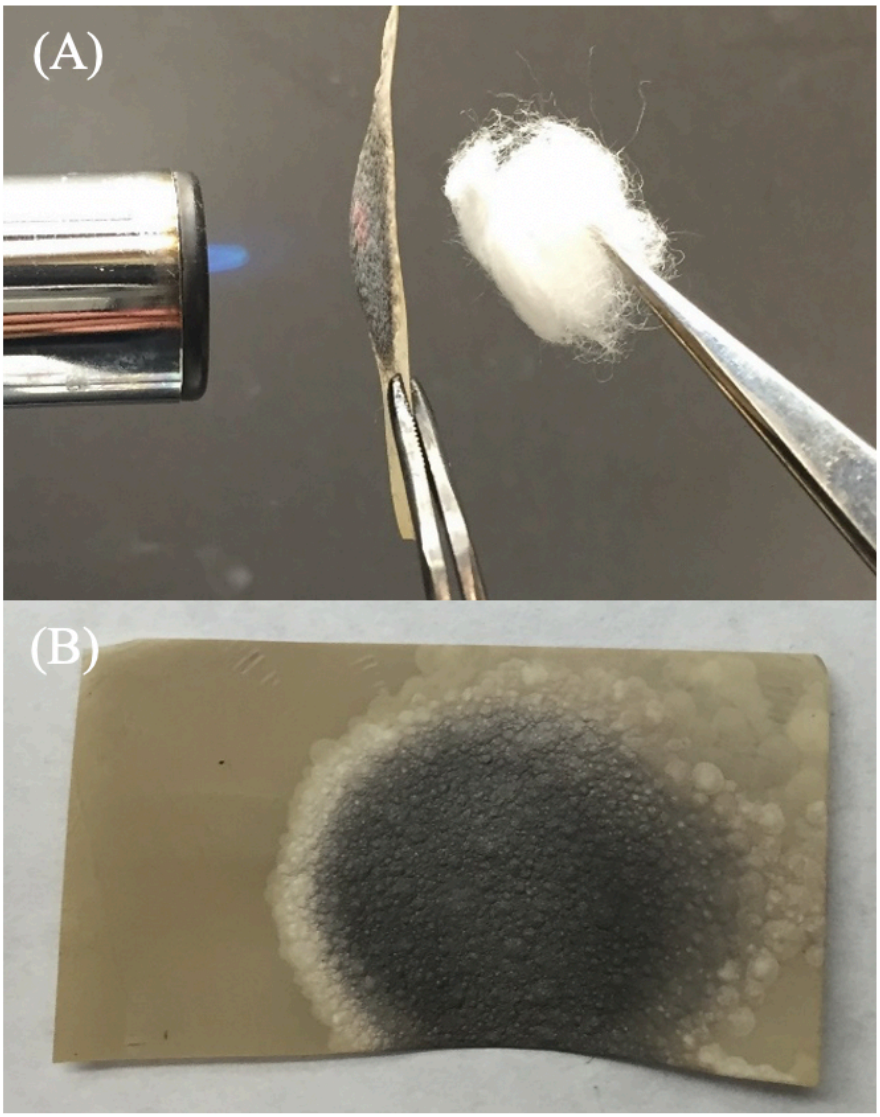

Figure 39. Images of (A) combustibility testing (1300 °C) of PVDF/MMT thin film under a butane torch for 12 s and (B) surface morphology after combustibility testing.

Table 7. Barrier properties of the formed PVDF/MMT nanocomposite film.

	Thickness (μm)	OTR (cm^3/m^2 · day)	O_2 Permeability [$10^{-16}cm^3$(STP)cm/cm^2•s• Pa]
MMT	16	85.1	15.55
PVDF	78	63.5	56.58
PVDF/MMT	27	1.2	0.37

6.10 Conclusion

A novel impregnation method for the preparation of PVDF/MMT nanocomposite films was developed. The introduction of PVDF into the system significantly increased the mechanical, barrier, and flame protection properties of the films. While PVDF was adopted in this preliminary exploration, other polymers may serve a similar role to prepare various functional nanocomposite films for different applications.

References

1. Podsiadlo, P.; Kaushik, A. K.; Arruda, e. M.; Waas, A. M.; Shim, b. S.; Xu, J.; Nandivada, H.; Pumplin, B. G.; Lahann, J.; Ramamoorthy, A.; Kotov, N. A., Ultrastrong and Stiff Layered Polymer Nanocomposites. *Science* **2007,** *318* (59847), 80-8.

2. Walther, A.; Bjurhager, I.; Malho, J. M.; Pere, J.; Ruokolainen, J.; Berglund, L. A.; Ikkala, O., Large-area, lightweight and thick biomimetic composites with superior material properties via fast, economic, and green pathways. *Nano Lett* **2010,** *10* (8), 2742-8.

3. Podsiadlo, P.; Tang, Z.; Shim, B. S.; Kotov, N. A., Counterintuitive Effect of Moldecular Strength and Role of Molecular Rigidity on Mechanical Properties of Layer-by-Layer Assembled Nanocomposited. *Nano Lett* **2007,** *7*.

4. Chang, S.; Slopek, R. P.; Condon, B.; Grunlan, J. C., Surface Coating for Flame-Retardant Behavior of Cotton Fabric Using a Continuous Layer-by-Layer Process. *Industrial & Engineering Chemistry Research* **2014,** *53* (10), 3805-3812.

5. Salamova, A.; Hites, R. A., Brominated and chlorinated flame retardants in tree bark from around the globe. *Environ Sci Technol* **2013,** *47* (1), 349-54.

6. Ebina, T.; Mizukami, F., Flexible Transparent Clay Films with Heat-Resistant and High Gas-Barrier Properties. *Advanced Materials* **2007,** *19* (18), 2450-2453.

7. Guin, T.; Krecker, M.; Hagen, D. A.; Grunlan, J. C., Thick growing multilayer nanobrick wall thin films: super gas barrier with very few layers. *Langmuir* **2014,** *30* (24), 7057-60.

8. Priolo, M. A.; Holder, K. M.; Gamboa, D.; Grunlan, J. C., Influence of clay concentration on the gas barrier of clay-polymer nanobrick wall thin film assemblies. *Langmuir* **2011,** *27* (19), 12106-14.

9. Priolo, M. A.; Holder, K. M.; Greenlee, S. M.; Stevens, B. E.; Grunlan, J. C., Precisely Tuning the Clay Spacing in Nanobrick Wall Gas Barrier Thin Films. *Chemistry of Materials* **2013,** *25* (9), 1649-1655.

10. Srivastava, S.; Kotov, N. A., Composite Layer-by-Layer (LbL) Assembly with Inorganic Nanoparticles and Nanowires. *Accounts of Chemical Research* **2008,** *41*, 1831-1841.

11. Das, P.; Schipmann, S.; Malho, J. M.; Zhu, B.; Klemradt, U.; Walther, A., Facile access to large-scale, self-assembled, nacre-inspired, high-performance materials with tunable nanoscale periodicities. *ACS Appl Mater Interfaces* **2013,** *5* (9), 3738-47.

12. Priolo, M. A.; Gamboa, D.; Holder, K. M.; Grunlan, J. C., Super gas barrier of transparent polymer-clay multilayer ultrathin films. *Nano Lett* **2010,** *10* (12), 4970-4.

13. Ding, F.; Liu, J.; Zeng, S.; Xia, Y.; Wells, K. M.; Nieh, M.-P.; Sun, L., Biomimetic nanocoatings with exceptional mechanical, barrier, and flame-retardant properties from large-scale one-stemp coassembly. *Science Advances* **2017,** *3*.

14. Patro, T. U.; Wagner, H. D., Layer-by-layer assembled PVA/Laponite multilayer free-standing films and their mechanical and thermal properties. *Nanotechnology* **2011,** *22* (45), 455706.

15. Kharlampieva, E.; Kozlovskaya, V.; Sukhishvili, S. A., Layer-by-Layer Hydrogen-Bonded Polymer Films: From Fundamentals to Applications. *Advanced Materials* **2009,** *21* (30), 3053-3065.

16. Barthelat, F., Biomimetics for next generation materials. *Philos Trans A Math Phys Eng Sci* **2007,** *365* (1861), 2907-19.

17. Chen, T.; Zhao, Y.; Song, S., Comparison of colloidal stability of montmorillonite dispersion in aqueous NaCl solution with in alcohol-water mixture. *Powder Technology* **2017,** *322*, 378-385.

18. Luckham, P. F.; Rossi, S., The colloidal and rheological properties of bentonite suspensions. *Advances in Colloid and Interface Science* **1999,** *83*, 43-92.

19. Rahman, W.; Ghosh, S. K.; Middya, T. R.; Mandal, D., Highly durable piezo-electric energy harvester by a super toughened and flexible nanocomposite: effect of laponite nano-clay in poly(vinylidene fluoride). *Materials Research Express* **2017,** *4* (9).

20. Jiang, X.; Xu, C.; Wang, Y.; Chen, Y., Polyvinylidene Fluoride/Acrylonitrile Butadiene Rubber Blends Prepared Via Dynamic Vulcanization. *Journal of Macromolecular Science, Part B* **2014,** *54* (1), 58-70.

Chapter 7. **Summary**

As noted in previous chapters, organic/inorganic nanocomposite coatings are of significant interest due to their excellent features of highly ordered structure,[1] outstanding properties (mechanical,[2] barrier,[3-5] flame retardant,[6-8] etc.), and scalable processing.[9, 10] The benefit of these properties is their diverse applications. However, the processing method significantly affects the properties and quality of the resultant nanocoatings. A one-step coassembly method was previously developed.[11] In combination with dip coating, the one-step coassembly is a successful method to produce well-aligned nanocoatings with outstanding barrier properties due to the flow on a surface generated during coating.[11]

Since dip coating provides such a highly aligned structure, a novel rotational coating method was further developed to apply centripetal acceleration to the nanocoating while continuously drying to understand the role different forces play in alignment. The centripetal acceleration ranged from 4.0 to 48.8 m/s^2 and was able to produce a highly aligned layered structure with superior barrier properties. In addition, spray coating was examined to work with large and irregularly shaped substrates. To examine the viability of spray coating, samples were spray coated for 15, 30, and 45 s for 1, 2, or 3 cycles at random. Each method contributes its unique features to coating, but a closer look at their turbidity and permeability helps reveal their efficiency. In Table 8, the turbidity of the nanocoatings prepared using rotational coating and spray coating are summarized. It is observed that rotational coating can produce highly ordered nanocoatings with a turbidity as low as -1.92×10^{-4} at 48.4 m/s^2, but spray coating could only achieve a turbidity of 1.29×10^{-4} at 45s:1×. The low turbidity values of the rotational coatings could be attributed to the high level nanosheet orientation (as supported by the presence of the Fabry-Pérot pattern)[12, 13] As discussed in the previous chapters, spray coating cannot form a uniform coating, while

rotational coating can form a uniform coating across a large substrate area. Also, the permeability in Table 9 depicts the same trend that rotational coating can produce nanocoatings with a low permeability. Dip coating data is also presented in this table since it has proven to produce nanocoatings with a highly aligned layered structure with a low permeability in the previous work.[11] It is observed that rotational coating provides promising results (0.0021 10^{-16}cm^3(STP)cm/cm^2•s•Pa), similar to that of dip coated samples (0.0015 10^{-16}cm^3(STP)cm/cm^2•s•Pa). Even though the current results from rotational coating are similar to those of dip coating, a higher centripetal acceleration is expected to lead to further improved performance, potentially superior to those of dip coating. The preliminary exploration has shown that spray coating can be used for one-step coassembly of nanocoatings. By adjusting the spray parameters, better results are expected. Besides, applying plasma or corona treatment to the surface of the substrate should also help improve surface wettability and thus coating quality.

Table 8. Turbidity of the nanocoatings produced by rotational coating and spray coating.

Rotational Coating			Spray Coating		
Centripetal Acceleration (m/s^2)	Thickness (nm)	Turbidity		Thickness (nm)	Turbidity
48.8	112 ± 26	-1.94×10^{-4}	15 s:1×	64 ± 10	1.50×10^{-4}
26.3	114 ± 10	-8.77×10^{-5}	15 s:2×	81 ± 11	2.11×10^{-4}
18.9	118 ± 8	3.42×10^{-5}	15 s:3×	115 ± 13	2.40×10^{-4}
10.1	123 ± 10	1.97×10^{-4}	30 s:1×	100 ± 16	1.29×10^{-4}
4.0	123 ± 23	2.53×10^{-4}	30 s:2×	139 ± 33	2.02×10^{-4}
			30 s:3×	208 ± 46	2.11×10^{-4}
			45 s:1×	140 ± 28	3.79×10^{-4}
			45 s:2×	219 ± 70	6.18×10^{-4}
			45 s:3×	309 ± 84	2.70×10^{-4}

Table 9. O_2 permeability of the nanocoatings by dip coating, rotational coating, and spray coating.

Dip Coating			Rotational Coating			Spray Coating		
Drying angle	Thickness (nm)	O_2 Permeability of coating layer [10^{-16}cm^3(STP) cm/cm^2•s• Pa]	Centripetal Acceleration (m/s^2)	Thickness (nm)	O_2 Permeability of coating layer [10^{-16}cm^3(STP)cm/ cm^2•s• Pa]	Spray Time/Cycles	Thickness (nm)	O_2 Permeability of coating layer [10^{-16}cm^3(STP)cm /cm^2•s• Pa]
Vertical	310 ± 12	0.0015	48.8	112 ± 26	0.0021	15 s:1×	64 ± 10	0.5883
			26.3	114 ± 10	0.0030	15 s:2×	81 ± 11	0.46956
			18.9	118 ± 8	0.0038	15 s:3×	115 ± 13	0.35047
			10.1	123 ± 10	0.0044	30 s:1×	100 ± 16	0.37844
			4.0	123 ± 23	0.0079	30 s:2×	139 ± 33	0.25943
						30 s:3×	208 ± 46	0.14482
						45 s:1×	140 ± 28	0.23653
						45 s:2×	219 ± 70	0.14325
						45 s:3×	309 ± 84	0.00615

Besides examining different coating methods to fabricate one-step coassembled nanocoatings, a new polymer binder, chitosan, was investigated to introduce antimicrobial functionality to the nanocoating, as well as to create a more degradable nanocoating. Chitosan is a natural polymer, and was proven to be able to partially replace PVA as the polymer binder in the nanocoating. PVA was still partially used due to its high film formability. The chitosan/PVA nanocoating also decreased the O_2 permeability to 0.00031 [10^{-16}cm^3(STP)cm/cm^2·s·Pa]. But more systematic evaluations are needed to give a comprehensive assessment of the antimicrobial properties of the coated PLA films for potential food packaging applications.

To create another sustainable packaging material, paper was examined as a possible substrate to help reduce the use of plastic packaging films. However, with the introduction of paper

substrate, difficulty arises in terms of coating process since it is a porous material and thus the conventional dip coating method did not work well. To overcome this issue, paper substrates were sonicated in the coating dispersion followed by dip coating. Through this method of coating, the water vapor transmission rates (WVTRs) of two paper substrates were significantly decreased. The WVTRs of regular paper and cotton paper were reduced from 5511.1 to 240.9 $g \bullet day^{-1} \bullet m^{-2}$ and from 1718.3 to 283.5 $g \bullet day^{-1} \bullet m^{-2}$, respectively, after applying the nanocoating. Future work is still needed to further improve the water vapor barrier and possibly introduce oxygen barrier properties as well.

Finally, an impregnation method was developed to form free-standing films. Lightweight nanocomposite thin films with excellent mechanical properties and other functionalities are always needed for various applications. The coating methods discussed above, including dip coating, rotational coating, spray coating, can create robust nanocoatings on various substrates but the formed nanocoatings are very difficult to be removed from the substrate as free-standing films. To address this problem, a new method was invented to prepare free-standing nanocomposite films with a high inorganic nanosheet loading. An all-MMT inorganic film was first prepared by casting a dispersion containing well-exfoliated MMT nanosheets. Once detached from the substrate, the all-MMT film was impregnated with a solution containing PVDF. The impregnated PVDF helped further align the inorganic MMT nanosheets and helped improve the mechanical properties of the resultant free-standing film dramatically. PVDF was adopted in this preliminary exploration because PVDF is flexible, biocompatible, and piezoelectric, which allows for a variety of functional applications.[14] Other polymers may serve a similar role to prepare various free-standing functional nanocomposite thin films via this method for widespread application, which is worth further investigation.

In conclusion, one-step coassembly has been well-investigated and proven to be a versatile method to form nanocoatings with various coating methods (e.g., dip coating, rotational coating, spray coating, etc.) and can be applied onto different substrates (polymer films, paper, etc.). In addition, a new polymer binder was introduced to broaden the scope and application of the formed nanocoatings. In the future, this one-step coassembly method might be further advanced by adopting new coating methods (e.g., roll-to-roll coating, etc.), new substrates (e.g., fabrics, wood, leather, etc.), and new coating ingredients (both new polymer binders and new inorganic nanosheets). Besides, it may inspire the invention of new processing methods to prepare nacre-like structures.

References

1. Choudalakis, G.; Gotsis, A. D., Permeability of polymer/clay nanocomposites: A review. *European Polymer Journal* **2009,** *45* (4), 967-984.

2. Chen, H.; Müller, M. B.; Gilmore, K. J.; Wallace, G. G.; Li, D., Mechanically Strong, Electrically Conductive, and Biocompatible Graphene Paper. *Advanced Materials* **2008,** *20* (18), 3557-3561.

3. Guin, T.; Krecker, M.; Hagen, D. A.; Grunlan, J. C., Thick growing multilayer nanobrick wall thin films: super gas barrier with very few layers. *Langmuir* **2014,** *30* (24), 7057-60.

4. Priolo, M. A.; Holder, K. M.; Gamboa, D.; Grunlan, J. C., Influence of clay concentration on the gas barrier of clay-polymer nanobrick wall thin film assemblies. *Langmuir* **2011,** *27* (19), 12106-14.

5. Priolo, M. A.; Holder, K. M.; Greenlee, S. M.; Stevens, B. E.; Grunlan, J. C., Precisely Tuning the Clay Spacing in Nanobrick Wall Gas Barrier Thin Films. *Chemistry of Materials* **2013,** *25* (9), 1649-1655.

6. Ebina, T.; Mizukami, F., Flexible Transparent Clay Films with Heat-Resistant and High Gas-Barrier Properties. *Advanced Materials* **2007,** *19* (18), 2450-2453.

7. Watanabe, I., Environmental release and behavior of brominated flame retardants. *Environment International* **2003,** *29* (6), 665-682.

8. Sun, L.; Boo, W. J.; Clearfield, A.; Sue, H. J.; Pham, H. Q., Barrier properties of model epoxy nanocomposites. *Journal of Membrane Science* **2008,** *318* (1-2), 129-136.

9. Srivastava, S.; Kotov, N. A., Composite Layer-by-Layer (LbL) Assembly with Inorganic Nanoparticles and Nanowires. *Accounts of Chemical Research* **2008,** *41*, 1831-1841.

10. Das, P.; Schipmann, S.; Malho, J. M.; Zhu, B.; Klemradt, U.; Walther, A., Facile access to large-scale, self-assembled, nacre-inspired, high-performance materials with tunable nanoscale periodicities. *ACS Appl Mater Interfaces* **2013,** *5* (9), 3738-47.

11. Ding, F.; Liu, J.; Zeng, S.; Xia, Y.; Wells, K. M.; Nieh, M.-P.; Sun, L., Biomimetic nanocoatings with exceptional mechanical, barrier, and flame-retardant properties from large-scale one-stemp coassembly. *Science Advances* **2017,** *3*.

12. Mamedov, A.; Ostrander, J.; Aliev, F.; Kotov, N. A., Stratified Assemblies of Magnetite Nanoparticles and Montmorillonite Prepared by the Layer-by-Layer Assembly. *Langmuir* **2000,** *16* (16), 3941-3949.

13. Guan, Y.; Yang, S.; Zhang, Y.; Xu, J.; Han, C. C.; Kotov, N. A., Fabry-Perot Fringes and Their Application To Study the Film Growth, Chain Rearrangement, and Erosion of Hydrogen-Bonded PVPON/PAA Films. *J. Phys. Chem. B* **2006,** *110* (13484-13490).

14. Rahman, W.; Ghosh, S. K.; Middya, T. R.; Mandal, D., Highly durable piezo-electric energy harvester by a super toughened and flexible nanocomposite: effect of laponite nano-clay in poly(vinylidene fluoride). *Materials Research Express* **2017,** *4* (9).